ROLE OF THE DORSAL PERIAQUEDUCTAL GRAY ACTIVATION IN THE NEURAL CONTROL OF BREATHING

By

WEIRONG ZHANG

A DISSERTATION PRESENTED TO THE GRADUATE SCHOOL
OF THE UNIVERSITY OF FLORIDA IN PARTIAL FULFILLMENT
OF THE REQUIREMENTS FOR THE DEGREE OF
DOCTOR OF PHILOSOPHY

UNIVERSITY OF FLORIDA

2004

THIS WORK IS DEDICATED TO MY SON DANIEL, AND MY WIFE YUMING.

ACKNOWLEDGMENTS

This dissertation would not have been possible without the help and input of many people. I would like to thank my supervisory committee including Dr. Paul Davenport, Dr. Donald Bolser, Dr. Linda Hayward, Dr. Daniel Martin, and Dr. Paul Reier for their support and guidance during my Ph.D. career.

Many people provided technical assistance during my studies. In particular, I would like to thank Mabelin Castellanos for her generous help on many techniques and softwares. I would like to express my appreciation to Vicki Dugan for teaching me how to make cuff electrodes, and Patrick Shahan for his help on histology processing.

I would also like to thank Dr. Kevin Anderson. Dr. Anderson showed me the fun of teaching and gave me a memorable TA experience.

I thank other members of the lab including Yang-Ling Chou, Kimberly Kelly, Erin Robertson, Camille Schwartz, and also the people sharing the student office including Lara DeRuisseau, Joslyn Hansen, and Cheng Wang. I thank them for the time we shared together. I thank Ken Marx, Dagan, and Neal for the night we together enjoyed a wonderful baseball game. I would also like to thank Cherith Davenport, Dr. Donald Demaray and Mrs. Demaray, Kathleen Davenport and Andy Cobble for their support. And I gave my special thanks to Matthew Davenport for those spiritual discussions.

I would also like to thank my Chinese friends including Daping Fan, Zhiqun Zhang and Jianghui Cao, Xiaochun Xu, Wei (Webster) Zhang, Weiying Zhao and Youzhong Liu, for their love, support, and everlasting friendship.

Finally, I give enormous thanks to my family. I am deeply indebted to my parents. They strongly supported me to seek my dream since I was a little boy. I am also indebted to my brother Weihong Zhang, my sister-in-law Yuehua Wu, and my niece Bingjie Zhang. They took the responsibility to take care of my parents, and always asked me to focus on my research. I would like to thank my wife Yuming Gong. We supported each other during these years here, especially when we were expecting my graduation and our first baby at the same time. My son Daniel came into this world at the time I was tired of revising my dissertation. He always reminds me of hope, either with crying or smiling. I am extremely blessed with the support and love from my family. They may not understand what is written in my dissertation. But without them, I could not write a single word.

TABLE OF CONTENTS

page

ACKNOWLEDGMENTS iv

LIST OF TABLES ix

LIST OF FIGURES x

ABSTRACT xii

CHAPTER

1 INTRODUCTION OF THE PERIAQUEDUCTAL GRAY 1

Overview 1
Columnar Structures of the PAG 2
Physiological Functions of the PAG 4
The dPAG and Neural Control of Breathing 6
Experimental Approach 10

2 RESPIRATORY MUSCLE RESPONSES ELICITED BY DORSAL PERIAQUEDUCTAL GRAY STIMULATION IN RATS 11

Introduction 11
Materials and Methods 13
General Preparation 13
Protocols 15
Data Analysis 17
Results 19
Effect of Stimulation Intensity 19
Effect of Stimulation Frequency 20
Onset Effect of dPAG Stimulation 24
Off-stimulation and Post-stimulation Effect 25
dPAG Stimulation Effect on Phrenic ENG, Abdominal EMG, and $P_{ET}CO_2$ 26
Discussion 29
Respiratory Response to dPAG Stimulation 30
Cardiovascular Responses to dPAG Stimulation 33
Summary 34

3 REGIONAL DISTRIBUTION IN DORSAL PERIAQUEDUCTAL GRAY ELICITED RESPIRATORY RESPONSES 35

Introduction 35
Materials and Methods 37
General Preparation 37
Protocols 39
Data Analysis 40
Results 42
Respiratory Response to Electrical Stimulation in the dPAG 42
Respiratory Response to DLH Stimulation in the dPAG 46
Cardiovascular Response to dPAG Stimulation 48
Reconstructed Stimulation and Microinjection Sites 51
Discussion 52
Respiratory Response to Rostro-caudal dPAG Activation 52
Diaphragm EMG Response to dPAG Activation 54
Cardiovascular Response to dPAG Activation 55
Summary 56

4 INFLUENCE OF THE DORSAL PERIAQUEDUCTAL GRAY ON RESPIRATORY RESPONSE TO PERIPHERAL CHEMORECEPTOR STIMULATION 57

Introduction 57
Materials and Methods 58
General Preparation 59
Protocols 60
Data Analysis 61
Results 63
Cario-respiratory Response to Intravenous KCN and Control Experiments 63
Cardio-respiratory Response to Bic Disinhibition in the dPAG 63
Effect of Bicuculline Disinhibition of the dPAG on KCN Response 64
Cardio-respiratory Response to DLH Stimulation in the dPAG 65
Effect of DLH Stimulation in the dPAG on KCN Response 67
Reconstructed Microinjection Sites 68
Discussion 68
Respiratory Response Elicited from the dPAG 69
Effect of dPAG Activation on Respiratory Response to KCN 70
Effect of dPAG Activation on Cardiovascular Response to KCN 72
Technical Considerations 73
Summary 75

5 INFLUENCE OF THE DORSAL PERIAQUEDUCTAL GRAY ACTIVATION ON RESPIRATORY OCCLUSION REFLEXES 76

Introduction 76
Materials and Methods 78

General Preparation 78
Protocols 80
Data Analysis 80
Results 81
Respiratory Response to dPAG Activation 81
The Vi-Ti Relationship with dPAG Activation 83
The Ve-Te Relationship with dPAG Activation 85
Diaphragm EMG Activity 85
Histology Reconstruction and Control Experiments 86
Discussion 86
Respiratory Response Elicited from the dPAG 87
Effect of dPAG Activation on Respiratory Occlusion Reflexes 88
DLH vs Bicuculline 91
Summary 92

6 ROLE OF THE DORDAL PERIAQUEDUCTAL GRAY IN THE NEURAL CONTROL OF BREATHING 93

Excitatory Effect of the dPAG on Respiratory Timing Response 93
Activation of the dPAG on Respiratory Muscle Activities and Ventilation 95
Influence of the dPAG on Respiratory Reflexes 96
Influence of the dPAG on Peripheral Chemoreflex 96
Influence of the dPAG on Respiratory Occlusion Reflexes 97
Physiological Significance of the Results 99

7 SUMMARY 101

LIST OF REFERENCES 103

BIOGRAPHICAL SKETCH 114

LIST OF TABLES

Table page

2-1. Peak cardio-respiratory response to electrical stimulation in the dPAG 21

2-2. On- and off-stimulus respiratory effect of electrical stimulation. 24

3-1. On- and off-stimulus respiratory effect of electrical stimulation. 50

4-1. Latencies to peak in cardio-respiratory response to KCN or dPAG activation.....66

5-1. Effect of inspiratory occlusion on respiratory timing change following the activation of the dPAG.....83

5-2. Effect of expiratory occlusion on respiratory timing change following the activation of the dPAG.....87

LIST OF FIGURES

Figure page

2-1. dPAG stimulation sites 15

2-2. Cardio-respiratory response elicited by dPAG stimulation 16

2-3. The schematic representation of analysis method on EMG activity. 18

2-4. Cardio-respiratory responses elicited from the dPAG with different current intensities 22

2-5. The relationships between peak cardio-respiratory responses and stimulation intensities 23

2-6. Cardio-respiratory responses elicited from the dPAG with different stimulus frequencies 25

2-7. The relationships between peak cardio-respiratory responses and stimulation frequencies. 27

2-8. External abdominal oblique muscle EMG activity following the electrical stimulation in the dPAG 28

3-1. Cardio-respiratory response elicited by caudal dPAG stimulation. 41

3-2. Respiratory responses following electrical stimulation in the rostral and caudal dPAG 43

3-3. Diaphragm EMG activity changes following electrical stimulation in rostral and caudal dPAG 44

3-4. Respiratory timing response to DLH stimulation in rostral and caudal dPAG 45

3-5. Ventilation response to DLH stimulation in rostral and caudal dPAG 46

3-6. Diaphragm EMG response to DLH stimulation in rostral and caudal dPAG 47

3-7. Cardiovascular responses following electrical stimulation in rostral and caudal dPAG. 48

3-8. Cardiovascular response to DLH stimulation in rostral and caudal dPAG. 49

3-9. Reconstructed dPAG stimulation sites 51

4-1. Influence of dPAG disinhibition on cardio-respiratory response to intravenous KCN in one animal. 64

4-2. Influence of DLH microinjection in the dPAG on cardio-respiratory activity and response to intravenous KCN in one animal 65

4-3. Effect of dPAG activation on respiratory timing response to intravenous KCN 67

4-4. Effect of dPAG activation on ventilation response to intravenous KCN 69

4-5. Effect of dPAG activation on diaphragm EMG activity response to intravenous KCN. 71

4-6. Effect of dPAG activation on cardiovascular response to intravenous KCN 73

4-7. Reconstructed dPAG microinjection sites 74

5-1. A sample of respiratory occlusions before and after microinjection of DLH in the dPAG from one single animal 82

5-2. Volume-timing relationships in respiratory occlusion during dPAG activation 84

5-3. Relatiopship between respiratory volume and timing with or without dPAG activation. 86

5-4. Reconstructed dPAG stimulation sites 88

6-1. A schematic model about the role of the dPAG in the neural control of breathing. ..98

Abstract of Dissertation Presented to the Graduate School
of the University of Florida in Partial Fulfillment of the
Requirements for the Degree of Doctor of Philosophy

ROLE OF THE DORSAL PERIAQUEDUCTAL GRAY ACTIVATION
IN THE NEURAL CONTROL OF BREATHING

By

Weirong Zhang

December, 2004

Chair: Paul W. Davenport
Major Department: Veterinary Medicine

This project investigated the influence of the dorsal periaqueductal gray (dPAG), a central neural integration structure of defense behaviors and emotional reactions, on respiratory activities and reflexes. Electrical stimulation and chemical microinjection were used to activate the dPAG. Chemical microinjection was performed with glutamate receptor angonist D,L-homocysteic acid (DLH), or $GABA_A$ (γ-aminobutyric acid) receptor antagonist bicuculline (Bic) into the dPAG. Cardio-respiratory parameters were assessed in spontaneously breathing, vagal intact, anesthetized Sprague-Dawley rats.

Electrical stimulation of the dPAG decreased inspiratory time (Ti) and expiratory time (Te) resulting in an increased respiratory frequency (f_R). Stimulation of the dPAG also increased respiratory muscle activities of both diaphragm and external abdominal oblique muscle, especially the baseline activities of muscle electromyography (EMG). There was a dose-dependent increase in the respiratory response following increased

electrical stimulus frequency and intensity. Activation of the dPAG elicited hypertension and tachycardia. There is regional difference in the dPAG elicited respiratory responses, but not the cardiovascular responses. Activation of the caudal dPAG elicited a greater increase in f_R than the rostral region, due to a greater decrease in Ti and Te, and a greater increase in diaphragm EMG activity.

Cardio-respiratory responses from the dPAG activation are similar to those elicited by peripheral chemoreceptor stimulation with intravenous potassium cyanide (KCN). When KCN was delivered after dPAG activation with Bic microinjection, or simultaneously with DLH microinjection in the dPAG, the peak respiratory response and latency-to-peak were similar to the response to KCN alone. This suggests that peripheral chemoreceptor stimulation blocked descending excitatory inputs from the dPAG to the brainstem respiratory network. Inspiratory or expiratory occlusion significantly increased Ti or Te during occlusion respectively. Activation of the dPAG significantly enhanced this prolongation effect. Inspiratory occlusion significantly increased diaphragm EMG activity during occlusion, which was further enhanced with dPAG activation.

In conclusion, activation of the dPAG stimulates the brainstem respiratory network. These descending excitatory inputs further interact with brainstem neural respiratory reflexes. These studies demonstrated the influence of the central affective system in the neural control of breathing, and enhanced our understandings of the neural mechanism of the respiratory behaviors in patients with emotional changes.

CHAPTER 1
INTRODUCTION OF THE PERIAQUEDUCTAL GRAY

Overview

The midbrain periaqueductal gray matter (PAG) refers to the cellular region that surrounds the mesencephalic aqueduct from the most rostral level at the posterior commisure to the most caudal level at the dorsal tegmental nucleus. This neural structure is known to have a significant role in defense behavior. Defense behavior in cats is a complex set of behaviors comprising an immobile aggressive display with hunching of back, flattening of the ears, teeth baring, hissing, growling, unsheathed claws, defecation, piloerection and mydriasis. This behavior pattern is expressed, either completely or partially, when the animal is facing a potential threatening circumstance. Based on the evaluation of the threat level, the response could culminate in either attack or flight behavior. These behaviors are always found to be accompanied by autonomic responses, especially cardiorespiratory changes. This autonomic regulation is an integral component of defense behavior (Hess et al., 1943).

Similar defense behavior patterns can be elicited from multiple central neural structures, including the amygdala, the perifornical hypothalamus and the PAG (Hess et al., 1943; Fernandez de Molina et al., 1962; Hunsperger, 1963). Lesion of the PAG attenuated both the amygdala- and hypothalamus-evoked defensive behaviors, while neither telencephalic ablation nor hypothalamic lesions blocked defense behavior evoked from the PAG. Thus, the PAG is considered as the final common path for these defense behaviors. Specific activation of neurons in the PAG with neurochemical microinjection

demonstrated that this structure is a major central neural component involved in defense behavior (Bandler et al., 1982; Bandler et al., 1985; Hilton et al., 1986). One major component of defense behavior is the modulation of autonomic function including changes in ventilation. However, very little is known about the respiratory response to dPAG activation.

Columnar Structures of the PAG

The PAG is a longitudinal column densely packed with small neurons. This cellular column is also somewhat funnel-shaped with its base located caudally. The PAG is not a homogeneous structure. Cytoarchitecture studies have revealed that the dorsal part of the PAG has the highest neuronal density, while the ventral part of the PAG has the largest neuronal size (Beitz, 1985). Neuronal density also decreases along the rostro-caudal axis of the PAG. Four longitudinal subdivisions in the PAG are generally recognized (Carrive, 1993; Bandler et al., 1994; Behbehani, 1995; Vianna et al., 2003): the dorsomedial (dmPAG), dorsolateral (dlPAG), lateral (lPAG), and ventrolateral (vlPAG) subdivisions. These regions are subdivided in a radial fashion, and each subdivision forms a longitudinal column along the rostro-caudal axis of the PAG. The sizes and shapes of these subdivisions are not identical along this axis. Both the lPAG and the vlPAG are well developed in the caudal third of the PAG, but disappear in the rostral PAG. While the dmPAG and the dlPAG are well developed in the intermediate third of the PAG, the dlPAG is very slender in the caudal third, and the dmPAG becomes wider in the rostral and caudal thirds. The boundaries of these subdivisions are based on anatomical, histochemical, and physiological studies (Carrive, 1993; Bandler et al., 1994; Behbehani, 1995; Vianna et al., 2003).

The dlPAG can be intensively stained for the enzyme NADPH diaphorase (Depaulis et al., 1994), and acetylcholinesterase (Illing et al., 1986). The subdivision of the PAG is also demonstrated by different afferents and efferent projection patterns, which are directly related to its physiological functions. All PAG subdivisions have output projections to the ventral medulla, except the dlPAG (Carrive, 1993). Both lPAG and vlPAG project to the same regions in the medulla, but only the vlPAG projects to the periambigual region, where vagal preganlionic neurons are located (Bandler et al., 1994). Both the lPAG and vlPAG receive direct somatic and visceral afferents from the spinal cord (Bandler et al., 2000). Only the afferent inputs to the lPAG are somatotopically organized. The vlPAG receives a direct projection from the medial nucleus of the tractus solitarius (NTS), which receives afferent inputs from both pulmonary stretch receptors (PSRs) and baroreceptors (Herbert et al., 1992). The complexity of these afferent and efferent projections is essential for the PAG to play an integration role in the somatic and autonomic responses of defense behaviors.

Many neurotransmitter receptors were found on the neurons of the PAG. All three subtypes of glutamate receptors, α-amino-3-hydroxy-5-methylisoxazole-4-propionate (AMPA)/kainate, *N*-methyl-*D*-aspartate (NMDA) and metabotropic glutamate receptors, are found in the PAG (Albin et al., 1990). The distribution of these glutamate receptors decreases along the dorso-ventral axis. Both $GABA_A$ and $GABA_B$ receptors were found in the PAG (Bowery et al., 1987). The dPAG, especially the dlPAG, had more labeling of both receptors than other regions of the PAG. There are more $GABA_A$ receptors than $GABA_B$ receptors (Chiou et al., 2000). A majority of those GABA-immunoreactivity neurons also showed co-localization of serotonin 5-HT_{2A} receptors (Griffiths et al.,

2002). The PAG has extensive serotonin-immunoreactive profiles, especially the ventral region (Clements et al., 1985). Serotonin mainly produces an inhibitory effect in the PAG, which is mediated by 5-HT_{1A} receptors. The PAG also has 5-HT_2 receptors that mediate an excitatory effect (Brandão et al., 1991; Behbehani et al., 1993, Lovick, 1994). The 5-HT_{2A} receptors are evenly distributed and do not show regional differences in the dPAG (Griffiths et al., 2002). The 5-HT_{1A} receptors are regionally distributed with more expressions in the ventral PAG (Pompeiano et al., 1992). There are also multiple opioid receptors in the PAG. These receptors are important components in the PAG antinociception function (Mansour et al., 1987). Expression of mu opioid receptors is moderate, and mainly in the dPAG. A similar level of kappa subtype receptor was found in the rostral ventral PAG and all subdivisions of the caudal PAG. The distribution of the delta subtype receptor did not have region variability (Wang et al., 2002). The physiological significance of the regional neurotransmitter distribution is still not fully understood, although it is clear that the functions of the different columns of the PAG depend on the balance between excitatory and inhibitory inputs. The co-localization of various neurotransmitter receptors makes the PAG an ideal central site to coordinate complex somatic and autonomic responses.

Physiological Functions of the PAG

It has been demonstrated that the PAG is a central neural structure that mediates defense behavior patterns elicited from other higher brains including the hypothalamus and the amygdala (Fernandez de Molina et al., 1962; Hunsperger, 1963; Bandler et al., 1985; Hilton et al., 1986). The major physiological functions of the PAG include antinociception, defense/aversive behaviors, vocalization, autonomic regulation, and lordosis (Behbehani, 1995). Defense behaviors are the adaptive/survival strategies of the

animals when facing challenging or threatening environments. These physiological functions of the PAG are integral components of the defense behavior.

Consistent with neuroanatomical regional differences, physiological functions of the PAG were also expressed as functional columns (Bandler et al., 1994; Bandler et al., 2000). Activation of the dPAG and lPAG elicited fight/flight behavior, hypertension, tachycardia, and non-opioid mediated analgesia. Activation of the vlPAG elicited freezing behavior, characterized by hyporeactivity, hypotension, bradycardia, and opioid mediated analgesia. The ventral PAG plays a crucial role in the expression of conditioned fear reactions (Kim et al., 1993; Leman et al., 2003; Walker et al., 2003), but the dPAG is important in acquisition of fear conditioning (De Oca et al., 1998).

The regional differences in physiological functions of the PAG are also evident along the rostro-caudal axis of the PAG. Rostral dPAG activation elicited fight behavior, decreased blood flow to the limbs and visceral bed and increased blood flow to the face. Caudal dPAG stimulation evoked flight behavior, increased blood flow to the limbs and decreased blood flow to the viscera and face. These cardiovascular response patterns could be elicited in paralyzed animals, which suggested this phenomenon was not secondary to changes in muscle activities (Depaulis et al., 1992; Bandler, 1994; Bandler et al., 2000). The blood flow distribution pattern fits the metabolic needs of different organs related to the behavioral patterns. These coordinated somatomotor activities confirmed the role of the PAG as an integration center mediating different strategies for various stressful situations.

The components of defense behavior are coordinated for the survival of animals. Analgesia is important for the recovery of injury or continuous fight after injury.

Vocalization is a communication mechanism. Autonomic responses adjust organ functions within the animal for specific behavior patterns. Cardiovascular depressor responses can be evoked from the vPAG, and a pressor response is elicited from the dPAG (Bandler et al., 1994; Bandler et al., 2000). The cardiovascular responses elicited from the dPAG resulted in a significant increase in both arterial blood pressure and heart rate, suggesting an attenuated baroreflex (Hilton, 1982). Inhibition of the baroreflex is essential for allowing sufficient blood supply to vital organs during defense behavior. Both the lateral parabrachial nucleus (LPBN) and the nucleus tractus solitarius (NTS) have been suggested as the target nuclei mediating the inhibition (Nosaka, et al., 1993; Inui et al., 1993; Nosaka et al., 1996; Sevoz-Couche et al., 2003). These studies also suggested complex influence of the dPAG on brainstem neural structures.

The dPAG and Neural Control of Breathing

The dPAG has been demonstrated to modulate respiratory activity. In anesthetized and paralyzed cats, electrical stimulation in the PAG elicited increased respiratory rate, mainly due to the shortening of expiratory time (Te) (Duffin et al., 1972; Hockman et al., 1974; Bassal et al., 1982). Similar results were observed when electrical stimulation was applied specifically to the dPAG (Lovick, 1985; Markgraf et al., 1991; Hayward et al., 2003). An increased respiratory frequency was reported following microinjection of DLH into the dPAG, which was due to the shortening of both inspiratory time (Ti) and Te (Lovick, 1992; Huang et al., 2000). These respiratory responses could also be evoked by the application of $GABA_A$ receptor antagonist bicuculline (Hayward et al., 2003). The magnitudes of the respiratory timing responses were dose-dependent (Huang et al., 2000; Hayward et al., 2003). Greater increases in respiratory frequency were found with increased dose of chemical stimulation. Activation of the dPAG was also associated with

increased diaphragm electromyography (EMG) amplitude and baseline activities (Huang et al., 2000; Hayward et al., 2003). The change in respiratory timing suggests that the modulation effect of the dPAG may be the result of changes in the brainstem respiratory neural network.

The current understanding of the neural circuits involved in dPAG modulation of neural control of breathing is limited. The lateral parabrachial nucleus (LPBN) has been reported to be the primary relay mediating dPAG elicited respiratory responses (Hayward et al., 2004). Microinjection of $GABA_A$ receptor angonist muscimol into the LPBN eliminated about 90% of dPAG evoked respiratory response, but only partially inhibited the accompanying cardiovascular responses. Furthermore, similar respiratory responses could be elicited by microinjection of DLH into the LPBN (Chamberlin et al., 1994). Other brainstem nuclei receive projections from the dPAG, and are known to be involved in neural control of breathing, including the A5 cell group (Coles et al., 1996), the rostral ventrolateral medulla (RVLM) (Weston et al., 2004) and caudal raphe system (Feldman et al., 2003). Their roles in dPAG elicited respiratory responses remain ambiguous.

Eupenic breathing is characterized by active inspiration and passive expiration. During behaviors requiring increased ventilation, such as exercise, expiration can become active. An increase in tracheal pressure and airflow in both inspiratory and expiratory directions was observed after dPAG activation (Lovick et al., 1992), which suggested enhanced activity of the inspiratory muscles and recruitment of expiratory muscles. However, it is unknown if dPAG stimulation elicits active expiratory muscle activity. Thus, it was hypothesized that activation of the dPAG will recruit external abdominal oblique muscle activity and generate activate expiration.

Studies on dPAG elicited respiratory responses have been done mainly by activation of the caudal dPAG. Rostral and caudal dPAG were involved in different strategies of defense behavior, i.e., fight and flight behaviors. While hypertension and tachycardia accompany both fight and flight behaviors, underlying neural mechanisms are different (Carrive, 1993; Bandler et al., 1994; Bandler et al., 2000). The fight defense behavior has extracranial vasodilation but limbs and visceral vasoconstriction. The flight behavior was accompanied with vasodilation in limbs but vasoconstriction in other regions. These changes in blood flow redistribution are to meet the metabolic requirements of specific organs. However, it is unclear if there is a regional difference in the respiratory response elicited from the dPAG. It was therefore hypothesized that there would be a regional difference in dPAG elicited respiratory response along the rostro-caudal axis.

Increased *c*-Fos expression in the dPAG was observed following hypoxia or peripheral chemoreceptor stimulation (Berquin et al., 2000; Hayward et al., 2002). The neuronal responsiveness to hypoxia has been confirmed in the dPAG using an *in vitro* preparation (Kramer et al., 1999). Hypoxia responsive neurons in the caudal hypothalamus project to the dPAG (Ryan et al., 1995). These data suggest that the dPAG could be in the neuronal circuit mediating autonomic responses to hypoxia. It has been suggested that suprapontine neural structures are not essential in respiratory response to peripheral chemoreflex (Koshiya et al., 1994). But after microinjection of excitatory amino acid antagonist kynurenic acid or synaptic blocker cobalt chloride in the caudal hypothalamus, the hypoxia respiratory response was significantly attenuated (Horn et al., 1997; Kramer et al., 1998). It has been reported that hypoxia could elicit autonomic and

behavioral response patterns similar to those observed with defense behavior (Hilton et al., 1982; Marshall, 1987). In addition, stimulation of the dPAG elicited a hyperventilation that decreased end-tidal PCO_2 (Zhang et al, 2003). The hypocapnia was sustained throughout the dPAG activation period with no evidence of hypocapneic ventilatory compensation. Thus, defense behavior may be affected by hypercapnia and hypoxia. Conversely, hypoxic and hypercapneic responses may be modulated by dPAG mediated defense behavior. It remains unknown, however, whether there is an interaction between dPAG activation and peripheral chemoreceptor stimulation. It was hypothesized that dPAG activation would modulate the respiratory response to peripheral chemoreceptor stimulation.

The effect of dPAG activation on respiratory mechanoreflexes has not been studied. During eupneic breathing, the mechanosensory information from the airways and lung, in part, determines the timing of inspiratory and expiratory phases of the respiratory cycle. This respiratory mechanical information is transduced by slowly adapting pulmonary stretch receptors (PSRs). The PSR afferent fibers are in the vagus nerves and project to brainstem respiratory nuclei. Decreased inspiratory volumes (Vi) or expiratory volumes (Ve) are associated with increased Ti or Te, respectively. This volume-timing reflex is mediated by PSRs (Zechman et al., 1976; Davenport et al., 1981; Davenport et al., 1986; Webb et al., 1994; Webb et al., 1996). It was demonstrated that changes in the central respiratory network can modulate the volume-dependent control of respiratory phase duration. It is also known that dPAG evoked respiratory responses are associated with no significant change in tidal volume but a significant decrease in both Ti and Te. This suggested that the relationship between respiratory volume and respiratory timing during

eupnea was altered and the respiratory central neural timing sensitivity to PSRs modulated by dPAG activation. While dPAG activation can elicit significant changes in respiratory timing (Huang et al., 2000; Hayward et al., 2003; Hayward et al., 2004), it is unknown if dPAG changes the respiratory volume-timing related control of breathing pattern. It is therefore hypothesized that dPAG activation modulates respiratory mechanoreflexes.

Experimental Approach

It has been demonstrated that

- Activation of the dPAG can elicit respiratory response, which is expressed primarily as increased respiratory frequency, accompanied by tonic discharges of respiratory muscles.
- The dPAG has multiple connections with higher brain centers including the prefrontal cortex, the hypothalamus, the amygdala, and various brainstem nuclei including the LPBN, A5 cell groups, RVLM, caudal raphe system.
- The dPAG elicited respiratory response is mediated by the LPBN.

Based on these previous studies, this dissertation investigated the following hypotheses:

- Hypothesis 1: The activation of the dPAG will modulate breathing pattern, and inspiratory and expiratory muscle activities
- Hypothesis 2: There is a regional difference in dPAG elicited respiratory responses along the rostro-caudal axis of the dPAG
- Hypothesis 3: The activation of the dPAG will modulate the respiratory response to stimulation of peripheral chemoreceptors
- Hypothesis 4: The activation of the dPAG will modulate respiratory mechanoreflexes

The overall goal of this dissertation is to determine the effect of dPAG activation on respiratory activity and reflexes. Urethane-anesthetized, vagal intact, adult, male, Sprague-Dawley rats were used. Both electrical stimulation and chemical microinjection methods were used to activate the dPAG. These results provide a new understanding of the role of the dPAG in modulation of respiratory activity.

CHAPTER 2
RESPIRATORY MUSCLE RESPONSES ELICITED BY DORSAL PERIAQUEDUCTAL GRAY STIMULATION IN RATS

Introduction

The periaqueductal gray matter (PAG) refers to the neural structure surrounding the mesencephalic aqueduct. This region is an important neural structure in defense behavior, analgesia, vocalization and autonomic regulation. Different behavior patterns have been elicited by activation of the longitudinal neuronal columns of the PAG (Bandler et al., 1994; Bandler et al., 2000; Behbehani, 1995; Carrive, 1993; Zhang et al., 1994). The dorsal subdivision (dPAG) has been demonstrated to play a crucial role in fight/flight behavior and associated autonomic responses. Furthermore, the activation of the dPAG is closely related to the emotional responses of anxiety, panic and fear (Bandler et al., 2000; Graeff et al., 1993; Nashold et al., 1969; Vianna et al., 2003). These emotional responses often have a respiratory component that may be mediated by the dPAG.

In anesthetized and paralyzed cats, electrical stimulation in the PAG elicited increased respiratory rate that was mainly due to shortening of expiratory time (Te) (Bassal et al., 1982; Duffin et al., 1972; Hockman et al., 1974). Similar results were observed in rats when electrical stimulation was applied specifically to just the dPAG (Hayward et al., 2003; Lovick, 1992; Markgraf et al., 1991). An increased respiratory rate due to the shortening of inspiratory time (Ti) and Te was reported with microinjection of the excitatory amino acid D,L-homocysteic acid (DLH) into the dPAG (Huang et al., 2000; Lovick, 1992). Similar respiratory responses could also be evoked by applying the

$GABA_A$ receptor antagonist bicuculline, activating this area by disinhibiting neurons in the dPAG (Hayward et al., 2003). Inspiratory and expiratory tracheal airflow have also been reported to increase following dPAG activation (Lovick, 1992) suggesting the possible recruitment of expiratory muscle activity. Previous studies, however, only measured increased respiratory activity in an inspiratory muscle, the diaphragm. The present study was undertaken to test the hypothesis that dPAG activation involves the simultaneous recruitment of both inspiratory and expiratory muscles. Furthermore, we hypothesized that the recruitment of expiratory muscles has the same stimulus threshold as recruitment thresholds for both inspiratory muscles and cardiovascular changes.

Stimulation of the dPAG may also elicit a sustained change in basal state of the dPAG (Hayward et al., 2003; Hilton, 1982). If this occurs, then the change of cardio-respiratory response behavior would be sustained after the cessation of stimulation. Electrical dPAG stimulation is the technique of choice since the on- and off-stimulation timing could be reliably determined. Although electrical stimulation activates both neurons and fibers of passage, it has been demonstrated that controlled stimulation in the dPAG could elicit cardio-respiratory responses similar to chemical stimulation (Behbehani, 1995; Hayward et al., 2003; van der Plas et al., 1995). It was hypothesized that electrical stimulation of the dPAG would elicit an immediate (within the first respiratory cycle) increase in ventilation and the increased ventilatory state would persist after the stimulation ceased. Thus, this project studied the effect of dPAG activation by electrical stimulation with systematic variation of stimulus intensities and frequencies. Both inspiratory and expiratory muscle activities were analyzed. The cardio-respiratory responses were analyzed during and after the electrical stimulation of the dPAG.

Materials and Methods

The experiments were performed on 11 adult male Sprague-Dawley rats (250 - 400g) housed in the University of Florida animal care facility. The rats were exposed to a normal 12hr light-12hr dark cycle. The experimental protocol was reviewed and approved by the Institutional Animal Care and Use Committee of the University of Florida.

General Preparation

The rat was anesthetized with urethane (1.4 g/kg, i.p.). Additional urethane (20 mg/ml) was administrated intravenously as necessary. The adequacy of anesthesia was regularly verified by the absence of a withdrawal reflex or blood pressure and heart rate responses to a paw pinch. A tracheostomy was performed. The femoral artery and vein were catheterized. The body temperature was monitored with a rectal probe and maintained between 37 - 39°C with the periodic use of a heating pad. The rats respired spontaneously with room air. End-tidal PCO_2 ($P_{ET}CO_2$) was measured with flow-through capnography (Capnogard, Novametris Medical System).

Inspiratory and expiratory electromyographic (EMG) activities were recorded with bipolar Teflon-coated wire electrodes. The bared tips of the electrodes were inserted into the diaphragm through a small incision in the abdominal skin. A third wire served as an electrical ground inserted in the skin beside the ear. Another pair of electrodes was inserted into the external abdominal oblique muscle, ipsilateral to the diaphragm electrodes through a second incision in the abdominal skin. For three animals, the phrenic nerve was isolated via a dorsal approach in the cervical region ipsilateral to the diaphragm electrodes. The intact nerve was placed *en passage* on bipolar platinum electrodes for recording phrenic neurogram (ENG) and covered with warm mineral oil.

The recording electrodes for muscle EMGs or phrenic ENG were connected to high-impedance probes connected to an AC preamplifier (P511, Grass Instruments), amplified and band-pass filtered (0.3-3.0 kHz). The analog outputs were then connected to a computer data sampling system (CED Model 1401, Cambridge Electronics Design) and processed by a signal analysis program (Spike 2, Cambridge Electronics Design). The arterial catheter and tracheal tube were attached to two calibrated pressure transducers connected to a polygraph system (Model 7400, Grass Instruments). The analog outputs of the polygraph were sent to the computer data sampling system. All signals were recorded simultaneously and stored for subsequent off-line analysis.

The animal was then placed prone in a small animal stereotaxic head-holder (Kopf Instruments). The cortex overlying the PAG was exposed by removal of small portions of the skull with a high-speed drill. The dura was reflected, and warm mineral oil was applied on the surface. A monopolar stainless steel stimulating electrode, insulated to within 30-50 μm of the tip, was advanced into the dPAG based on a stereotaxic atlas of the rat brain (Paxinos et al., 1997). The coordinates for the caudal dPAG were 7.64 to 8.72 mm caudal to the bregma, 0.1 to 0.6 mm lateral to the midline and depths of 3.8 to 4.5 mm below the dorsal surface of the brain. The dPAG was stimulated (S48 stimulator, Grass Instruments) with a 10 s train of electrical pulses (0.2 ms pulse width).

In all animals, the stimulation site was marked at the end of the experiment by electrolytic lesion (1 mA, 30 s). The animal was then euthanized, the brain removed and fixed in 4% paraformaldehyde solution. The fixed tissue was then cut coronally into 40-μm-thick sections with a crytostat (HM101, Carl Zeiss). The sections were mounted and stained with cresyl violet. The stained sections were examined to identify the lesion,

stimulation site, and corresponding electrode tract. The atlas from Paxinos and Watson (Paxinos et al., 1997) was used to reconstruct the stimulation site (Fig. 2-1).

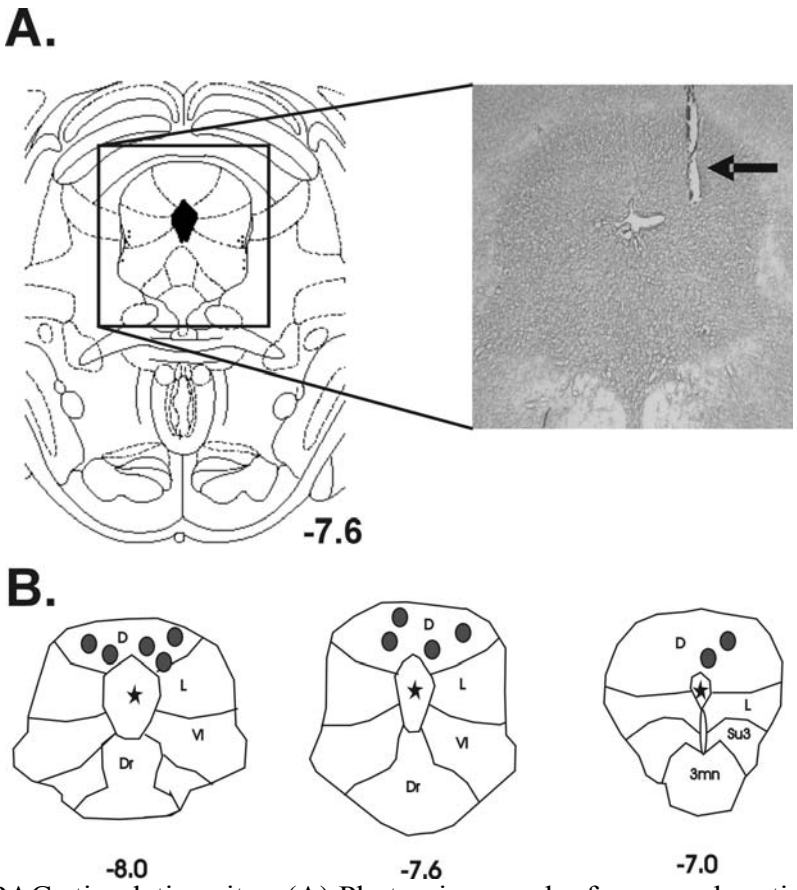

Figure 2-1. dPAG stimulation sites. (A) Photomicrograph of a coronal section through the dPAG. The electrode tract is marked by the arrow in the photomicrograph. (B) The lower panel represents the positions of the electrode tips of all animals. Schematic drawings based on the rat brain atlas (Paxinos et al., 1997). The ★ indicates the aqueduct; dr: dorsal raphe. d: dorsal PAG; l: lateral PAG; vl: ventrolateral PAG; su3: supraoculomotor PAG; 3mn: oculomotor nucleus.

Protocols

In the first set of experiments (n=8), electrical stimulation was delivered unilaterally into the dPAG. The stimulating electrode was stereotaxically guided to sites within the caudal dPAG. The EMGs from the diaphragm (dEMG) and external abdominal oblique muscle (aEMG), and arterial blood pressure were recorded. Two sets of stimulation were used: 1) fixed magnitude with varying frequency, 75 μA at 10, 30,

and 100 Hz, and 2) fixed frequency with varying magnitude, 100 Hz at 10, 50, 75, and 100 μA. The stimuli were delivered in random order.

In the second set of experiments (n=3), electrical stimulation was delivered into the dPAG with a single stimulus paradigm: pulse trains of 10 s, 100 Hz frequency, 0.2 ms pulse width, 50 μA current magnitude. The dEMG, ipsilateral phrenic ENG, HR and blood pressure were recorded. The objective of this group of animals was to confirm that the dEMG response correlated with phrenic nerve activity during stimulation of the dPAG.

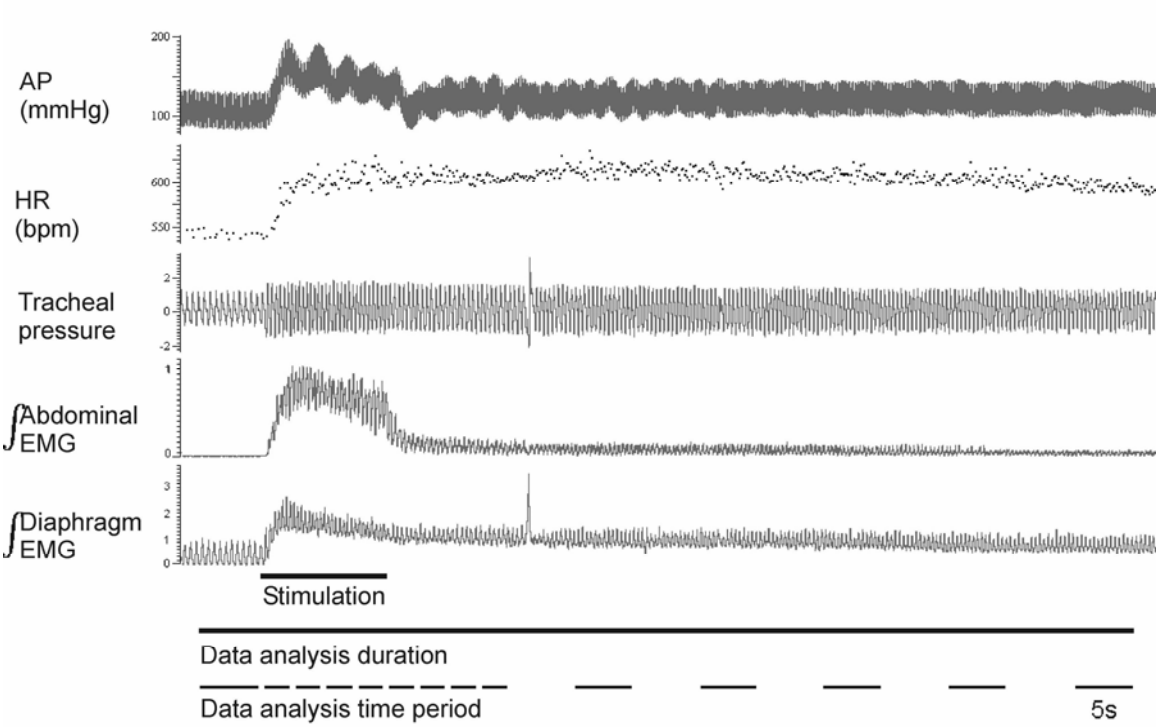

Figure 2-2. Cardio-respiratory response elicited by dPAG stimulation with 75 μA intensity, 100 Hz frequency, 10 s duration, 0.2 ms pulse width from a single animal. The top trace is the arterial blood pressure. The second trace is the HR response. The third trace is the tracheal pressure. The fourth trace is integrated EMG from the external abdominal oblique muscle. The bottom trace is the integrated EMG from the diaphragm. The horizontal bar represents the 10 s stimulation duration. The second horizontal bar represents total time duration for data analysis (70 s). The third horizontal broken line represents each time period for data analysis, the long bar represents 5 s while the short bar represents 2.5 s.

Data Analysis

All data were analyzed off-line using Spike2 software (Cambridge Electronics Design). The dEMG, aEMG and ENG were rectified and integrated (time constant = 50 ms). The Ti, Te, and respiratory rate (f_R) were calculated from the tracheal pressure. Baseline dEMG, aEMG and ENG were defined as the minimum value measured between bursts at end of expiration. The amplitudes of integrated dEMG (ΔdEMG), aEMG (ΔaEMG) or ENG (ΔENG) were calculated as the difference between baseline and peak burst amplitudes. The mean arterial blood pressure (MAP) was calculated as the diastolic pressure plus 1/3 of the pulse pressure. Heart rate (HR) was derived from the average interval between peak systolic pressure pulses in the arterial pressure trace.

The control respiratory and cardiovascular parameters were averaged over the 5 s prior the onset of stimulation. The on- and off-stimulus respiratory effects were measured from the complete respiratory cycle or breath taken immediately before and after the onset of stimulation, and the first complete respiratory cycle following cessation of stimulation. During electrical stimulation, Ti, Te, f_R, baseline aEMG, baseline dEMG, ΔdEMG amplitude, MAP and HR were averaged every 2.5 s. After the cessation of stimulation, these values were averaged for every 2.5 s during the first 10 s. Then, the parameters were averaged for 5 s of each 10 s period for the next 50 s (Fig. 2-2). MAP, HR, Ti, Te, and f_R were compared before, during, and after dPAG stimulation. The peak value for each analyzed parameter was defined as the highest average value that occurred during electrical stimulation. For diaphragm activity, baseline dEMG and ΔdEMG were expressed as a percentage of control (Fig. 2-3). For the aEMG signal, the activity under the control condition was treated as zero since there was no control activity. The peak

aEMG baseline activity or ΔaEMG was considered as arbitrary unit one. All aEMG measurements were calculated as a ratio to peak values (Fig. 2-3).

A two-way ANOVA with repeated measures (factors: frequency and time, or factors: intensity and time) was performed for comparisons of respiratory and cardiovascular responses due to the different stimulating conditions in the dPAG. A one-way ANOVA with repeated measures (factor: treatment) was performed for comparisons on respiratory parameter changes in two single breaths immediate before and after electrical stimulation, or the cessation of stimulation. When differences were indicated, a Tukey post-hoc multiple comparison analysis was used to identify significant effects. A Pearson correlation test was performed to measure the correlation between dEMG and phrenic ENG activity. Probabilities $p<0.05$ were considered significant. All data are reported as means ± SE.

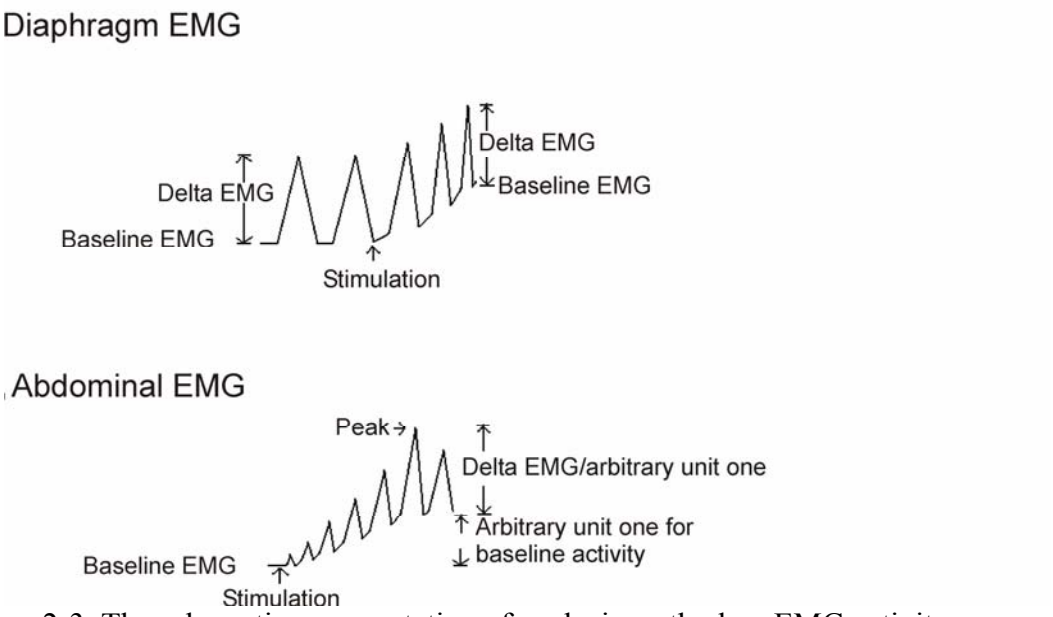

Figure 2-3. The schematic representation of analysis method on EMG activity.

Results

In all animals, the tips of the electrical stimulation electrodes were in the dPAG (Fig. 2-1). Before the stimulation, average f_R was 102±2 breath/min, HR 462±3 beat/min, and MAP 80±3 mmHg. A typical response observed during and immediately following electrical stimulation (75μA, 100Hz, 10s) of the dPAG is shown in Fig. 2-2. At these stimulation parameters, the maximal tracheal pressure increased immediately in both negative and positive directions indicating increased inspiratory and expiratory efforts. Associated with these changes in trachea pressure was a rapid increase in f_R, peak tracheal pressure, dEMG activity and recruitment of aEMG activity. The aEMG was silent during eupenic breathing, but aEMG activity was recruited after the onset of stimulation, and persisted after the cessation of stimulation (Fig. 2-2). Parallel to the immediate change in respiratory function there was a slower rate of change in both blood pressure and heart rate.

Effect of Stimulation Intensity

To identify the dPAG stimulation intensity sufficient to increase respiratory activity, animals were stimulated with a 10s electrical stimulus train of 100 Hz with various intensities of 10, 50, 75, or 100 μA (Fig. 2-4 and 2-5). Stimulation with 10 μA did not elicit significant changes in cardio-respiratory pattern. For those stimuli greater than 10μA, baseline activity of dEMG during stimulation increased significantly compared with control. In the first 2.5 s measurement period, both 75 μA and 100 μA evoked a greater increase in baseline activity than 50 μA (p<0.05). Ti and Te significantly decreased, and f_R significantly increased for stimulus intensities of 50, 75, and 100 μA. No significant changes in ΔdEMG were observed for all stimulus intensities.

MAP and HR significantly increased with stimulus intensities of 50, 75, and 100 μA, and no significant group differences were observed among these three stimulation intensities.

The relationships between peak cardio-respiratory responses and stimulus intensity are presented in Table 2-1 and Fig. 2-5. The respiratory timing parameters and MAP reached their peaks during the 2nd 2.5 s measurement period. Baseline dEMG peaked during the 1st 2.5 s measurement period with stimulation intensities of 75 and 100 μA. HR increased to peak at the 4th 2.5 s measurement period during stimulation. Stimulation with 10 μA did not significantly change peak cardio-respiratory parameters compared to control. No significant difference in peak values was found among 50, 75, and 100 μA stimulus intensities.

Effect of Stimulation Frequency

To identify the dPAG stimulation frequency sufficient to increase respiratory activity, the animals were stimulated with a 10 s electrical stimulus train of 75 μA with 10, 30, and 100 Hz. Stimulation at 10 Hz did not elicit significant changes in cardio-respiratory pattern (Fig. 2-6). Baseline dEMG significantly increased at the 4^{th} measurement period during stimulation with 30 Hz ($p<0.05$), while 100 Hz stimulation elicited a significant increase in the 1^{st} 2.5 s measurement period, ($p<0.001$). Stimulation with 100 Hz elicited a significantly greater increase in baseline dEMG compared to 10 Hz and 30 Hz ($p<0.001$). There was no significant change in ΔdEMG across all frequencies of stimulation. Ti and Te significantly decreased with 100 Hz stimulation, thus there was a significant increase in f_R (Fig. 2-6). Stimulation with 30 Hz significantly decreased Ti and Te, and increased f_R from the 2^{nd} 2.5 s measurement period. There was a significant difference in the Ti, Te, and f_R between 30 Hz and 100 Hz ($p<0.05$).

Table 2-1. Peak cardio-respiratory response to electrical stimulation in the dPAG.

	100 Hz					75 μA			
	control	+10 μA	+50 μA	+75 μA	+100 μA	control	+10 Hz	+30 Hz	+100 Hz
Ti (ms)	218±16	211±19	147±12^{**++}	127±7^{**++}	134±13^{**++}	219±17	223±22	171±15^{**+}	127±7$^{**++\#}$
Te (ms)	377±39	325±33	168±10^{*++}	147±8^{*++}	152±6^{*++}	382±39	375±34	202±16^{**++}	147±8^{**++}
f_R (/min)	104±7	116±9	195±15^{*++}	222±14^{**++}	215±13^{**++}	100±4	102±7	166±17^{**++}	222±14$^{**++\#\#}$
Baseline dEMG activity (%)	1.00±0.00	1.24±0.14	11.96±2.02^{*++}	16.28±3.39$^{**++\&}$	15.11±3.22^{*++}	1.00±0.00	1.01±0.06	5.85±3.39*	16.28±3.39$^{**++\#\#}$
dEMG activity amplitude (%)	1.00±0.00	1.04±0.05	1.30±0.28	2.08±1.02	1.48±0.50	1.00±0.00	1.03±0.03	1.09±0.09	2.08±1.02
MAP (mmHg)	80±9	90±7	141±13^{*++}	151±11^{*++}	152±17^{*++}	80±7	80±68	125±12^{*++}	151±11$^{**++\#}$
HR (bpm)	462±9	476±8	511±13^{*++}	535±16^{*++}	527±16^{*++}	463±9	461±8	500±13^{**++}	535±16$^{**++\#\#}$

All data are mean ± SE. dEMG: diaphragm EMG.
*: $p<0.05$; **: $p<0.001$, comparing with control level. +: $p<0.05$; ++: $p<0.001$, comparing with peak values from 10μA 100Hz or 75μA 10Hz stimulation. &: $p<0.05$, comparing with peak values from 50μA 100Hz stimulation. #: $p<0.05$; ##: $p<0.001$, comparing with peak values from 75μA 30Hz stimulation.

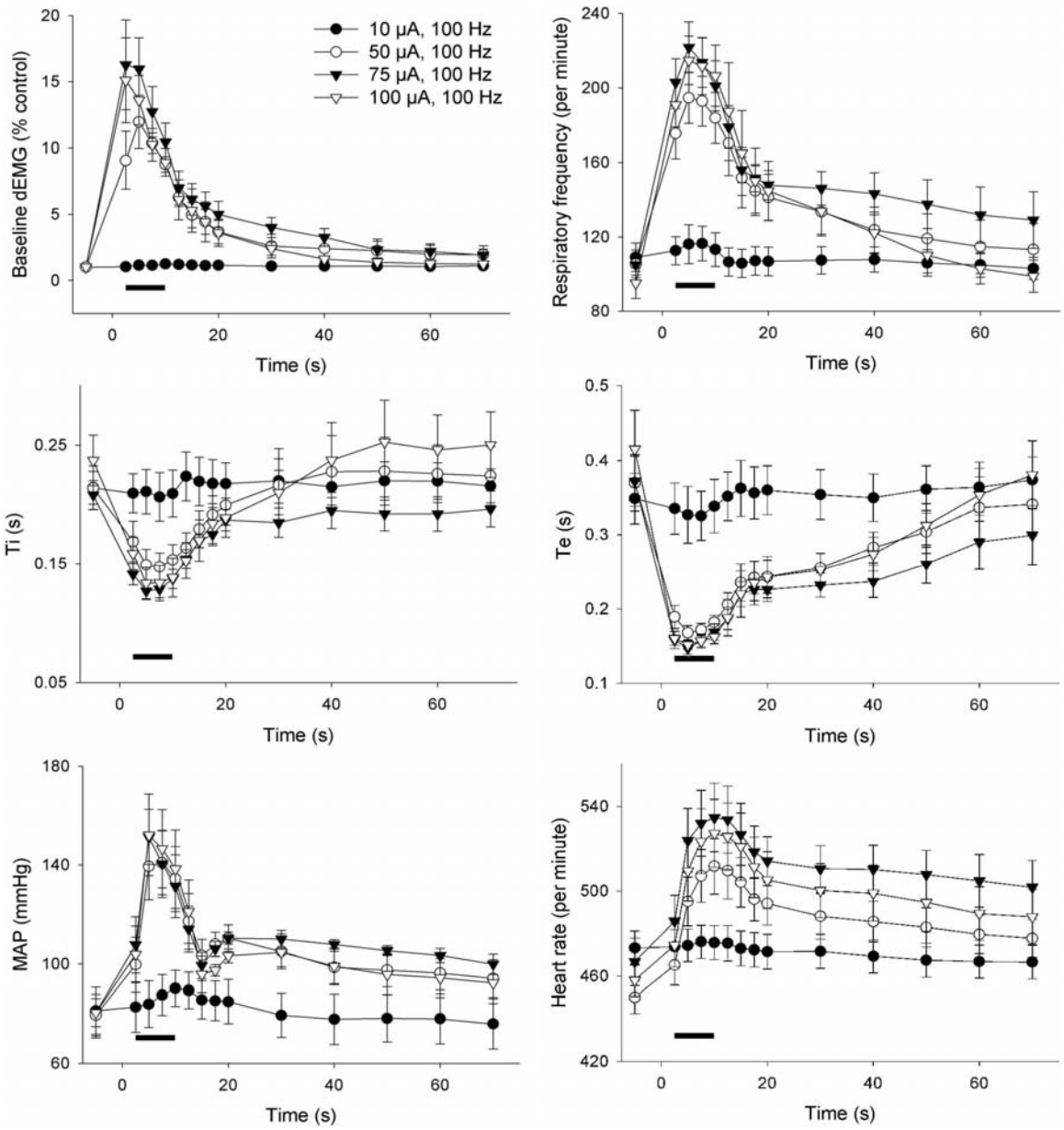

Figure 2-4. Cardio-respiratory responses elicited from the dPAG with different current intensities (100 Hz at 10 μA, 50 μA, 75 μA and 100 μA). The bar in each panel represents the duration of electrical stimulation (n=6).

Stimulation with 30 Hz increased both MAP and HR significantly at the 2nd 2.5 s measurement period (Fig. 2-6). Stimulation at 100 Hz significantly increased MAP and HR at the 1st 2.5 s measurement period (p<0.001). A significant difference in HR was observed with 30 Hz and 100 Hz stimulation frequencies. There was no significant difference in the MAP change between 30 Hz and 100 Hz.

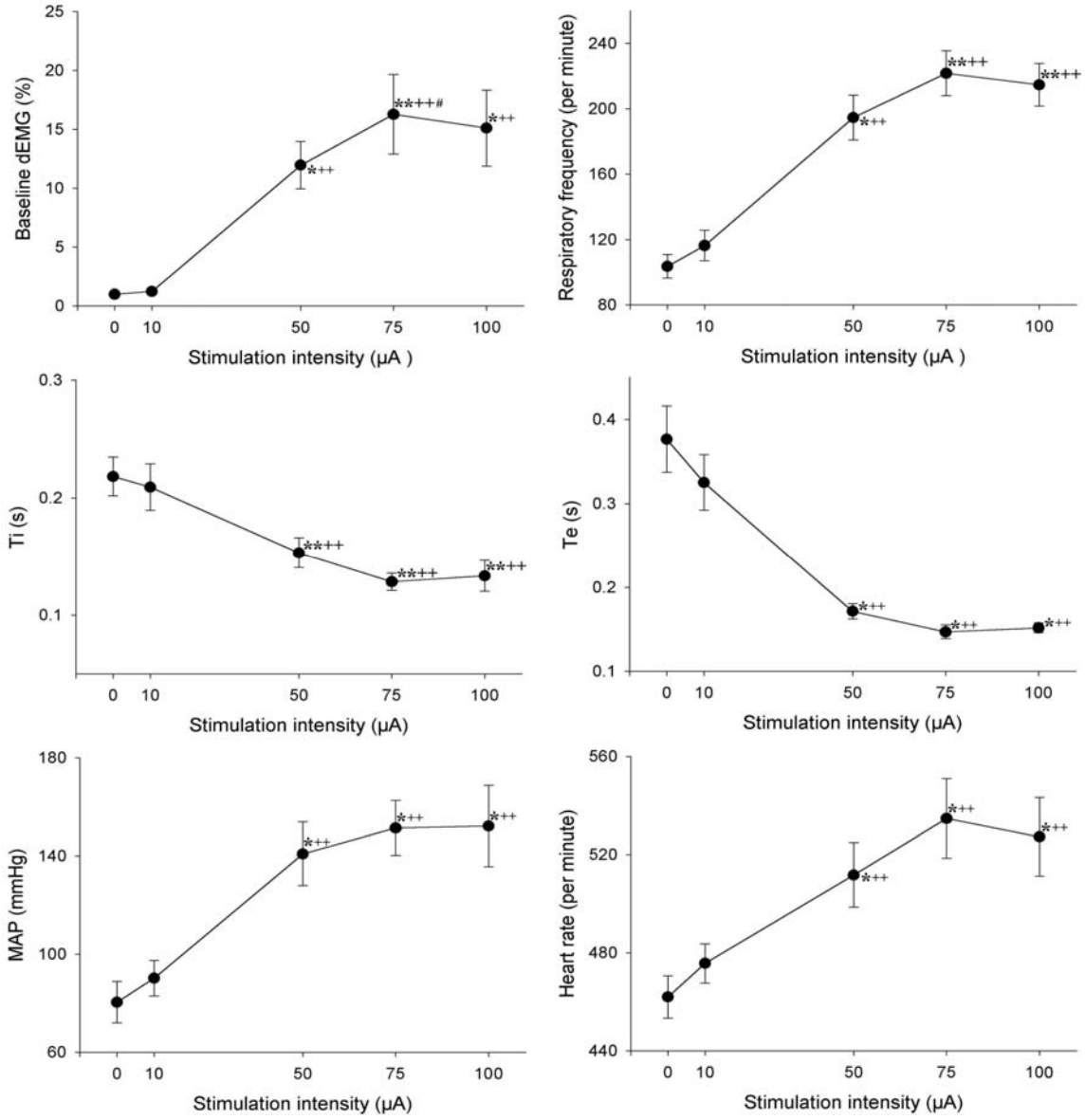

Figure 2-5. The relationships between peak cardio-respiratory responses and stimulation intensities (n=6). The value at 0 μA represents the averaged control value before stimulation. *: $p<0.05$; **: $p<0.001$, comparing with control level. +: $p<0.05$; ++: $p<0.01$, comparing with peak values from lowest stimulation intensity (10 μA). #: $p<0.05$ comparing 50 μA with 75 μA.

The peak cardio-respiratory response relationships as a function of stimulus frequency are presented in Table 2-1 and Fig. 2-7. Ti, Te and f_R reached their peaks during the 2nd 2.5 s measurement period with 100 Hz stimulation, and reached peak at the 4th 2.5 s measurement period with 30 Hz. Baseline dEMG peaked during the 1st 2.5 s period with 100 Hz stimulation. Baseline dEMG peaked at the 4th 2.5 s measurement

period with 30 Hz stimulation. HR peak was at the 4th 2.5 s measurement period for 30 Hz and 100 Hz stimulation. Stimulation at 30 Hz and 100 Hz elicited significant changes in peak Ti, Te, f_R, MAP and HR compared to 10 Hz stimulation (p<0.05).

Table 2-2. On- and off-stimulus respiratory effect of electrical stimulation with 100 μA and 100 Hz in the dPAG.

	On-stimulus effect		Off-stimulus effect	
	Control	Stimulus-on	Stimulus-on	Stimulus-off
Ti (ms)	217±7	143±13**	136±2	144±1##
Te (ms)	404±54	212±9*	169±1	197±2
f_R (/min)	100±8	170±5**	200±12	178±8
Baseline dEMG (%)	100±0	226±67	813±133	754±192
dEMG amplitude (%)	100±0	135±14*	134±36	123±37

All data are mean ± SE. dEMG: diaphragm EMG. *: p<0.05; **: p<0.001, comparing with control level. ##: p<0.001, comparing with stimulus-on.

Onset Effect of dPAG Stimulation

The specific changes in respiration that occurred within the first breath following the onset of dPAG stimulation were analyzed in more detail. The respiratory timing and dEMG activity was compared in breaths immediately before and after the onset of electrical stimulation with 100 μA and 100 Hz (Table 2-2). Within this first breath, Ti significantly decreased from 217±7 ms to 143±13 ms (p<0.001), and Te significantly decreased from 404±54 ms to 212±9 ms (p <0.05). Respiratory frequency significantly increased from 100±8 to 170±5 breaths/min (p <0.001). There were significant increases in baseline dEMG activity (226±67%).

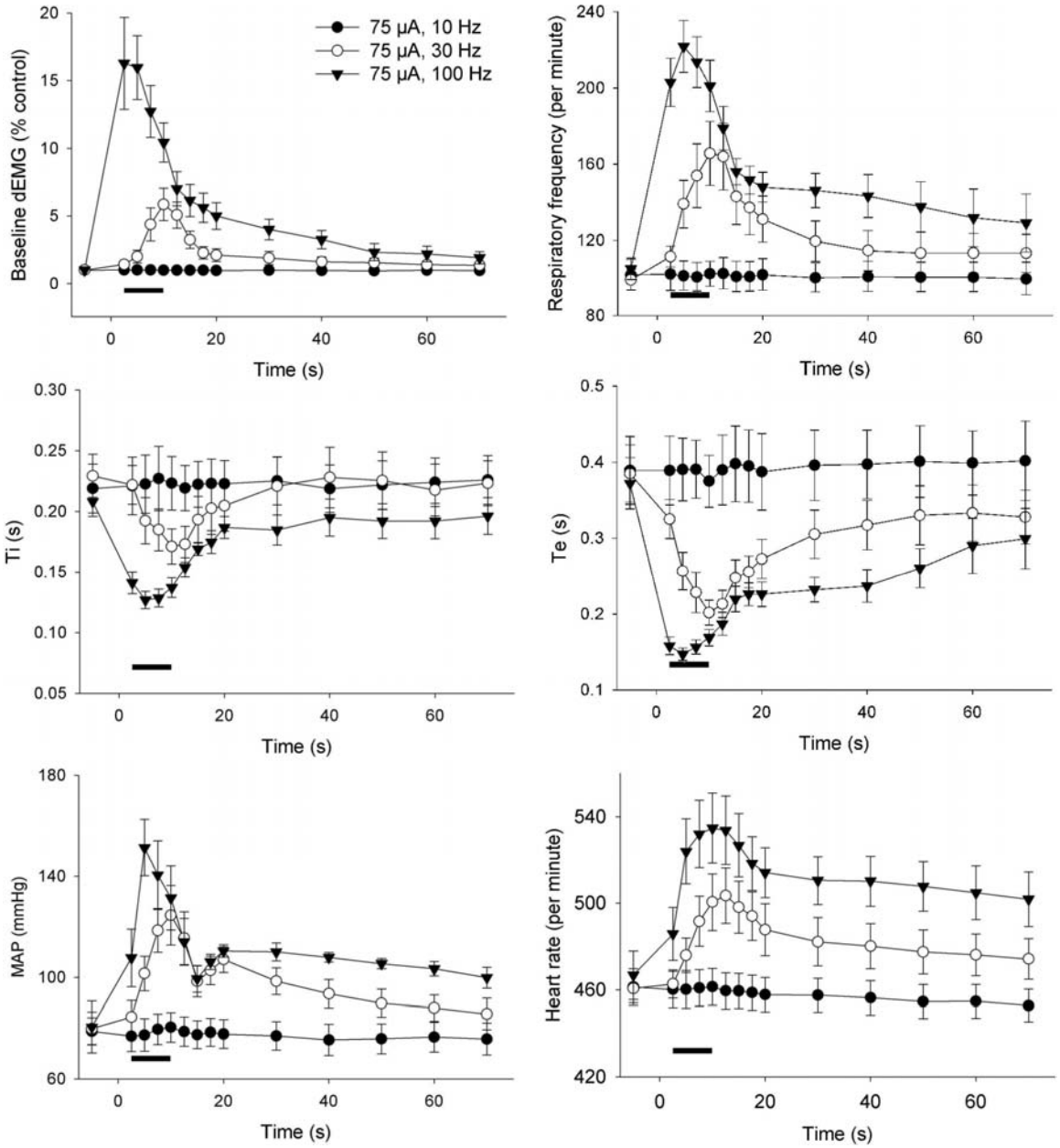

Figure 2-6. Cardio-respiratory responses elicited from the dPAG with different stimulus frequencies (75 µA at 10 Hz, 30 Hz, and 100 µA). The bar in each panel represents the duration of electrical stimulation (n=6).

Off-stimulation and Post-stimulation Effect

Following the cessation of stimulation, dPAG induced changes in cardio-respiratory activity persisted for a minimum of 60 s (Fig. 2-2). After the cessation of stimulation at 100 Hz there were sustained and significant increases in baseline dEMG and f_R compared to control, until the 7.5 s time period with 50 µA, the 20 s time period

with 75 μA, and the 10 s time period with 100 μA (p>0.05). Ti returned to control level at the 5 s time period following cessation of stimulation with 50 μA and 75 μA and the 10 s time period with 100 μA (p>0.05). Te was significantly decreased after the cessation of stimulation until the 20 s time period with 50 μA, the 40 s time period with 75 μA (p<0.05) and the 30 s time period with 100 μA (p<0.05). With 50, 75 and 100 μA, HR remained significantly greater than control during the entire 1 minute post-stimulation measurement period (p<0.001). MAP returned to control level after cessation of stimulation by the 20 s time period with 50 μA, the 50 s time period with 75 μA and the 30 s time period with 100 μA.

The first breath pattern following the offset of dPAG stimulation with 100 μA and 100 Hz (Table 2-1) was determined. The Ti, Te, f_R and dEMG activity were compared between the breaths immediate before and after the cessation of electrical stimulation. Ti significantly increased from 136±2 ms to 144±1 ms (p<0.001). Te was not significantly different (169±1 ms to 179±2 ms). The f_R significantly decreased from 200±12 to 178±8 breath/min (p>0.05). There were no significant change of baseline dEMG activity (813±133% to 754±192%) and ΔdEMG amplitude (134±36% to 123±37%).

dPAG Stimulation Effect on Phrenic ENG, Abdominal EMG, and $P_{ET}CO_2$

In the three animals tested, the phrenic ENG increased in parallel with the ipsilateral dEMG during the electrical stimulation of the dPAG. Baseline dEMG and phrenic ENG activities increased in the first breath following the onset of stimulation. The pattern of the phrenic ENG activity was significantly correlated with the dEMG activity (r=0.825, p<0.001).

The aEMG was silent during control breathing (Fig. 2-2 and 2-8). aEMG activity was recruited later and recovered earlier during dPAG stimulation than dEMG. dPAG

stimulation increased ΔaEMG amplitude and aEMG baseline activity. There was increased aEMG baseline discharge during the inspiratory phase. The ΔaEMG was modulated with a respiratory rhythm in phase with expiration. aEMG activity persisted after the cessation of stimulation with stimulus intensities of 50, 75, and 100 μA and stimulus frequencies of 30 and 100 Hz.

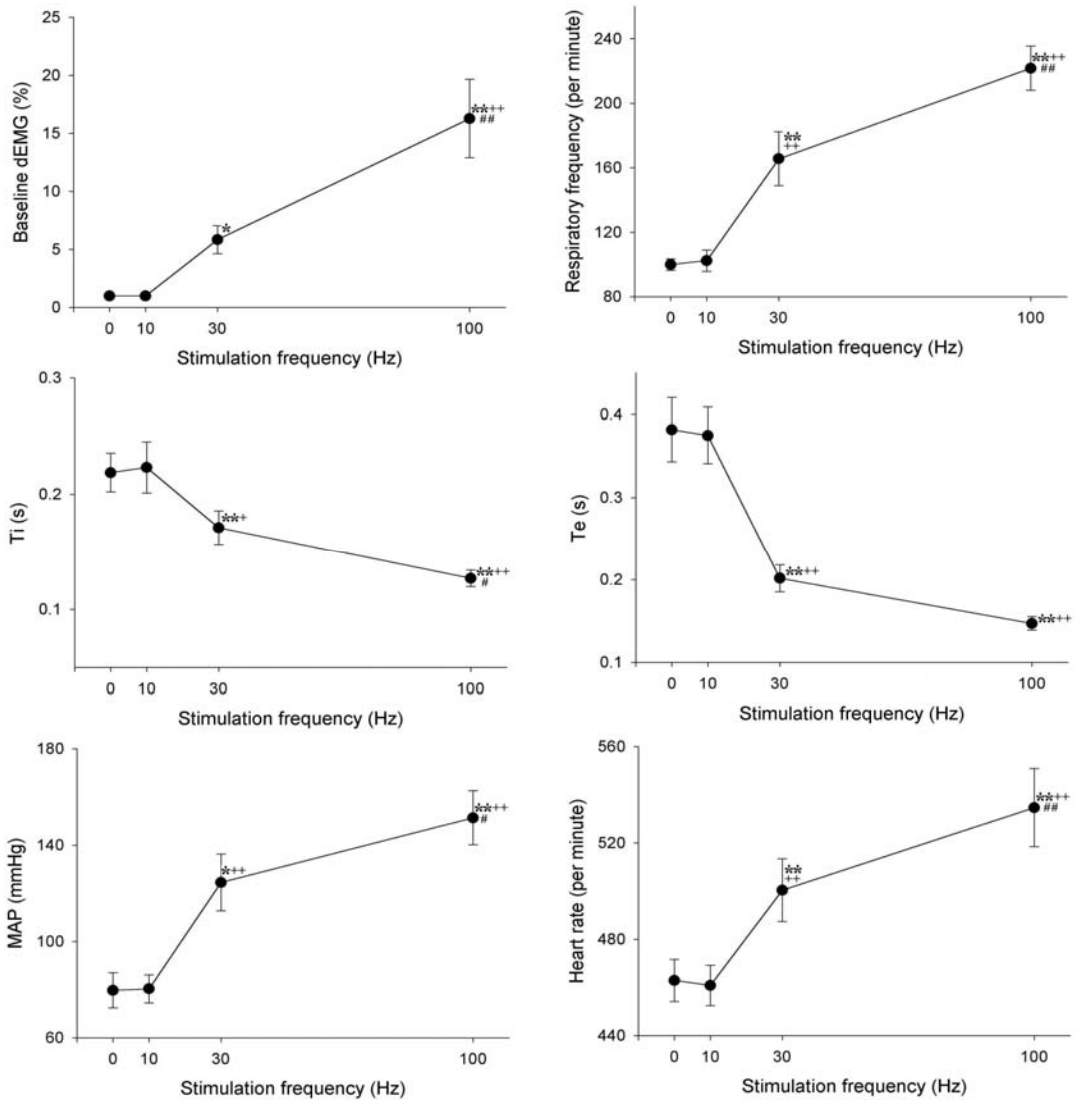

Figure 2-7. The relationships between peak cardio-respiratory responses and stimulation frequencies (n=6). The value at 0 Hz represents the averaged control value before stimulation. *: $p<0.05$; **: $p<0.001$, comparing with control level. +: $p<0.05$; ++: $p<0.01$, comparing with peak values from lowest stimulation frequency (10 Hz). #: $p<0.05$, ##: p<0.01 comparing with peak values from 75 μA and 30 Hz.

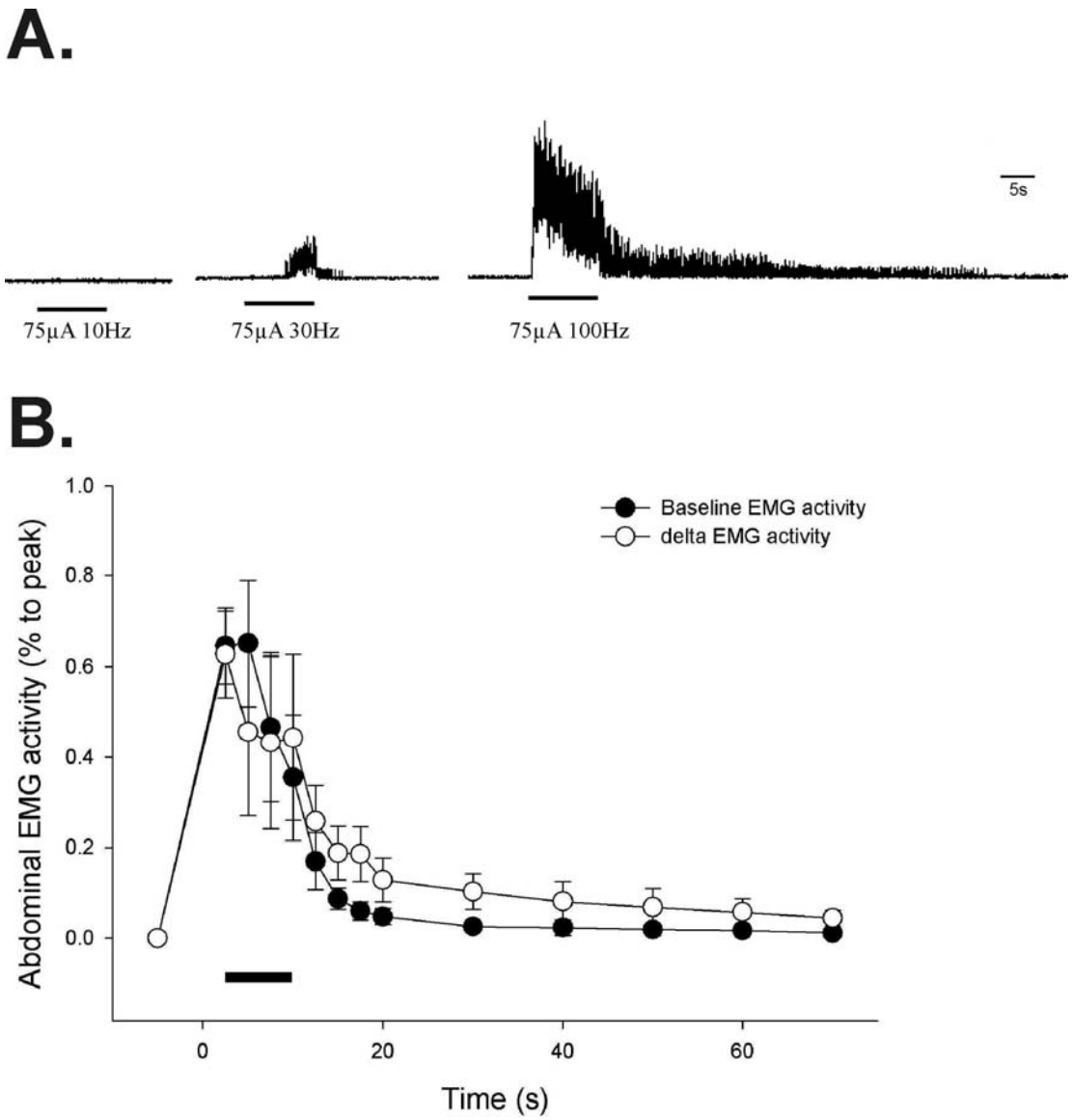

Figure 2-8. External abdominal oblique muscle EMG activity following the electrical stimulation in the dPAG. (A) Data from one animal. Note there was no EMG activity under the pre-stimulation control condition. (B) Mean abdominal EMG response to 100 Hz, 75 µA stimulation of the dPAG. The horizontal bar represents stimulation duration of 10 s.

$P_{ET}CO_2$ was recorded during electrical stimulation in the dPAG with 75 µA at 100 Hz. $P_{ET}CO_2$ decreased from 39.5±0.6 mmHg to 27.8±2.3 mmHg on the first breath after the onset of stimulation. The $P_{ET}CO_2$ remained decreased throughout the stimulation. After the cessation of stimulation, $P_{ET}CO_2$ returned to control by the first post-stimulus measurement period.

Discussion

The results of this investigation demonstrated that electrical stimulation in the dPAG elicited enhanced respiratory activity that included both inspiratory and expiratory muscle recruitment. Respiratory frequency increased significantly following dPAG activation, which included shortening of both Ti and Te. The changes in breath phase timing were the result of increased active inspiratory and expiratory motor output. The increase in respiratory activities was accompanied by significant increases in both HR and MAP. There were stimulus intensity and frequency thresholds for eliciting the dPAG mediated respiratory response. Electrical stimulation in the dPAG also produced an immediate elevated respiratory dEMG and aEMG baseline activity, which was sustained after the cessation of electrical stimulation in dPAG. This sustained post-stimulation effect may represent a sustained change of basal state of the dPAG and/or changes in descending respiratory pathways.

Electrical stimulation to activate neural structures in the PAG has inherent strengths and limitations as an electrophysiological research tool. The advantage of the electrical stimulation is the ability to observe the timing of on- and off-stimulus effects. This is especially important when studying time related changes in neural structures. In the present study, the use of electrical stimulation allowed for the observation of a first breath onset effect, while the site in the brainstem respiratory network activated by dPAG related descending input is unknown. It is clear that there is a short-latency response to dPAG activation. However, current spread is a concern, especially with monopolar electrodes. It has been suggested (Rank, 1975) that the current spread can range 0.3 – 1.0 mm when the stimulus intensity was 50-200 μA in the CNS. In the present study the highest intensity was 100 μA, so the current spread range would be less than 1.0 mm.

Although electrical stimulation can activate both neurons and fibers of passage, the thresholds of these neuronal elements are different. Indeed, electrical stimulation can still be used to specifically activate different components with specific stimulating parameters (Behbehani, 1995; van der Plas et al., 1995). As previously suggested (Hayward et al., 2003), low intensity and high frequency electrical stimulation elicited similar cardiovascular and respiratory responses from the dPAG as chemical disinhibition. Thus, while electrical stimulation reduces the specificity of the structures activated, it has the advantage of allowing the observation of the timing of the onset of the respiratory response and sustained respiratory activity after the stimulation has ceased.

Respiratory Response to dPAG Stimulation

dPAG electrical stimulation elicited a significant increase in respiratory frequency with no significant change in ΔdEMG amplitude. This resulted in a frequency dependent increase in neural minute ventilation. The increased respiratory frequency was the result of shortening of both Ti and Te. The results also showed that activation of the dPAG has a greater effect on Te than Ti. In addition, the reduction in Te was sustained after cessation of stimulation. Electrical stimulation frequencies at 25 and 40 Hz were previously reported to reduce Te with minimal effect on Ti (Hayward et al., 2003). This effect on Te is consistent with the report in cats that electrical stimulation in the PAG decreased Te, but the specific region within the PAG that was stimulated was not identified (Bassal et al., 1982; Duffin et al., 1972; Hockman et al., 1974). Thus, there is a dPAG modulation of respiratory timing that appears to be greatest on modulation of expiration.

Stimulation of dPAG neurons by excitation with microinjection of DLH or disinhibition with bicuculline significantly reduced both Ti and Te in a dose-dependent

manner (Hayward et al., 2003; Huang et al., 2000). In the present study, the magnitude of the respiratory responses was increased with increased current intensity and stimulation frequency in a dose-dependent manner, consistent with chemical stimulation (Hayward et al., 2003; Huang et al., 2000). There was a threshold for eliciting the response evidenced by the observation that low stimulation intensity or low frequency did not elicit significant changes of cardio-respiratory pattern. As the intensity or frequency increased, the cardio-respiratory responses were recruited and increased to a plateau. The modulation of respiratory timing could therefore be attributed to dPAG elicited modulation of brainstem respiratory center activities by yet to be determined pathways.

Anatomical studies have reported direct and indirect connections between the PAG and brainstem respiratory network. A retrograde labeling study reported a connection between rostral ventral respiratory group (rVRG) and the PAG (Gaytan et al., 1998). Neuronal inhibition with GABA receptor angonist muscimol in the lateral parabrachial nucleus (LPBN) almost completely blocked the respiratory response elicited from the dPAG (Hayward et al., 2004). Anatomical connections between the PAG and LPBN had been confirmed in various studies (Cameron et al., 1995; Bianchi et al., 1998; Krout et al., 1998). The LPBN has been demonstrated as a critical region in neural control of breathing (Chamberlin et al., 1994; St. John, 1998). Thus, it is likely that the respiratory response elicited by electrical stimulation in the present study is mediated by a LPBN pathway.

Electrical stimulation in the dPAG also elicited a significant change of dEMG that was evident in the first breath following the onset of electrical stimulation. The change in dEMG was due to an increase in the baseline dEMG activity with no significant change

in ΔdEMG. The increase in inspiratory muscle activity is consistent with previous reports of electrical and chemical stimulation of the dPAG (Huang et al., 2000; Hayward et al., 2003). However, while it has been reported that dPAG activation decreases Te, there are no previous reports of active expiration and recruitment of expiratory muscle activity. dPAG activation recruited aEMG activity in this normally silent expiratory muscle. The dPAG mediated activation of the abdominal muscle was sustained after the cessation of stimulation. The activation of both inspiratory and expiratory muscles was further associated with an increase of tracheal pressure changes in both inspiratory and expiratory directions. Thus, the respiratory response elicited from the dPAG included recruiting of active expiration.

Elevated baseline activity in dEMG and phrenic ENG was observed in the present study. In a report by Huang et al (Huang et al., 2000), DLH was microinjected into dPAG and there was an increased respiratory rate and the baseline dEMG activity (their Fig.1). This increase in dEMG baseline was also reported with dPAG activation by electrical stimulation and GABA disinhibition (Hayward et al., 2003). The increase in phrenic ENG activity parallels the change in dEMG demonstrating that the change in dEMG was due to dPAG mediated changes in respiratory neural mechanisms. Alternatively, baseline dEMG and phrenic ENG elevation is not due to the stimulation artifact since the elevation continued after the completion of stimulation. The change in respiratory drive was also not an artifact of the enhanced intrinsic contraction of the diaphragm since this tonic activity was also observed in the phrenic neurogram. The tonic activity appears to be the result of increased neural output to respiratory muscles from spinal motor respiratory drive although the exact source is not yet known. This tonic activity would

represent an increase in resting muscle tone and may change functional residual capacity (FRC) as previously suggested (Hayward et al., 2003). The results of the present study extend these observations by showing that increased respiratory muscle tone occurs in both inspiratory and expiratory muscles. Stimulation of the hypothalamic locomotion region, another suprapontine structure involved in defense behaviors, with both electrical stimulation and GABA disinhibition elicited enhanced cardio-respiratory responses and elevation of baseline activity in the phrenic ENG in anesthetized and decorticated cats (Eldridge, 1994; Eldridge et al., 1981). This elevation was evident without chemoreceptor or vagal inputs. Thus, this enhancement and recruitment of respiratory muscles in response to stimulation of central neural defense regions may be a common characteristic of these elicited behaviors.

Cardiovascular Responses to dPAG Stimulation

Both chemical and electrical stimulation in the dPAG evoked significant increase in MAP and HR. The response pattern in the present study was similar to previous studies with both conscious and anesthetized animals (Behbehani, 1995). The increase in MAP and HR was related to the intensity of stimulation of the dPAG, which were similar to dose-dependent responses of disinhibition (Hayward et al., 2003) or DLH stimulation (Huang et al., 2000) of the dPAG. The rostral ventrolateral medulla has been demonstrated to mediate the pressor and tachycardia responses elicited from the dPAG (Lovick, 1993). Huang, et al (Huang et al., 2000) suggested that dPAG-elicited cardiovascular and respiratory responses could be separated at brainstem level. Microinjection of propranolol into the NTS attenuated the respiratory response elicited from the dPAG, but not the cardiovascular response. Blocking the LPBN eliminated 90% of the respiratory response evoked from the dPAG, while the cardiovascular response

was only partially attenuated (Hayward et al., 2004). These data suggest that cardiovascular and respiratory responses elicited from dPAG may descend by different pathways to the brainstem.

Summary

The results of the present study demonstrated that the respiratory response elicited with stimulation of the dPAG was characterized by increased active ventilation for both inspiration and expiration. The activity of the diaphragm was increased and expiratory muscle activity was recruited. There is an activation threshold in the dPAG for both respiratory and cardiovascular responses. The cardio-respiratory response pattern is stimulus intensity and frequency dependent. Electrical dPAG stimulation that exceeded the threshold elicited a change in respiratory timing in the first breath following the onset of stimulation. Respiratory timing changes were sustained after the cessation of stimulation and may represent short-term respiratory neuroplasticity elicited from the dPAG. The increase in ventilation persisted in spite of a decreased PCO_2. The neural mechanisms of enhanced respiratory muscle EMG activities and breathing pattern changes remains to be determined, but may involve brainstem and spinal control systems.

CHAPTER 3
REGIONAL DISTRIBUTION IN DORSAL PERIAQUEDUCTAL GRAY ELICITED RESPIRATORY RESPONSES

Introduction

The periaqueductal gray (PAG) is the neural structure surrounding the mesencephalic aqueduct and is an important neural structure for defense behavior, analgesia, vocalization and autonomic regulation (Carrive, 1993; Bandler et al., 1994; Behbehani, 1995; Bandler et al., 2000). The dorsal PAG (dPAG) plays a crucial role in fight/flight behavior and accompanied autonomic responses. Both animal and human studies have demonstrated that the dPAG is one central neural structure involved in the emotional responses of anxiety and fear (Graeff et al., 1993; Nashold et al., 1969). Physiological responses are not, however, homogenous throughout the dPAG. Stimulation in the rostral dPAG evoked active fight defense behavior including upright postures and vocalizations. Caudal dPAG stimulation elicited flight/escape behavior. Both types of behaviors are accompanied by increased blood pressure and heart rate (Carrive, 1993; Bandler et al., 1994; Bandler et al., 2000). These different behavior strategies are based on the risk assessment of threatening environments (Blanchard et al., 1986). These behaviors have respiratory and cardiovascular changes that provide autonomic adaptation to support these behaviors. However, it is poorly understood if these autonomic responses similarly vary within the dPAG.

In anesthetized and paralyzed cats, electrical stimulation in the PAG elicited increased respiratory frequency (f_R) that was mainly due to the shortening of expiratory

time (Te), however the specific PAG region stimulated was not reported (Duffin et al., 1972; Hockman et al., 1974; Bassal et al., 1982). Similar results were observed during dPAG electrical stimulation (Lovick, 1985; Markgraf et al., 1991; Hayward et al., 2003; Hayward et al., 2004). An increased f_R was also reported with microinjection of the excitatory amino acid D,L-homocysteic acid (DLH) and $GABA_A$ receptor antagonist bicuculline into the dPAG. The change in f_R was the results of shortening inspiratory time (Ti) and Te (Lovick, 1992; Huang et al., 2000; Hayward et al., 2003). These results demonstrated that activation of the dPAG has excitatory effects on respiratory activity. However, it is unknown whether there is a regional difference in respiratory responses elicited from rostral and caudal dPAG. Labeling studies reported that efferent flow of rostral dPAG goes through caudal dPAG before it reaches its descending targets in the brainstem (Cameron et al., 1995; Sandkuhler et al., 1995). It was therefore hypothesized that respiratory responses elicited with activation of the caudal dPAG will be greater than that from rostral dPAG.

Defense behavior is considered as a preparatory reflex or visceral alerting reflex (Hilton, 1982). Activation of the dPAG mobilizes body resources to meet challenging environments. The respiratory response persisted after cessation of electrical stimulation of the dPAG (Hayward et al, 2003). This suggests that dPAG stimulation modulates basal respiratory activity causing a prolonged post-stimulation facilitation of respiration. The regional dPAG distribution and the pattern of this sustained post-stimulation response are unknown. Thus, it was further hypothesized that stimulation of the dPAG would elicit a sustained change in its basal respiratory state, and this change is greater with activation of the caudal dPAG. To investigate these effects, electrical dPAG stimulation was chosen

because the on- and off-stimulation timing could be reliably determined. Although electrical stimulation activates both neurons and fibers of passage, it has been demonstrated that controlled electrical stimulation of the dPAG elicits cardio-respiratory responses similar to chemical stimulation (Behbehani, 1995; van der Plas et al., 1995; Hayward et al., 2003). The relationship between electrical stimulation, regional response characteristics, and cardio-respiratory response was further investigated using DLH microinjection in the rostral and caudal dPAG. It was hypothesized that neuronal activation of the dPAG could elicit similar cardio-respiratory responses as electrical stimulation.

Materials and Methods

The experiments were performed on eighteen male Sprague-Dawley rats (350 - 420g) housed in the University of Florida animal care facility. The rats were exposed to a normal 12hr light 12hr dark cycle. The experimental protocol was reviewed and approved by the Institutional Animal Care and Use Committee of the University of Florida.

General Preparation

The rat was anesthetized with urethane (1.4 g/kg, i.p.). Additional urethane (20 mg/ml) was administrated intravenously as necessary. The adequacy of anesthesia was verified by the absence of a withdrawal reflex or blood pressure and heart rate responses to a paw pinch. A tracheostomy was performed. The femoral artery and vein were catheterized. The body temperature was monitored with a rectal probe and maintained between 37 ± 1°C with a thermostatically controlled heating pad (NP 50-7053-F, Harvard Apparatus). The rats respired spontaneously with room air.

Diaphragm EMG (dEMG) activity was recorded with thin, Teflon-coated wire bipolar EMG electrodes. The bared tips of the electrodes were inserted into the

diaphragm through a small incision in the abdominal skin. The recording electrodes were connected to a high-impedance probe connected to an AC preamplifier (P511, Grass Instruments), amplified and band-pass filtered (0.3-3.0 kHz). The analog output was then connected to a computer data sampling system (CED Model 1401, Cambridge Electronics Design) and processed by a signal analysis program (Spike 2, Cambridge Electronics Design). The tracheal tube was connected to a pneumotachograph (8431 series, Hans Rudolph) to measure tracheal airflow. The pneumotachograph was connected to a differential pressure transducer which was connected to a polygraph (Model 7400, Grass Instruments). The analog outputs of the polygraph were led into a computer data sampling system. All signals were digitalized and stored for subsequent offline analysis.

The animal was placed prone in a stereotaxic head-holder (Kopf Instruments). The cortex overlying the PAG was exposed by removal of portions of the skull with a high-speed drill. The dura was reflected and warm mineral oil was applied to the surface. The coordinates for the rostral dPAG were 5.30 to 6.30 mm caudal to the bregma, 0.1 to 0.6 mm lateral to the midline and depths of 3.8 to 4.5 mm below the surface of the brain. The caudal dPAG was 7.64 to 8.72 mm caudal to the bregma, 0.1 to 0.6 mm lateral to the midline and depths of 3.8 to 4.5 mm. For electrical stimulation, a monopolar stainless steel microelectrode, insulated to within 30-50 μm of the tip, was advanced into the dPAG based on a stereotaxic atlas of the rat brain (Paxino et al., 1997). The dPAG was stimulated (S48 stimulator, Grass Instruments) with a 10 s train of electrical pulses (75 μA, 100 Hz, 0.2 ms pulse width). The electrical stimulation site was marked at the end of the experiment by an electrolytic lesion (1 mA, 30 s). DLH was dissolved in artificial

cerebrospinal fluid (aCSF: 122 mM NaCl, 3 mM KCl, 25.7 mM $NaHCO_3^-$ and 1 mM $CaCl_2$), with pH adjusted to 7.4. DLH stimulation was performed with a single-barrel microinjection pipette, attached to a pneumatic injection system (PDES-02P, NPI, Germany). Small amounts of fluorescent carboxylate-modified microspheres (Molecular Probes, Eugene, OR) were added into the solutions for identification of the microinjection sites. The volume of injection was monitored by measuring the movement of the meniscus through a magnifying eye-piece equipped with a calibrated reticule (50×; Titan Tools). One minute after completion of an injection, the pipette was retracted from the brain.

After completion of experiment, the animal was euthanized, the brain removed and fixed in 4% paraformaldehyde solution. The fixed tissue was then cut coronally into 40-μm-thick sections with a crytostat (HM101, Carl Zeiss). For electrical stimulation experiments, sections were mounted and stained with cresyl violet. The stained sections were examined to identify the lesion and corresponding electrode tract. For DLH stimulation experiments, sections were mounted and imaged with a microscope equipped with bright field and epifluorescence. After identifying the location of fluorescence beads, the slices were then stained with neutral red. A rat brain atlas (Paxinos et al., 1997) was used to reconstruct stimulation site.

Protocols

After the animal was surgically prepared, electrical stimulation was delivered unilaterally into the dPAG (n=8). The stimulating electrode was stereotaxically guided to sites within the dPAG. The dEMG activity, tracheal airflow, and arterial blood pressure were recorded simultaneously. The stimulation was delivered to the rostral and caudal

dPAG in same animal in separate trials. The order was randomized, and there was at least 15 minutes between the two stimulations. The last stimulation tract was lesioned (1 mA, 30 s) for histology identification.

For chemical stimulation (n=7), the experimental preparation was the same as electrical stimulation. DLH (45 nl 0.2 M) was microinjected into the rostral and caudal dPAG in same animal in separate trials. The order was randomized, and there were at least 30 minutes between the two microinjections. Control aCSF (45 nl) microinjection was performed in three rats.

Data Analysis

All data were analyzed using Spike2 software (Cambridge Electronics Design). The EMGs were rectified and integrated (time constant = 50 ms). The Ti, Te, and f_R were calculated from the integrated dEMG signals. Ti was measured from the onset of the dEMG burst activity to the point at which the peak EMG activity began to decline. Te was measured from the end of Ti to the onset of following inspiration. Baseline dEMG activity was defined as the minimum value measured between bursts. The amplitude of integrated dEMG (ΔdEMG) was calculated as the difference between baseline and peak burst amplitude. Mean arterial blood pressure (MAP) was calculated as the diastolic pressure plus 1/3 of the pulse pressure. HR was derived from the interval between peak systolic pressure pulses in the arterial pressure trace. For electrical stimulation experiments, neural minute ventilation was calculated by multiplying ΔdEMG by the instantaneous f_R (Eldridge, 1975).

For electrical stimulation, the control respiratory and cardiovascular parameters were averaged over a 5 s time period prior to the onset of stimulation. These parameters were then averaged every 2.5 s during the 10 s stimulation. After the cessation of

stimulation, these values were averaged for every 2.5 s during the first 10 s post-stimulation time period, then averaged for 5 s of each 10 s period for the next 50s post-stimulation time period (Fig. 1). MAP, HR, Ti, Te, and f_R were compared before, during, and after electrical stimulation. Baseline dEMG and ΔdEMG were expressed as a percentage of control. The on- and off-stimulus respiratory effects were measured from the complete respiratory cycle immediately before and after the onset of stimulation, and the first complete respiratory cycle following cessation of stimulation.

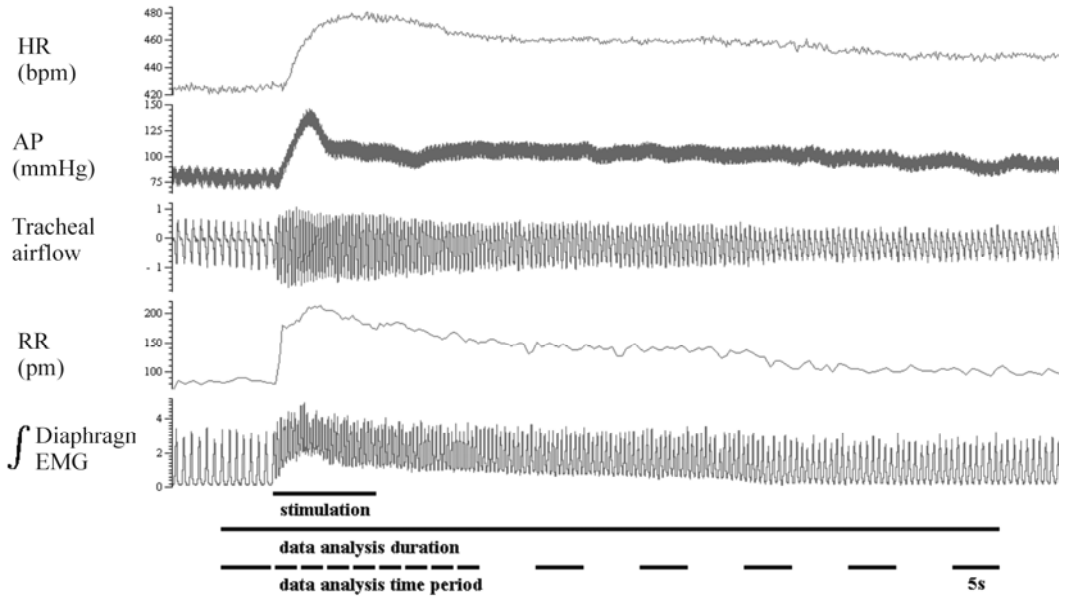

Figure 3-1. Cardio-respiratory response elicited by caudal dPAG stimulation with 75 μA intensity, 100 Hz frequency, 10 s duration, 0.2 ms pulse width from a single animal. The first horizontal bar represents the 10 s stimulation duration. The second horizontal bar represents total time duration for data analysis (70s). The third horizontal broken line represents each time measurement period for data analysis.

For chemical stimulation, cardio-respiratory parameters were collected at control, peak response, and one minute after the completion of microinjection. Both control and one minute post-injection values were averaged over 5 s. Peak respiratory responses were measured at the peak DLH response and averaged for 5 breaths at the peak rate. Peak HR was averaged from a 10 s time period.

A two-way ANOVA with repeated measures (factors: region and time) was performed for comparisons of cardio-respiratory responses as a function of the stimulation in the rostral and caudal dPAG. When differences were indicated, a Tukey post-hoc multiple comparison analysis was performed to identify significant effects. A two-way ANOVA with repeated measures (factors: region and treatment) was performed for comparisons of respiratory parameter changes in two single breaths immediate before and after the onset of electrical stimulation or the cessation of stimulation. Statistical significance was accepted at probability $p<0.05$, and analyses were completed using SigmaStat (v2.03, SPSS software, Chicago, IL). All data are reported as means ± SE.

Results

Respiratory Response to Electrical Stimulation in the dPAG

Electrical stimulation in the dPAG elicited an immediate increase in respiratory activity. A typical response following electrical stimulation in the caudal dPAG is shown in Fig. 3-1. There was an increase in f_R, peak tracheal airflow, baseline dEMG activity, HR and MAP.

The respiratory timing and dEMG activity were compared in breaths immediate before and after the onset of electrical stimulation (Table 3-1). With rostral dPAG stimulation, Ti was not significantly different (213±20 ms to 183±1 ms). Te significantly decreased from 376±57 ms to 194±4 ms ($p<0.001$). f_R significantly increased from 104±16 to 162±10 breaths/min ($p<0.001$). There was a significant increase in baseline dEMG activity to 336±123% ($p<0.05$). There was no significant difference in ΔdEMG (114±7%; $p>0.05$). With caudal dPAG stimulation, Ti was not significantly different (212±9 ms to 167±15 ms; $p>0.05$). Te significantly decreased from 415±4 ms to 184±18 ms ($p<0.001$). f_R significantly increased from 99±7 to 172±6 breaths/min ($p<0.001$).

Baseline dEMG activity increased to 212±59% (p>0.05), and ΔdEMG significantly increased to 130±12% (p<0.05). There was no significant difference in the onset response between rostral and caudal dPAG stimulation groups.

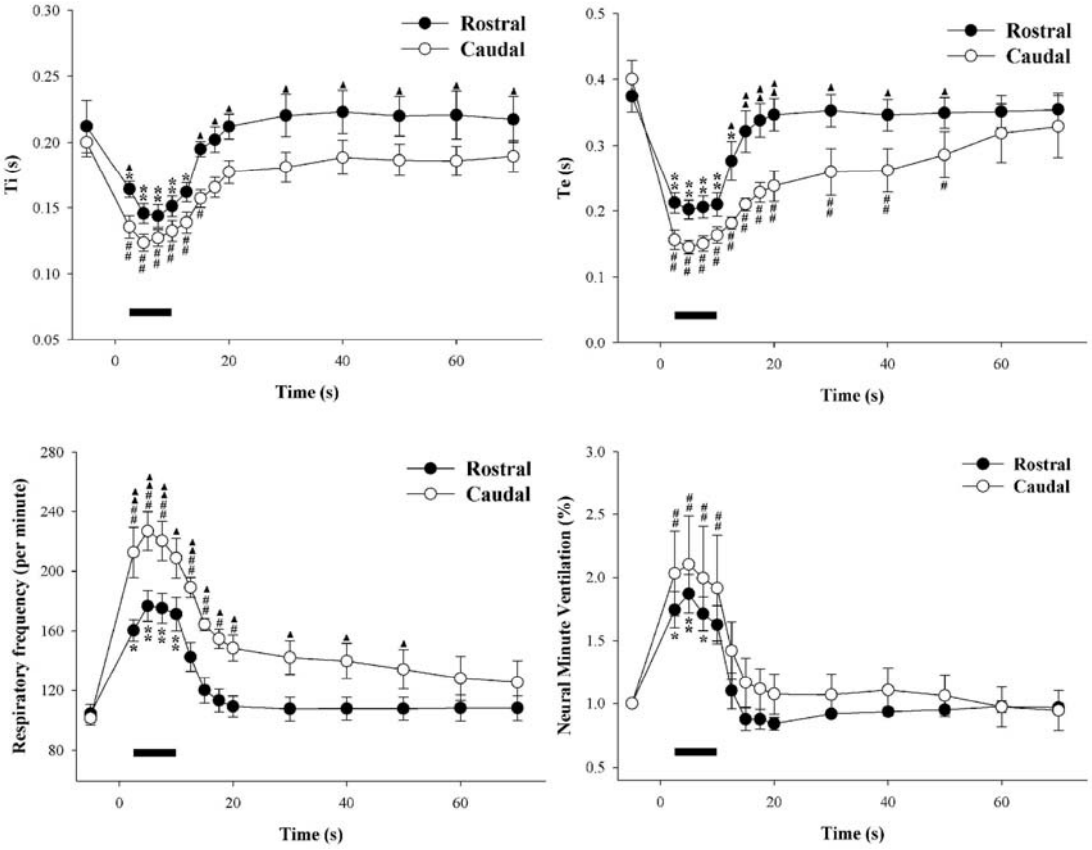

Figure 3-2. Respiratory responses following electrical stimulation in the rostral and caudal dPAG. The filled bar under the tracing represents 10 s stimulation duration. *: p<0.05; **: p<0.001, comparing with control level during stimulation in rostral dPAG. #: p<0.05; ##: p<0.01, comparing with control level during stimulation in caudal dPAG. ▲: p<0.05, ▲▲: p<0.01 comparing between rostral and caudal dPAG stimulation.

Rostral dPAG electrical stimulation elicited significant decrease in both Ti and Te, and increase in f_R during the 10 s stimulation period (Fig. 3-2). All these respiratory timing parameters reached peak during the 2nd 2.5 s measurement period. Rostral stimulation elicited a significant increase in baseline dEMG activity, which reached peak at the 3rd 2.5 s measurement period during stimulation (Fig. 3-3). There was no significant change of ΔdEMG during stimulation. There was significant increase in

neural minute ventilation during stimulation which peaked at the 2nd 2.5 s measurement period (Fig. 3-2). Caudal dPAG stimulation elicited similar respiratory response pattern during the 10 s stimulation period. There were significant changes in Ti, Te, f_R, baseline dEMG activity, neural minute ventilation, but not ΔdEMG (Fig. 3-2 and 3-3). The peak of the respiratory timing response with caudal stimulation occurred at the 2nd 2.5 s measurement period during stimulation. The dEMG baseline reached peak at the 1st 2.5 s measurement period. Caudal dPAG stimulation elicited a significantly greater increase in f_R (Fig. 3-2), and less increase in dEMG baseline than rostral stimulation (Fig. 3-3).

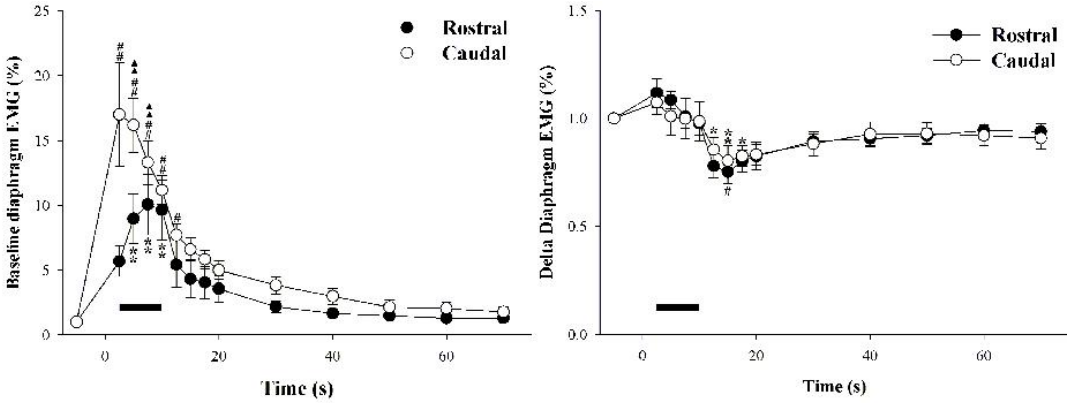

Figure 3-3. Diaphragm EMG activity changes following electrical stimulation in rostral and caudal dPAG. The filled bar under the tracing represents 10 s stimulation duration. *: $p<0.05$; **: $p<0.001$, comparing with control level during stimulation in rostral dPAG. #: $p<0.05$; ##: $p<0.01$, comparing with control level during stimulation in caudal dPAG.

The respiratory timing and dEMG activity were compared in breaths immediate before and after the cessation of electrical stimulation (Table 3-1). With rostral stimulation, the off-stimulus Ti was not significantly different (149±11 ms to 161±10 ms). The off-stimulus Te significantly increased from 205±19 ms to 255±13 ms ($p<0.001$). The off-stimulus f_R significantly decreased from 174±11 to 146±7 breaths/min ($p<0.05$). The relative level of baseline dEMG activity decreased from 1176±279% to 700±266% ($p<0.05$) and ΔdEMG did not significantly change (99±6% to 88±9%). With

caudal dPAG stimulation, the cessation of stimulation did not significantly change Ti (134±10 ms to 143±10 ms). The off-stimulus Te significantly increased from 172±8 ms to 185±9 ms (p<0.001). The off-stimulus f_R significantly decreased from 199±10 to 184±6 breaths/min (p<0.001). The relative level of dEMG baseline was not significantly changed (919±129% to 868±168%). The off-stimulus ΔEMG significantly decreased from 102±13% to 86±10% (p<0.05). There was significant difference in off-stimulus respiratory effect on Te and f_R between rostral and caudal dPAG (p<0.05).

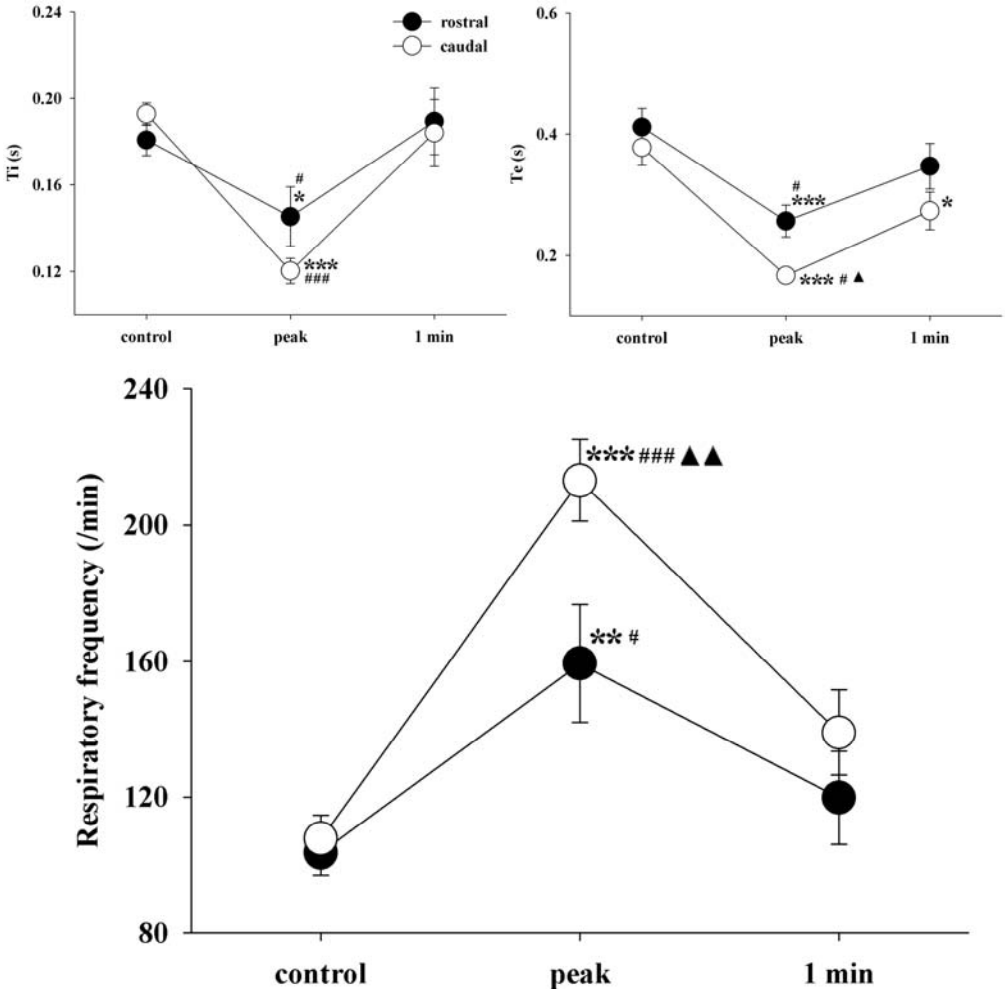

Figure 3-4. Respiratory timing response to DLH stimulation in rostral and caudal dPAG. *: significant difference comparing with control value, p<0.05; **: p<0.01; ***:p<0.001. #: significant difference comparing with recovery value at one minute, p<0.05; ###: p<0.001. ▲: significant difference comparing with rostral group, p<0.05; ▲▲: p<0.01.

After the cessation of stimulation, respiratory parameters recovered to control level. With rostral dPAG stimulation, Ti, Te, f_R, dEMG activity, and neural minute ventilation recovered to non-significant levels within 5 s after the cessation of stimulation (Fig. 3-2 and 3-3). With caudal dPAG stimulation, Ti and f_R recovered to control levels within 10 s. Te was significantly decreased until 40 s after the cessation of stimulation. There were significant differences in Ti, Te, and f_R between rostral and caudal trials after the cessation of stimulation (p<0.05), which was slower recovery of respiratory timing after caudal dPAG stimulation (Fig. 3-2).

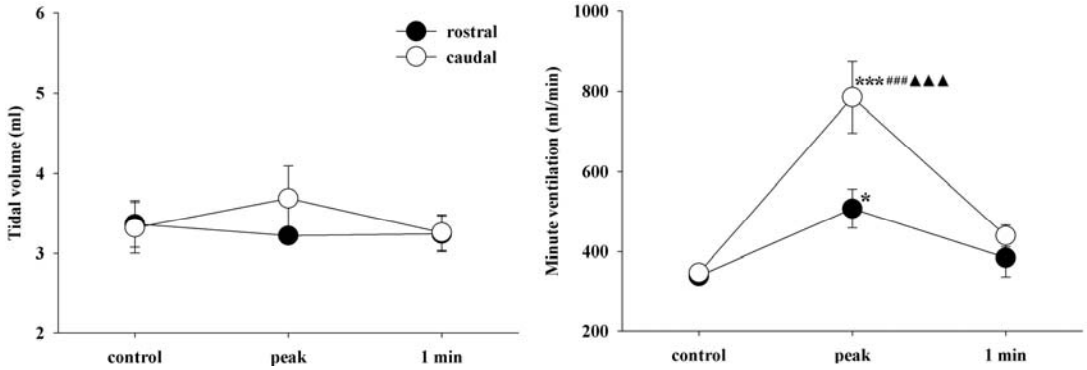

Figure 3-5. Ventilation response to DLH stimulation in rostral and caudal dPAG. *: significant difference comparing with control value, p<0.05; ***: p<0.001. ###: significant difference comparing with recovery value at one minute, p<0.001. ▲▲▲: significant difference comparing with rostral group, p<0.001.

Respiratory Response to DLH Stimulation in the dPAG

Similar to electrical stimulation, DLH microinjection in the dPAG elicited increased respiratory activity (Fig. 3-4). Rostral microinjection increased f_R from 104±6 breaths/min to 159±17 breaths/min (p<0.01). This was the result of significant shortening of both Ti (181±7 ms to 145±14 ms, p<0.05) and Te (411±31 ms to 257±26 ms, p<0.001). Rostral DLH microinjection elicited a significant increase in minute ventilation (p<0.05), but not tidal volume (Fig. 3-5). Caudal DLH microinjection elicited a similar respiratory response pattern. Caudal DLH microinjection increased f_R from 108±7

breaths/min to peak 213±12 breaths/min (p<0.001). The Ti decreased from 193±5 ms to 120±6 ms (p<0.001), and Te from 377±29 ms to 166±10 ms (p<0.001). Caudal DLH microinjection did not affect tidal volume, but significantly increased minute ventilation (p<0.001). Caudal dPAG activation elicited significantly greater increase of f_R (p<0.01) and decrease of Te than rostral dPAG (p<0.05). There was no significant difference in latency-to-peak respiratory response between rostral and caudal DLH microinjections (12.4±0.6 s vs 11.2±1.6 s). Caudal DLH microinjection elicited a greater increase in minute ventilation than rostral DLH microinjection (p<0.001) (Fig. 3-5).

Rostral DLH microinjection elicited a significant increase in baseline dEMG activity by 925±336% (p<0.01), but there was no significant difference in ΔdEMG (105±7%; p>0.05). Caudal DLH microinjection significantly increased dEMG baseline activity by 1138±281% (p<0.001), and ΔdEMG by 137±10% (p<0.01). There was a significant difference in dEMG response between rostral and caudal DLH microinjection (p<0.01). DLH microinjection in the caudal dPAG elicited greater increase in ΔdEMG than rostral microinjection (Fig. 3-6).

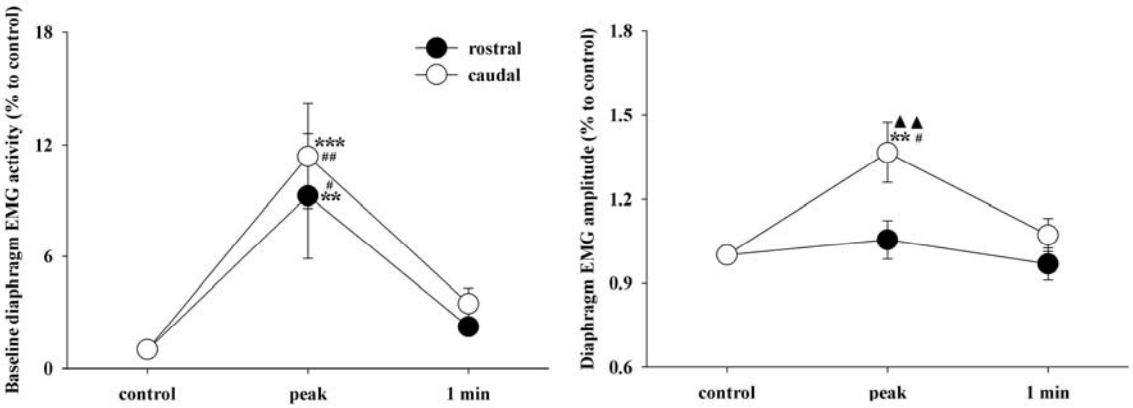

Figure 3-6. Diaphragm EMG response to DLH stimulation in rostral and caudal dPAG. **: significant difference comparing with control, p<0.01; ***:p<0.001. #: significant difference comparing with recovery value at one minute, p<0.05; ##: p<0.01. ▲▲: significant difference comparing with rostral group, p<0.01.

At one minute after the completion of DLH microinjection, respiratory timing and dEMG activities recovered to control level in both rostral and caudal dPAG groups. However, Te with caudal dPAG microinjection was still significantly decreased from control level (Fig. 3-4, 3-5, and 3-6). There was no significant difference in respiratory response between rostral and caudal microinjection groups.

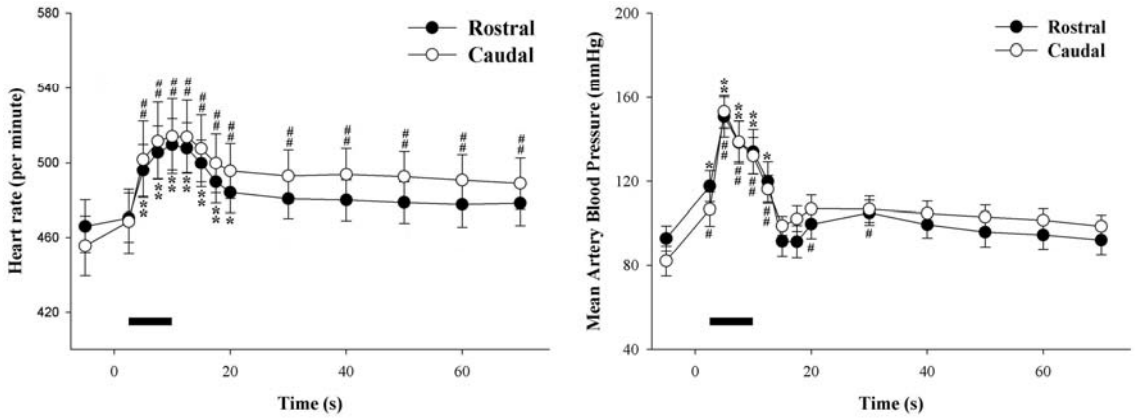

Figure 3-7. Cardiovascular responses following electrical stimulation in rostral and caudal dPAG. The filled bar under the tracing represents 10 s stimulation duration. *: $p<0.05$; **: $p<0.001$, comparing with control during stimulation in rostral dPAG. #: $p<0.05$; ##: $p<0.01$, comparing with control during stimulation in caudal dPAG.

Cardiovascular Response to dPAG Stimulation

Cardiovascular responses elicited by electrical stimulation in rostral and caudal dPAG were similar (Fig. 3-7). Stimulation in the rostral dPAG caused a significant increase in HR from the 2nd 2.5 s measurement period during stimulation until 10 s after the cessation of stimulation. HR reached peak at the 4th 2.5 s measurement period during stimulation. Rostral dPAG stimulation significantly increased MAP, and the peak response occurred at the 2nd 2.5 s measurement period. After the cessation of stimulation, MAP recovered to control. Caudal dPAG stimulation elicited a similar cardiovascular pattern as rostral dPAG (Fig. 3-7). During caudal dPAG stimulation, the HR response reached peak at the 4th 2.5 s measurement period. The MAP reached peak at 2nd 2.5 s

measurement period. The HR response to caudal dPAG stimulation persisted until the end of measurement period. No significant difference was found between rostral and caudal groups before, during, and after stimulation.

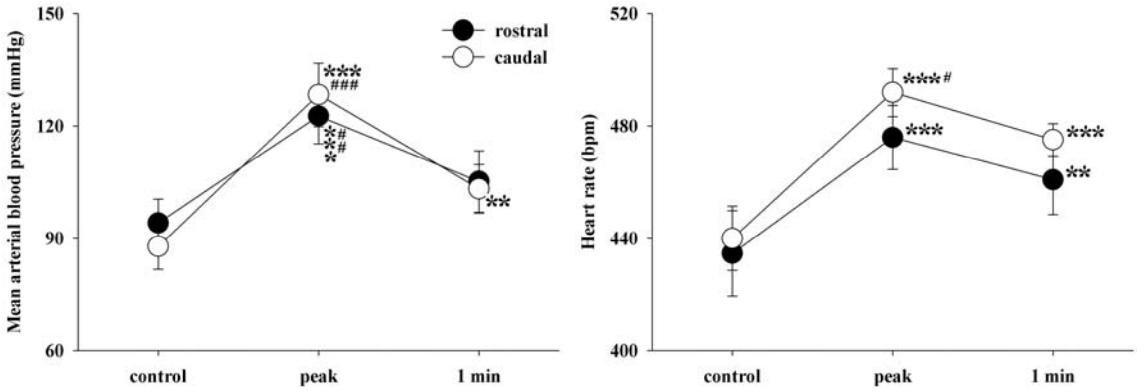

Figure 3-8. Cardiovascular response to DLH stimulation in rostral and caudal dPAG. **: significant difference compared with control, $p<0.01$; ***:$p<0.001$. #: significant difference compared with recovery value at one minute, $p<0.05$; ###: $p<0.001$.

Stimulation with DLH in the dPAG evoked similar cardiovascular response as electrical stimulation (Fig. 3-8). Rostral DLH microinjection elicited significant increases in both MAP (94.10±6.33 to 122.67±7.47 mmHg) and HR (434±15 to 476±11 beats/min), with a latency of 16.3±1.5 s and 25.9.3±2.5 s respectively. At one minute after the completion of microinjection, both MAP and HR were elevated, but only the HR response reached statistical significance. Caudal dPAG microinjection elicited a similar cardiovascular response pattern to rostral dPAG. MAP increased from 87.81±6.16 to 128.39±8.56 mmHg, HR from 440±11 to 492±9 beats/min. One minute after the completion of DLH microinjection, MAP and HR were still significantly greater than control. There was no significant difference in the cardiovascular response. The latency-to-peak for both MAP and HR responses were 12.3±1.9 s and 23.7±1.8 s, respectively, and were not significantly different from those in rostral dPAG trials. In control experiments with aCSF (n=3), no significant change of MAP and HR was observed.

Table 3-1. On- and off-stimulus respiratory effect of electrical stimulation with 75 μA and 100 Hz in the dPAG.

	On-stimulus respiratory effect				Off-stimulus respiratory effect			
	Rostral dPAG		Caudal dPAG		Rostral dPAG		Caudal dPAG	
	Control	On-sti.	Control	On-sti.	On-sti.	Off-sti.	On-sti.	Off-sti.
Ti (ms)	213±20	183±1	212±9	167±15	149±11	161±10	134±10	143±10
Te (ms)	376±57	194±4**	415±4	184±18**	205±19	255±13**	172±8	185±9
f_R (/min)	104±16	162±10**	99±7	172±6**	174±11	146±7*	199±10	184±6
Baseline dEMG (%)	100±0	336±123*	100±0	212±59	1176±279	700±266*	919±129	868±168
dEMG amplitude (%)	100±0	114±7	100±0	130±12*	99±6	88±9	102±13	86±10*

All data are mean ± SE. dEMG: diaphragm EMG.
*: $p<0.05$; **: $p<0.001$, comparing with control level or on-stimulation condition in off-stimulus study.

Reconstructed Stimulation and Microinjection Sites

The tips of the microelectrode tracts were in the rostral or caudal dPAG (Fig. 3-9C). DLH microinjection sites were reconstructed from all experiments and were located in rostral and caudal dPAG (Fig. 3-9A, B).

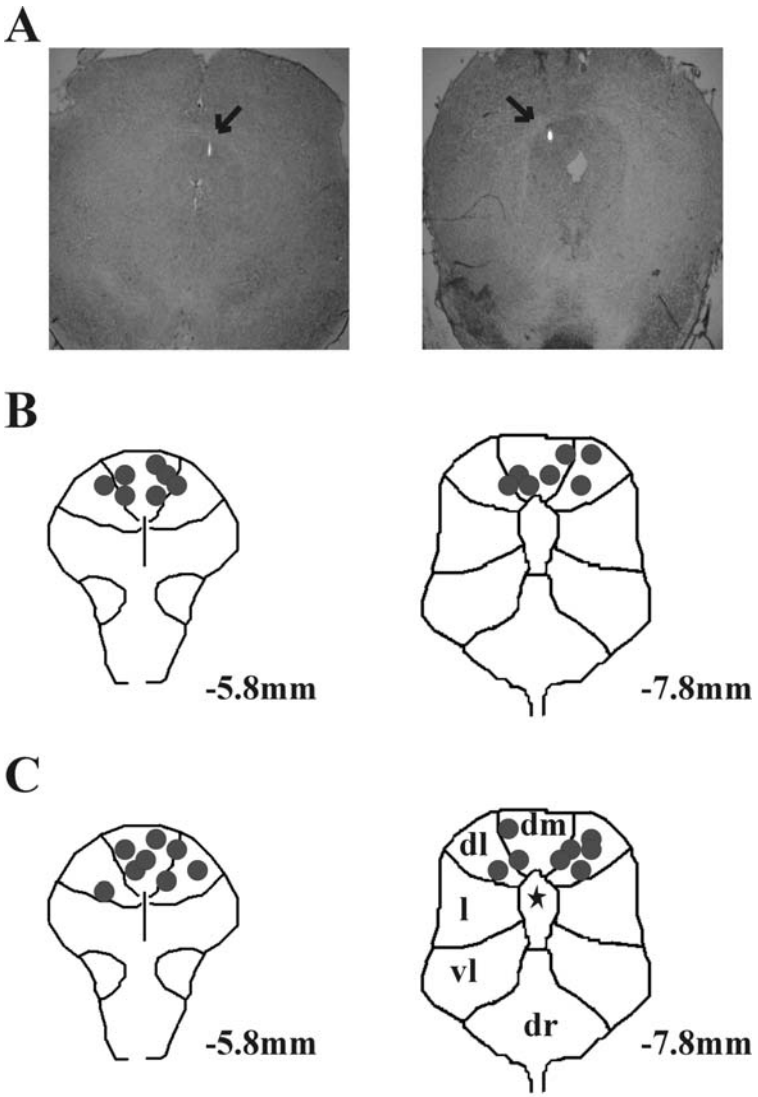

Figure 3-9. Reconstructed dPAG stimulation sites. (A) Photomicrographs of two coronal sections through rostral and caudal dPAG with chemical microinjection protocol. Arrows represent microinjection sites. (B) Reconstruction of DLH microinjection sites. (C) Reconstruction of electrical stimulation sites. Number to the right of the PAG images indicate of brain section relative to bregma. Schematic drawings based on the rat brain atlas (Paxinos et al., 1997). The ★ indicates the aqueduct; dr: dorsal raphe. dm: dorsomedial PAG; dl: dorsolateral PAG; l: lateral PAG; vl: ventrolateral PAG

Discussion

The results of this study demonstrated a regional difference in the respiratory pattern elicited by electrical and DLH stimulation in the rostral and caudal dPAG. The f_R increased significantly with dPAG activation as a result of shortening of both Ti and Te. With electrical stimulation, caudal dPAG elicited a significantly greater reduction in Ti and Te than rostral dPAG stimulation. Caudal dPAG stimulation elicited a significantly greater elevation of baseline dEMG activity, which was sustained after the cessation of electrical stimulation in both groups. At the peak response to DLH stimulation, f_R was greater in caudal dPAG trials, and the Te was more significantly reduced. Caudal dPAG stimulation elicited greater peak ΔdEMG than rostral dPAG trials. There was a significant increase in HR and MAP after dPAG activation, however, no regional difference was found.

Respiratory Response to Rostro-caudal dPAG Activation

Following stimulation of the dPAG, there was significant increase in f_R, and decreases in Ti and Te. The results also showed that activation of the dPAG has a greater effect on Te than Ti, and the reduced Te was sustained after cessation of electrical stimulation, particularly during caudal stimulation. The change of Te with dPAG activation has been previously reported in both cats and rats (Duffin et al., 1972; Hockman et al., 1974; Bassal et al., 1982; Hayward et al., 2003). Stimulation of the dPAG neurons with DLH excitation or bicuculline disinhibition can affect respiratory timing in a dose-dependent manner (Huang et al., 2000; Hayward et al., 2003). The modulation of respiratory timing can be attributed to dPAG elicited changes in the brainstem respiratory neural network. The results further suggested that dPAG activation may have differential effect on neural elements controlling Ti and Te.

The dPAG is the crucial component of an integrated neural mechanism that controls defense behavior and accompanying emotional and autonomic responses. The rostral and caudal dPAG are involved in different defense behavior patterns. Both fight and flight behaviors are accompanied with hypertension and tachycardia (Carrive, 1993; Bandler et al., 1994; Bandler et al., 2000). These different behavior strategies are based on the risk assessment, and the rostral or caudal dPAG contributes to the execution of these behaviors. The respiratory system provides essential oxygen to organ systems for their functions, which is crucial for these motor-related behaviors. In the current study, a difference in the respiratory response elicited from the rostral and caudal dPAG was observed. Caudal dPAG stimulation evoked greater respiratory responses than rostral dPAG stimulation. The change in respiratory pattern lasted longer with caudal dPAG stimulation, especially Te. It has been reported that both ascending and descending projection patterns from the rostral and caudal dPAG are similar (Cameron et al., 1995; Cameron et al., 1995). But same study also showed that these descending efferent fibers run caudally in the dPAG (Cameron et al., 1995). Caudal dPAG may be located between the rostral dPAG and the brainstem target nuclei. This is further supported by the observation that *c*-Fos expression was enhanced in the caudal dPAG when the rostral dPAG was activated (Sandkuhler et al., 1995). Thus, the regional difference in the respiratory response could be due to the interaction along the rostro-caudal axis within the dPAG, or the anatomical difference in descending projection target neural structures in the brainstem. The lateral parabrachial nucleus (LPBN) mediates, in part, the dPAG elicited respiratory response (Hayward et al., 2003; Hayward et al., 2004). The LPBN receives projections from both the rostral and caudal dPAG (Cameron et al., 1995; Krout

et al., 1998). These findings suggest that suprapontine mechanisms may contribute a major part in the regional difference in dPAG elicited respiratory response.

Huang et al (Huang et al., 2000) observed that DLH microinjection in rostral dPAG (6.8–7.3 mm caudal to bregma) could elicit cardio-respiratory responses, while in the caudal dPAG (7.8–8.3 mm caudal to bregma) only respiratory response could be elicited. Their rostral dPAG site was located immediately caudal to the rostral dPAG defined in current study. Their findings were not supported by current and other studies (Hayward, et al., 2003; Hayward, et al., 2004; Lovick, 1985; Markgraf et al., 1991), hence the difference could be due to the different stimulation sites. It is likely that during defense behavior, animals are able to motivate both cardiovascular and respiratory systems for distributing essential body resources.

Diaphragm EMG Response to dPAG Activation

Electrical stimulation in the dPAG elicited a significant change of dEMG immediately following the onset of stimulation. The increase in inspiratory muscle activity after dPAG activation is consistent with previous reports (Huang et al., 2000; Hayward et al., 2003; Hayward et al., 2004). Elevated dEMG baseline activity was observed in the present study, as reported previously (Hayward et al., 2003). This may represent an increase in resting muscle tone and a reduced functional residual capacity (Hayward et al., 2003). These results suggest that dPAG activation could change the neural output to the respiratory muscles. The tonic activity appears to be the result of increased and persistent neural drive.

With electrical stimulation, caudal dPAG elicited greater elevation in baseline dEMG activity, and reached peak early than rostral dPAG stimulation. This difference was not observed with DLH stimulation. No difference in latency-to-peak with DLH

microinjection was found between rostral and caudal trials. With stimulus intensity used in current project, caudal dPAG elicited a greater response in the baseline dEMG activity than that with DLH microinjection. A dose dependent response has been reported with chemical stimulation in the dPAG (Huang et al., 2000; Hayward et al., 2003). Thus, the difference can be explained by the difference in stimulus intensity, although a non-specific activation effect with electrical stimulation can not be excluded.

Cardiovascular Response to dPAG Activation

Stimulation in the dPAG elicited significant increase in MAP and HR with no regional difference. The response pattern observed in this study was similar to previous reports (Behbehani, 1995; Huang et al., 2000; Hayward et al., 2003; Hayward et al., 2004). In the LPBN, inhibition with muscimol eliminated 90% of dPAG elicited f_R response, but only 72% of HR response and 57% of MAP response (Hayward et al., 2004). In the caudal NTS, beta-adrenergic block attenuated the dPAG elicited respiratory response, but not the cardiovascular response (Huang et al., 2000). These data suggest that dPAG elicited cardiovascular and respiratory responses are mediated by different descending pathways. The rostral ventrolateral medulla mediates dPAG elicited pressor and tachycardia responses (Lovick, 1993). The dPAG also has projections to the noradrenergic A5 cell group, and the medulla raphe system (Cameron et al., 1995). These anatomical differences may contribute to the lack of regional difference was observed in dPAG elicited cardiovascular response.

While hypertension and tachycardia accompany both fight and flight behaviors, the neural mechanisms are different (Carrive, 1993; Bandler et al., 1994; Bandler et al., 2000). Rostral dPAG elicited fight behavior was accompanied by extracranial vasodilation and limb and visceral vasoconstriction. Caudal dPAG elicited flight behavior

was accompanied by vasodilation in limbs and vasoconstriction in other regions. Regional blood flow redistribution was the result of sympathetic outflow since it was sustained in paralyzed animals. These cardiovascular response patterns are consistent with those elicited by stimulation in different regions of the ventrolateral medulla (VLM) where different dPAG regions have corresponding projections (Carrive, 1993). The viscerotopic representation of vascular beds in PAG regions and corresponding VLM regions explains these cardiovascular response patterns. Since the MAP and HR are the overall effects of sympathoexcitation, no regional difference was found in this project.

Summary

The results of the current study demonstrated that enhanced ventilation was elicited from the stimulation of the dPAG. Enhanced respiratory activity was accompanied by increases in HR and MAP. Caudal dPAG stimulation elicited greater respiratory responses than rostral dPAG. Both regions changed respiratory timing and dEMG activity. No significant regional difference in cardiovascular responses was observed. Respiratory timing changes were sustained after the cessation of stimulation and may represent short-term respiratory neuroplasticity. The neural mechanisms of rostro-caudal difference remain to be determined.

CHAPTER 4
INFLUENCE OF THE DORSAL PERIAQUEDUCTAL GRAY ON RESPIRATORY RESPONSE TO PERIPHERAL CHEMORECEPTOR STIMULATION

Introduction

Arterial PO_2 and arterial H^+ circulation are detected by peripheral chemoreceptors in the carotid bodies and aortic bodies. The neural responses to hypoxia include arousal, increased ventilation, aversive responses and autonomic responses that compensate for the direct vasodilating effect of hypoxia and redistribute bloodflow to crucial organs (Marshall, 1994; Guyenet et al., 1995; Guyenet, 2000). It has been suggested that peripheral chemoreceptor inputs could be an alerting stimulus, thus evoke similar behavior and autonomic response patterns as those elicited from the brain defense regions, including the periaqueductal gray (PAG) (Hilton, 1982; Hilton et al., 1982; Marshall 1987). Defense reactions were considered as adaptive/preparatory reflexes that mobilize body resources to meet the challenging or threatening environments. Such reflexes were not compatible with short-term homeostasis. Thus, the inhibition of baroreflex could be expected to maintain the preparatory adaptation. On the other hand, the peripheral chemoreflex would be facilitated. The PAG is an important neural structure in defense behavior, analgesia, vocalization and autonomic regulation (Hilton et al., 1986; Carrive, 1993; Behbehani, 1995; Bandler et al., 2000). Of all the subdivisions in the PAG, the dorsal part (dPAG) involves in fight/flight defense behavior, and emotional responses like anxiety, fear, and panic (Nashold et al., 1969; Graeff, 2004). Activation of the dPAG consistently elicited hypertension and tachycardia, which are

integral autonomic components in those defense behaviors, and represent baroreflex inhibition (Hilton, 1982). Recently it has been demonstrated that dPAG activation would have excitatory effects on respiratory activity (Huang et al., 2000; Hayward et al., 2003; Hayward et al., 2004). These enhanced respiratory activities were achieved by hyperventilation due to shortening of inspiratory time (Ti) and expiratory time (Te), and tonic discharge of the diaphragm electromyography (dEMG) activity. The hyperventilation resulted in a decreased expired PCO_2 that was reported to persist throughout the activation of the dPAG (Hayward et al, 2003). However, the influence of dPAG activation on respiratory chemoreflexes is unknown.

Although it has been suggested that during the activation of the central defense regions, the peripheral chemoreflex would be facilitated (Hilton, 1982), it has not been tested. The caudal hypothalamus has been reported to modulate respiratory chemoreflex responses (Peano et al., 1992; Horn et al., 1998). Thus, it was hypothesized that dPAG activation would modulate the respiratory response to peripheral chemoreceptor stimulation. Peripheral chemoreflex responses were elicited by intravenous bolus injections of potassium cyanide (KCN). Intravenous KCN is a brief potent stimulus for arterial chemoreceptors and elicits reproducible reflex responses when repeated administration occurs at 5- to 10-min intervals (Hayward et al., 1999). Activation of the dPAG was performed with microinjection of excitatory amino acid D,L-homocysteic acid (DLH), or $GABA_A$ receptor antagonist bicuculline (Bic). Then, changes of respiratory response to intravenous KCN were compared before and after dPAG activation.

Materials and Methods

The experiments were performed on adult male Sprague-Dawley rats (350 - 420g) housed in the University of Florida animal care facility. The rats were exposed to a 12hr

light 12hr dark cycle. The experimental protocol was reviewed and approved by the Institutional Animal Care and Use Committee of the University of Florida.

General Preparation

The rats were anesthetized with urethane (1.4 g/kg, i.p.). Additional urethane (20 mg/ml) was administrated intravenously as necessary. The adequacy of anesthesia was verified by the absence of a withdrawal reflex or blood pressure and heart rate responses to a paw pinch. A tracheostomy was performed, and the rats respired spontaneously with room air. The femoral artery and vein were catheterized. The body temperature was monitored with a rectal probe and maintained between 36 - 38°C with a thermostatically controlled heating pad (NP 50-7053-F, Harvard Apparatus).

The dEMG activity was recorded with bipolar Teflon-coated wire electrodes. The bared tips of the electrodes were inserted into the diaphragm through a small incision in the abdominal skin. A third wire served as an electrical ground inserted in the skin beside the ear. The recording electrodes were connected to a high-impedance probe led into an AC preamplifier (P511, Grass Instruments), amplified and band-pass filtered (0.3-3.0 kHz). The analog output was then connected to a computer data sampling system (CED Model 1401, Cambridge Electronics Design) and processed by a signal analysis program (Spike 2, Cambridge Electronics Design). The arterial catheter was attached to a calibrated pressure transducer connected to a polygraph system (Model 7400, Grass Instruments). Tracheal tube from each animal was connected to a pneumotach (8431 series, Hans Rudolph) to measure tracheal pressure and tidal volume (Vt) and displayed on a polygraph. The analog outputs of the polygraph were sent to the computer data sampling system, and the signals were recorded and stored for subsequent offline analysis.

The animal was placed prone in a stereotaxic head-holder (Kopf Instruments). The cortex overlying the PAG was exposed by removing small pieces of skull with a high-speed drill. Chemicals were dissolved in artificial cerebrospinal fluid (aCSF) containing 122 mM NaCl, 3 mM KCl, 25.7 mM $NaHCO_3^-$, and 1 mM $CaCl_2$, with pH adjusted to 7.4. Chemical stimulation was performed with a single-barrel microinjection pipette, attached to a pneumatic injection system (PDES-02P, NPI, Germany). The pipette was stereotaxically lowered into the dPAG with the coordinates of 7.64 to 8.72 mm caudal to the bregma, 0.1 to 0.6 mm lateral to the midline and depths of 3.8 to 4.5 mm below the dorsal surface of the brain. Small amounts of fluorescent carboxylate-modified microspheres (Molecular Probes, Eugene, OR) were mixed into the microinjection solutions to facilitate later identification of the microinjection sites. The volume of injection was monitored by measuring the movement of the meniscus through a small magnifying eye-piece equipped with a calibrated reticule (50×; Titan Tools). One minute after completion of microinjection, the pipette was retracted from the brain.

Protocols

Protocol 1: The rats were stabilized after surgical preparation. Peripheral chemoreceptor stimulation and dPAG activation by disinhibition were then performed: 1) Intravenous KCN (90μg/kg wt) was injected; a second injection was delivered after 5 min; 2) Bic was microinjected (0.5mM, 45nl). A bolus of KCN was delivered (Bic+KCN 1 trial) 3 min after Bic injection. This was followed by a second KCN injection 5 min later (Bic+KCN 2 trial). The sequences of these presentations were randomized. At least one hour separated the presentations. Protocol 2: Peripheral chemoreceptor was stimulated and dPAG was activated by glutamate receptor agonist DLH microinjection: 1) Intravenous KCN (60μg/kg wt) was injected; a second injection was delivered after 5

min; 2) DLH (0.2M, 45nl) was microinjected into the dPAG; 3) DLH and intravenous KCN were injected simultaneously (DLH+KCN 1 trial). This was followed by a second injection of KCN 5 min later (DLH+KCN 2 trial). The orders of the three procedures were randomized. At least one hour separated each procedure. Control experiments were performed with microinjection of aCSF in the dPAG and intravenous KCN following the DLH protocol.

At the end of the experiment, the animal was euthanized. The brain removed and fixed in 4% paraformaldehyde solution for 72 hrs. The fixed tissue was frozen to -16°C, and cut coronally into 40-μm-thick sections with a crytostat (model HM101, Carl Zeiss). The sections were mounted and visualized with a microscope equipped with bright field and epifluorescence. The location of fluorescence beads was identified. The sections were then stained with neutral red, and sealed with a cover-slip. A rat brain atlas (Paxinos et al., 1997) was used to reconstruct the microinjection site.

Data Analysis

All data were analyzed off-line using Spike2 software (Cambridge Electronics Design). The dEMG was rectified and integrated (time constant = 50 ms). The Ti, Te, and respiratory frequency (f_R) were calculated from the integrated dEMG. Ti was measured from the onset of the dEMG activity to the point at which the dEMG peak activity began to decline. Te was measured from the end of Ti to the onset of following inspiration. Baseline dEMG activity was defined as the minimum expiratory activity. The amplitude of dEMG (ΔdEMG) was calculated as the difference between baseline and peak burst amplitude. Minute ventilation $\dot{V}_E$ was calculated by multiplying the Vt by the instantaneous f_R. The mean arterial blood pressure (MAP) was calculated as the diastolic

pressure plus 1/3 of the pulse pressure. HR was derived from the average interval between peak systolic pressure pulses in the arterial pressure trace.

The control breathing pattern was measured from a 5 s period before KCN injection. The peak respiratory response was determined from the maximum increase in f_R. Peak respiratory timing and dEMG responses were averaged from 3 breaths at the peak response. HR and MAP peaks were averaged from 10 heart beats at the same time point. The latency-to-peak was calculated as the time from the completion of KCN injection, Bic or DLH microinjection to peak of cardio-respiratory response. DLH control measurements were made at the peak, and the time corresponding to KCN response peak. Cardio-respiratory parameters were averaged for 5 breaths or 10 heart beats at the time corresponding to KCN response peak.

A two-way ANOVA with repeated measures (factors: treatment and time) was performed to compare the respiratory and cardiovascular response parameters as a function of peripheral chemoreceptor stimulation with or without dPAG activation. A one-way ANOVA with repeated measures (factor: treatment) was performed to for comparisons of cardio-respiratory parameters during control aCSF, Bic and DLH stimulation. One-way ANOVA with repeated measures (factor: treatment) was performed to compare the latency to peak among different groups, and peak response among different trials of control, DLH control, and DLH+KCN trials. When differences were indicated, a Tukey post-hoc multiple comparison analysis was used to identify significant effects. Statistical significance was accepted at probability $p<0.05$, and all analyses were completed using SigmaStat (v2.03, SPSS software, Chicago, IL). All data are reported as means ± SE.

Results

Cario-respiratory Response to Intravenous KCN and Control Experiments

Mean resting f_R, HR, and MAP of all animals were 107±2 breaths/min, 440±10 beats/min, and 93±6 mmHg. Intravenous KCN elicited hyperventilation, hypertension, and tachycardia in spontaneously breathing and anesthetized rats (Fig. 4-1, and 4-2). In Bic trials, peak KCN cardio-respiratory responses of f_R, HR, and MAP were 165±3 breaths/min, 493±23 beats/min, and 148±12 mmHg (all $p<0.001$). In DLH trials, KCN peak responses were 165±3 breaths/min for f_R, 473±36 beats/min for HR, and 153±8 mmHg for MAP (all $p<0.001$). Average latency-to-peaks were 3.25±0.11 s for f_R, 4.69±0.23 s for MAP, and 8.69±0.20 s for HR. Neither the insertion of micropipette itself nor aCSF (n=4) microinjection significantly change the cardio-respiratory parameters. No statistically significant difference was found in cardio-respiratory response to intravenous KCN before and after microinjection of aCSF into the dPAG.

Cardio-respiratory Response to Bic Disinhibition in the dPAG

Bic microinjection in the dPAG elicited increased f_R, dEMG baseline activity, MAP, and HR (Fig. 4-1). At 3 min and 8 min after the completion of bicuculline microinjection, f_R increased from 109±3 pre-Bic to 238±8 and 197±10 breaths/min respectively. There was a significant decrease in Ti and Te at 3 min ($p<0.001$) (Fig. 4-3). At 8 min after the completion of microinjection, Ti was not statistically different from control Ti, but Te was significantly decreased ($p<0.001$). There was no significant change in Vt during Bic disinhibition. $\dot{V}_E$ was increased due to an increased f_R (Fig. 4-4). Bic disinhibition significantly increased baseline dEMG activity at 3 and 8 min post Bic microinjection. The ΔdEMG was not significantly changed (Fig. 4-5).

Bic disinhibition of the dPAG significantly increased MAP from 84±9 pre-Bic to 137±7 and 117±10 mmHg at 3 min and 8 min after the completion of microinjection respectively. HR significantly increased from 443±21 pre-Bic to 522±7 and 510±8 beats/min respectively (Fig. 4-1 and -6). There was no statistic difference from HR and MAP between the 3 and 8 min measurement periods. Peak Bic control f_R was 245±10 breaths/min, HR 522±6 beats/min, and MAP 139±6 mmHg.

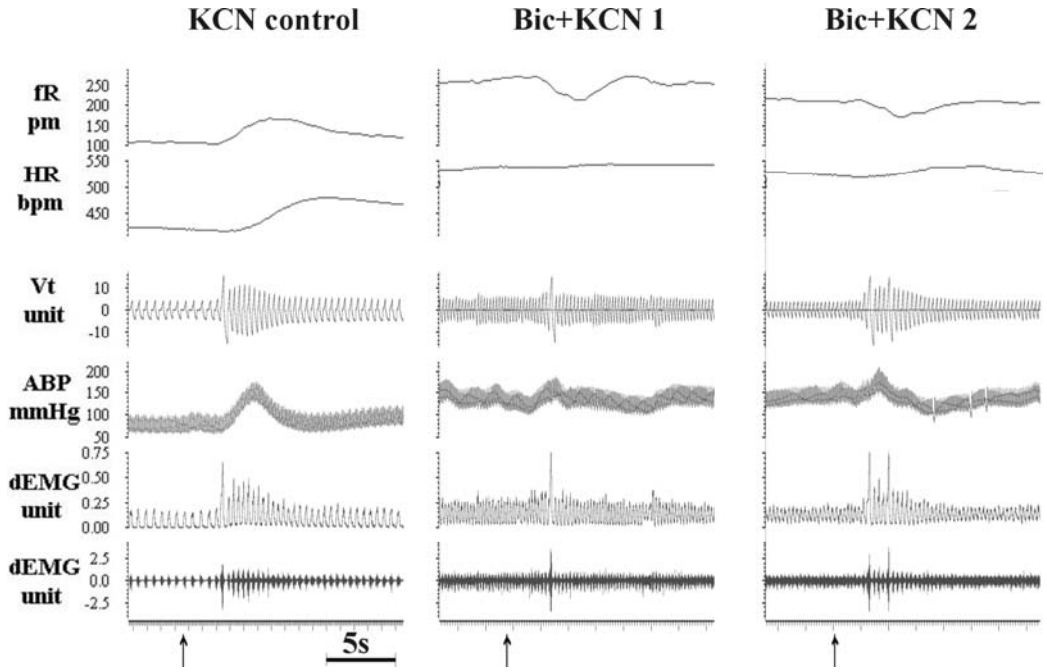

Figure 4-1. Influence of dPAG disinhibition on cardio-respiratory response to intravenous KCN in one animal. All panels are in same scale. Arrows represent the completion of intravenous KCN injection. Upper direction represents inspiration.

Effect of Bicuculline Disinhibition of the dPAG on KCN Response

The response to KCN during Bic disinhibition resulted in a significant decrease in f_R (Fig. 4-1 and 4-3). At 3 min after Bic microinjection (Bic+KCN 1), KCN significantly decreased Ti from 109±6 to 128±9 ms (p<0.01), and Te from 145±5 to 202±20 ms (p<0.01). Bic+KCN 1 significantly decreased f_R from 238±8 to 187±15 breaths/min (p<0.001). There were significant increases in Vt and $\dot{V}_E$ in response to Bic+KCN 1 (Fig.

4-4). There was no significant change of dEMG baseline activity in Bic+KCN 1 trials. Bic+KCN 1 significantly increased ΔdEMG (Fig. 4-5). Both MAP and HR increased in response to Bic+KCN 1 (Fig. 4-6).

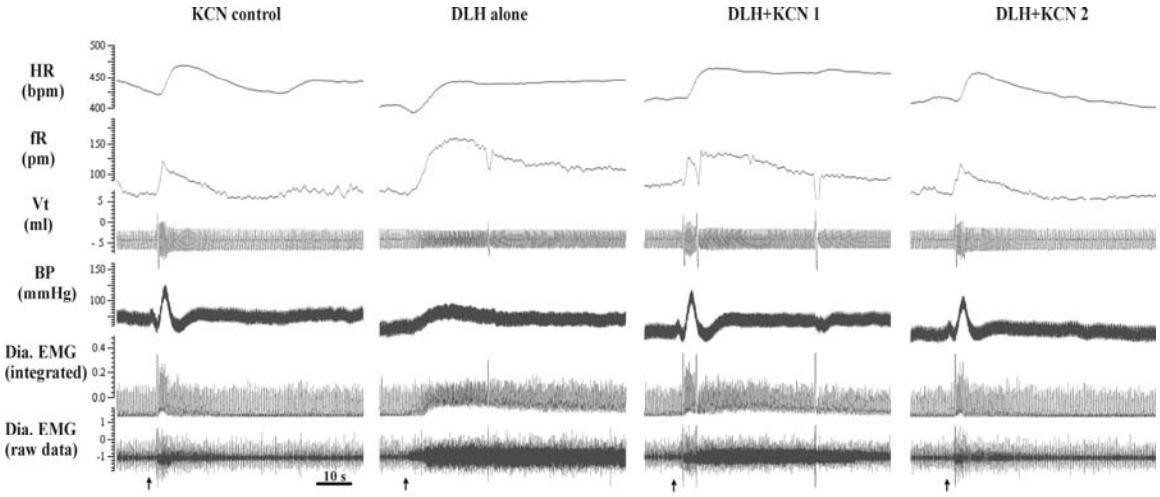

Figure 4-2. Influence of DLH microinjection in the dPAG on cardio-respiratory activity and response to intravenous KCN in one animal. All panels are in same scale. Arrows represent the completion of KCN injection or DLH (45nl, 0.1M) microinjection. Upper direction represents inspiration.

At 8 min after Bic microinjection (Bic+KCN 2), KCN significantly decreased f_R from 197±10 to 174±9 breaths/min (p<0.01). Ti increased from 127±8 to 128±4 ms (p>0.05), and Te from 181±8 to 222±18 ms (p<0.05). There were significant increases in Vt and $\dot{V}_E$ in response to Bic+KCN 2 (Fig. 4-4). No significant change of dEMG baseline activity was observed during Bic+KCN trial. Bic+KCN 2 significantly increased ΔdEMG (Fig. 4-5). Both MAP and HR increased in response to Bic+KCN 2 (Fig. 4-6). Among different experimental conditions, there was no difference in latency-to-peak of cardio-respiratory response to KCN (Table 4-1).

Cardio-respiratory Response to DLH Stimulation in the dPAG

DLH stimulation of the dPAG evoked a short duration cardio-respiratory response when compared to Bic disinhibition (Fig. 4-2). DLH stimulation increased f_R from 106±1

pre-DLH to 171±7 breaths/min. The latency-to-peak was 9.95±1.23 s (Table 4-1). DLH microinjection elicited significant decrease in Vt (Fig. 4-4). DLH elicited a significant decrease in Te (410±5 ms to 223±9 ms, $p<0.001$), and Ti (158±3 ms to 132±7 ms, $p<0.01$). The f_R significantly increased and $\dot{V}_E$ was also significantly increased. DLH stimulation evoked significant increase in baseline dEMG activity, but no significant change of ΔdEMG. Five minutes after the completion of DLH microinjection, cardio-respiratory parameters returned to pre-DLH levels. DLH microinjection increased MAP from 94±7 to 132±9 mmHg with a latency of 10.50±1.37 s, and HR from 428±14 to 456±12 beats/min with a latency of 16.35±3.52 s. Latency-to-peak cardio-respiratory response with DLH was significantly longer than the KCN response (Table 4-1).

Table 4-1. Latencies to peak in cardio-respiratory response to KCN or dPAG activation

	f_R	MAP	HR
Bic tests (n=5)			
KCN Control	3.37±0.13	5.25±0.36	8.79±0.46
Bic+KCN 1	3.01±0.35	4.28±0.53	8.50±1.18
Bic+KCN 2	3.23±0.23	4.76±0.64	8.02±0.93
DLH tests (n=7)			
KCN Control	3.17±0.17	4.30±0.21	8.62±0.17
DLH control	9.95±1.23***	10.50±1.37***	16.35±3.52*
DLH+KCN 1	2.29±0.08	3.79±0.22	8.93±0.36
DLH+KCN 2	3.04±0.20	4.23±0.22	8.45±0.26

Values are means ± SE. All values are given in second.
*****: significantly different from all other experimental conditions, $p < 0.05$; ***: $p<0.001$.

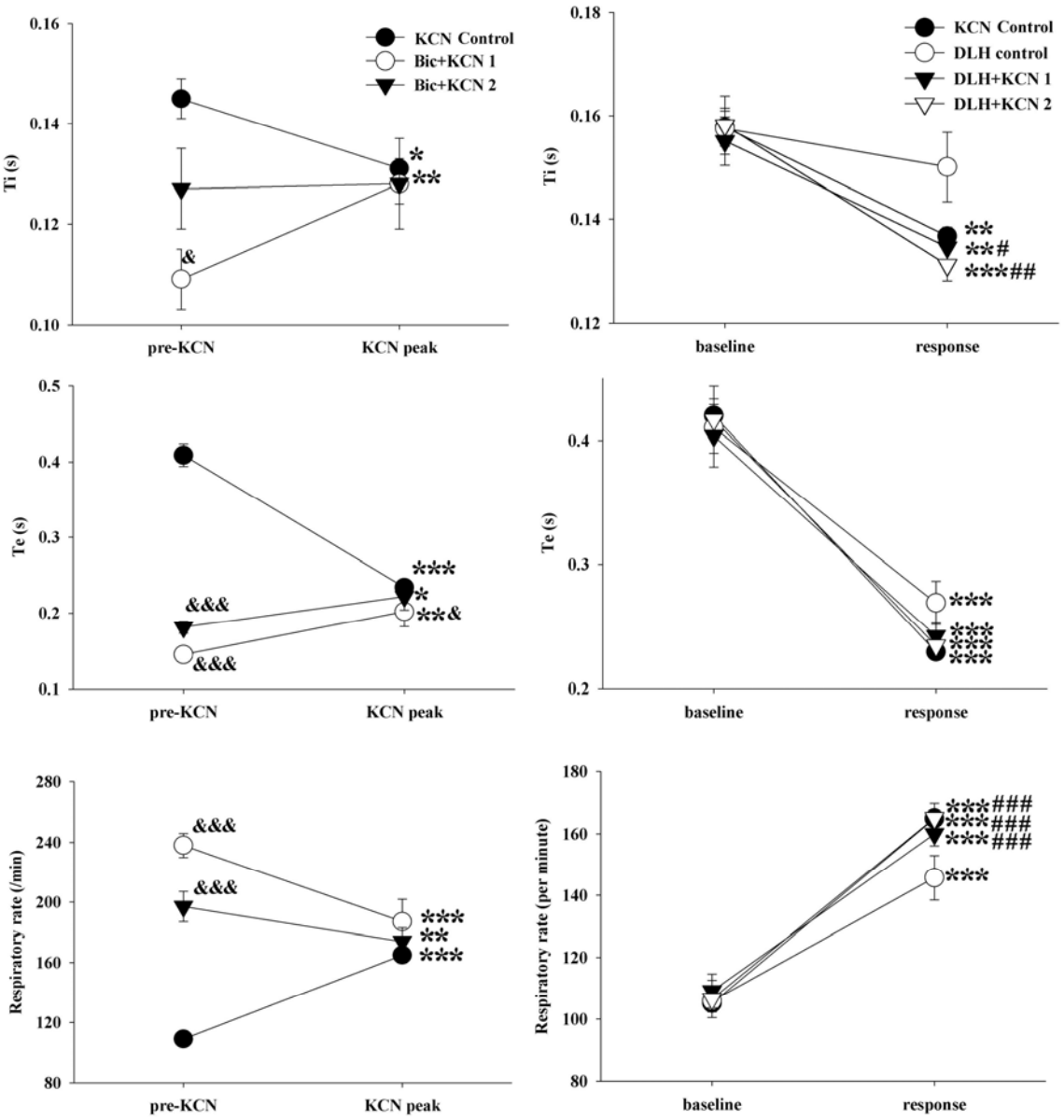

Figure 4-3. Effect of dPAG activation on respiratory timing response to intravenous KCN. *Left*: bicuculline group (n=5); *Right*: DLH group (n=7). *: significant difference from pre-KCN/baseline value, $p<0.05$; **: $p<0.01$; ***: $p<0.001$; &: significant difference from corresponding value in control experiment, $p<0.05$; &&&: $p<0.001$; #: significant difference from that during corresponding time in DLH control experiment, $p<0.05$; ##: $p<0.01$; ###: $p<0.001$.

Effect of DLH Stimulation in the dPAG on KCN Response

The simultaneous injection of DLH and KCN (DLH+KCN 1) significantly decreased Ti and Te resulting in a significantly increased f_R (Fig. 4-2 and 4-3).

DLH+KCN 1 significantly increased Vt and $\dot{V}_E$ (Fig. 4-4). DLH+KCN 1 significantly increased baseline dEMG activity and ΔdEMG above pre-KCN level (Fig. 4-5). MAP and HR were also significantly increased during DLH+KCN 1 trial (Fig. 4-6). These DLH+KCN 1 changes were not significantly different from KCN alone. During DLH alone response, at the time corresponding to KCN alone response peak, there was significant increase in f_R (146±7 vs 106±1 breaths/min) and HR (448±12 vs 428±14 beats/min). No significant change of dEMG activity and MAP was observed. The latencies to cardio-respiratory response peaks were not significantly different between DLH+KCN 1 and KCN alone (Table 4-1). Thus, underlying dPAG activation did not significantly change cardio-respiratory response to KCN. When DLH microinjection and intravenous KCN were delivered simultaneously, both HR and f_R took a slow decay pattern from peak response (Fig. 4-2, DLH+KCN 1 panel). At 5 min after simultaneous injection of DLH and KCN, there was no significant difference in cardio-respiratory response between KCN alone and DLH-KCN 2 trial (Fig. 4-3, 4-4, 4-5, and 4-6).

Reconstructed Microinjection Sites

Drug microinjection sites were reconstructed from histological sections containing the highest density of fluorescent beads (Fig. 4-7). Reconstructed microinjection sites from all experiments were located inside the dorsal column of the dPAG.

Discussion

This study investigated the effect of dPAG activation on cardio-respiratory responses to peripheral chemoreceptor stimulation. Peripheral chemoreceptor stimulation was elicited by intravenous KCN. Both DLH and Bic microinjected into the dPAG increased respiratory and cardiovascular activities. When KCN was delivered after the disinhibition of the dPAG with Bic, KCN slowed respiratory timing to the level of KCN

only trial. When KCN was delivered simultaneously with DLH microinjection, the respiratory activity increased to the level of KCN only trial. These data suggested that although dPAG activation could modulate activity of the brainstem respiratory network, peripheral chemoreceptor stimulation might functionally block this excitatory effect.

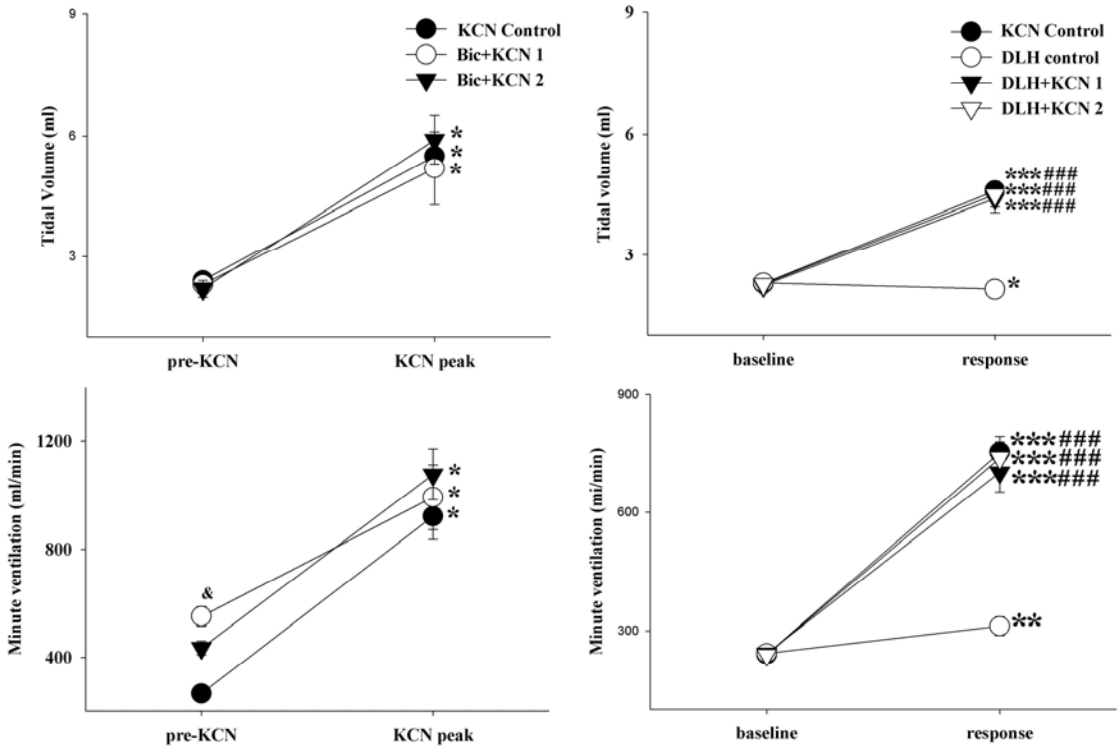

Figure 4-4. Effect of dPAG activation on ventilation response to intravenous KCN. *Left*: bicuculline group (n=5); *Right*: DLH group (n=7). *: significant difference from pre-KCN/baseline value, $p<0.05$; **: $p<0.05$; ***: $p<0.001$; &: significant difference from corresponding value in control experiment, $p<0.05$; ###: significant difference from that during corresponding time in DLH control experiment; $p<0.001$.

Respiratory Response Elicited from the dPAG

As reported previously (Huang et al., 2000; Hayward et al., 2003), dPAG activation elicits enhanced respiratory and cardiovascular activities. The respiratory response is characterized by significantly increased f_R and dEMG activity. In Bic disinhibition experiments, there were significant decreases in both Te and Ti at 3 min after

microinjection. But at 8 min, Ti has recovered to near control level while Te was still significantly reduced. This result is consistent with previous observation that low intensity electrical stimulation in the dPAG could only evoke significant decrease in Te, not Ti (Hayward et al., 2003). These data suggested that expiratory phase, and the underlying neuronal network, is more vulnerable to dPAG activation. This study further demonstrated that activation (DLH) and disinhibition (Bic) dPAG has differential effects on respiratory timing. In current experimental settings, at 8 min after the completion of Bic microinjection in the dPAG, there was still significant increase in f_R. In DLH microinjection trial, respiratory response has completely recovered at 5 min after microinjection. These results show that Bic elicits a greater change in respiration than DLH, and this effect is sustained for a longer period of time.

Effect of dPAG Activation on Respiratory Response to KCN

Bic disinhibition of the dPAG increased f_R, at a level higher than peak response to KCN only. Injection of KCN in the presence of Bic decreased f_R to a level that was approximately equal to KCN alone. When KCN was given simultaneously with DLH microinjection, the peak respiratory response again was approximately equal to KCN alone. These results suggest that the respiratory excitatory input form the dPAG was modulated by peripheral chemoreceptor stimulation. This further suggests that peripheral chemoreceptor afferents overrode descending excitatory inputs from the dPAG to the brainstem respiratory neural network.

The posterior hypothalamus has been demonstrated to modulate respiratory response to hypoxia (Peano et al., 1992; Horn et al., 1998). The neurons in the hypothalamus were activated by hypoxia, and projected to the PAG (Ryan et al., 1995). Within the dPAG, there are neurons respond to hypoxia (Kramer et al., 1999). Peripheral

chemoreceptor stimulation increased immediate-early gene *c-fos* expression in the dPAG (Berquin et al., 2000; Hayward et al., 2002). Furthermore, there are neurons in the dPAG have respiratory-related discharge rhythm (Ni et al., 1990). These data suggest that the PAG itself could be directly involved in the respiratory reflex to peripheral chemoreceptor stimulation.

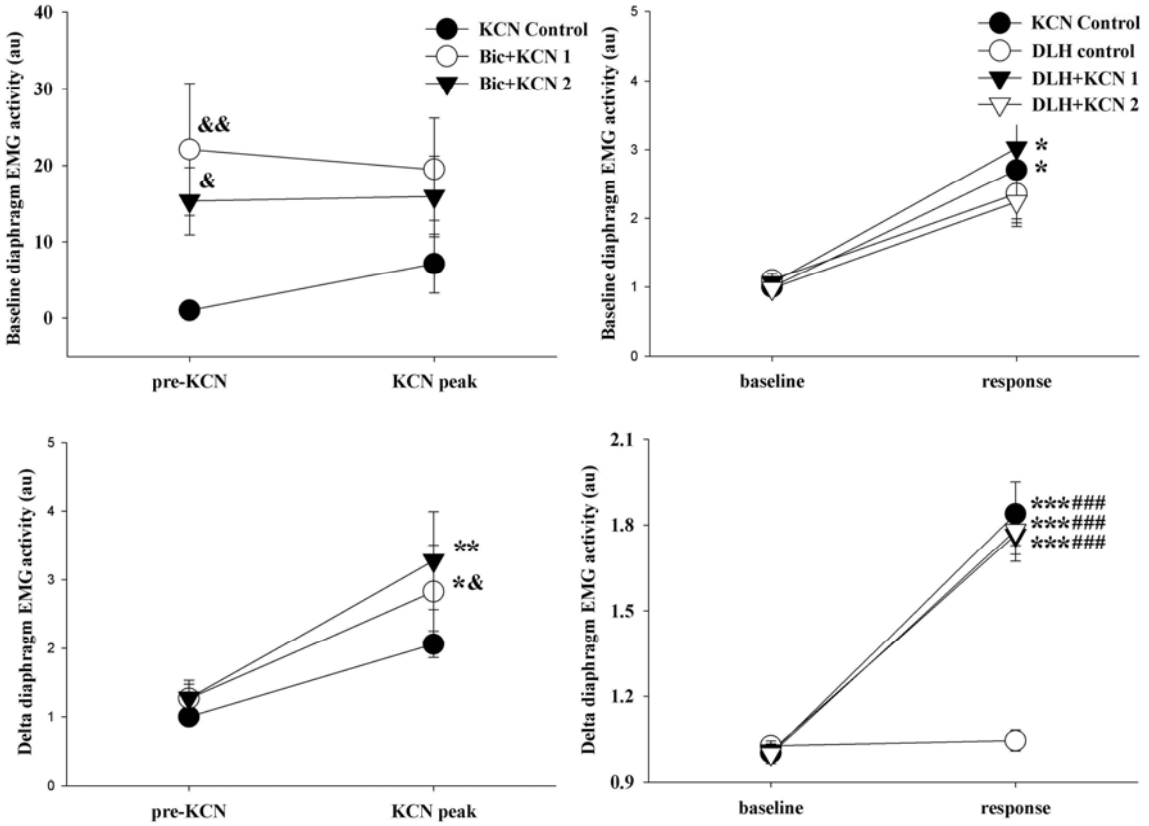

Figure 4-5. Effect of dPAG activation on diaphragm EMG activity response to intravenous KCN. *Left*: bicuculline group (n=5); *Right*: DLH group (n=7). *: significant difference from pre-KCN/baseline value, $p<0.05$; **: $p<0.01$; ***: $p<0.001$; &: significant difference from corresponding value in control experiment, $p<0.05$; &&: $p<0.01$; ###: significant difference from that during corresponding time in DLH control experiment; $p<0.001$.

The LPBN is a relay between the dPAG and the brainstem respiratory network (Hayward et al., 2004). Activation of the dPAG has excitatory effects on the LPBN (Hayward et al., 2003). Thus, dPAG descending inputs can be modulated by changing neuronal activities of the LPBN. But very few neurons in the LPBN were inhibited by the

peripheral chemoreceptor inputs (Hayward et al., 1995). It suggested that the LPBN might not be the site where the blocking happens. Peripheral chemoreceptor afferents may modulate respiratory drive by modulating neuronal activities in the ventral respiratory group (VRG) via the NTS (Marshall, 1994; Guyenet et al., 1995; Guyenet, 2000). This ascending excitatory input may block the descending excitatory inputs from the dPAG, as suggested by the observation that peripheral chemoreceptor stimulation could inhibit neuronal activities in the ventral medulla (Carroll et al., 1996). Peripheral chemoreceptor stimulation is suggested to be an alerting stimulus to animals, which may be mediated by the PAG. However, results from current project suggest that the peripheral chemoreceptor respiratory response may have higher priority than descending autonomic responses during defense behavior.

Effect of dPAG Activation on Cardiovascular Response to KCN

Bic disinhibition elicited moderate but significant increase in MAP and HR compared to their pre-KCN levels. DLH peak cardiovascular response was not significantly different under all experimental conditions (Fig. 4-6). It has been reported that the dPAG does not play an essential role in cardiovascular response to peripheral chemoreceptor stimulation (Koshiya et al., 1994; Haibara et al., 2002). In those studies, tissue dissection or neural inhibition methods were used. In the present study, Bic disinhibition of the dPAG attenuated the cardiovascular response to KCN. Neuronal blocking of the LPBN inhibited about ~72% of HR response, and oppressed about ~57% of the MAP response to dPAG stimulation (Hayward et al., 2004). The dPAG has direct projections to the LPBN (Krout et al., 1998), ventrolateral pontine A5 cell group, rostral ventrolateral medulla, and medulla raphe system (Carrive et al., 1988; Cameron et al., 1995; Hudson et al., 1996). This suggests that there are multiple descending pathways

from the dPAG mediating these autonomic responses. Thus, the different effect of dPAG activation on cardiovascular response to KCN may be the results of a neural mechanism that differs from the respiratory pathways.

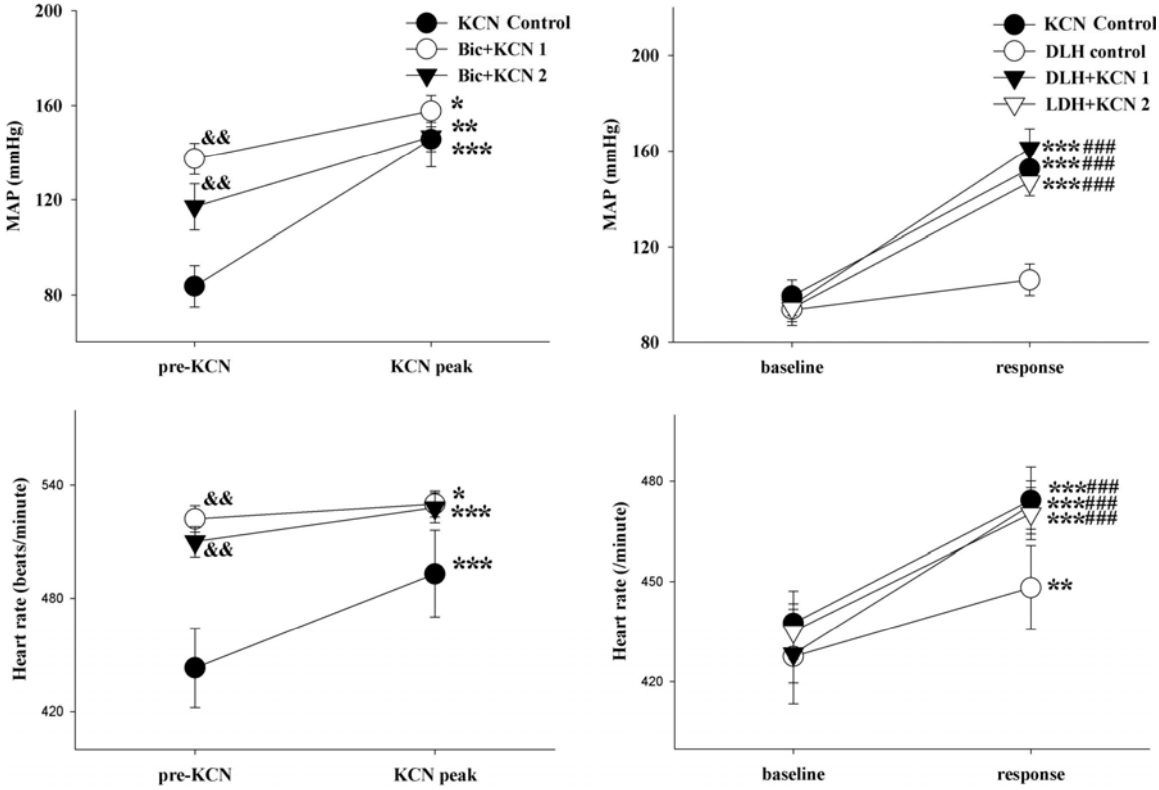

Figure 4-6. Effect of dPAG activation on cardiovascular response to intravenous KCN. *Left*: bicuculline group (n=5); *Right*: DLH group (n=7). *: significant difference from pre-KCN/baseline value, $p<0.05$; **: $p<0.01$; ***: $p<0.001$; &&: significant difference from corresponding value in control experiment, $p<0.01$; ###: significant difference from that during corresponding time in DLH control experiment; $p<0.001$.

Technical Considerations

KCN used in this project briefly stimulates the carotid body chemoreceptors. KCN provides a brief, rapid-onset, and potent activation of arterial chemoreceptors, and elicits a reproducible reflex response with repeated administration (Koshiya et al., 1994; Carroll et al., 1996; Hayward et al., 1999). Repeated KCN injection in the present study elicited a similar peak respiratory response. KCN provides a stimulus to carotid body

chemoreceptors without the confounding influence of systemic hypoxia. The cardio-respiratory response to KCN in both conscious and anesthetized rats is dependent on an intact carotid sinus nerve (Franchini et al., 1992; Hayward et al., 1999). KCN has very limited influence on baroreceptor afferents (Franchini et al., 1993). Thus, the use of KCN allowed investigation of the interaction of peripheral chemoreceptor stimulation and dPAG activation without confounding with systemic hypoxemia.

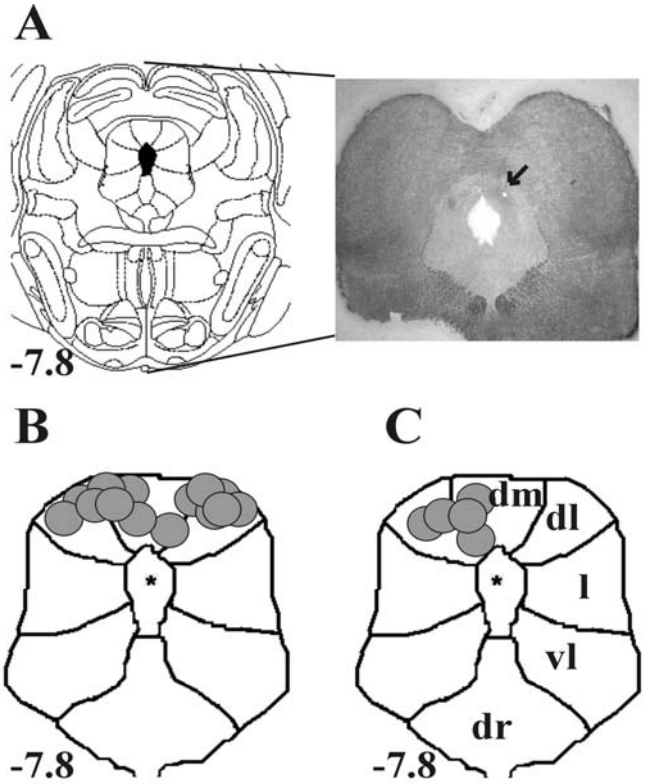

Figure 4-7. Reconstructed dPAG microinjection sites. *A*: the outline of the PAG (Paxinos et al., 1997) and corresponding histology section from the same approximate region taken from one animal illustrating a typical microinjection site (arrow). *B*: reconstructed dPAG microinjection sites from DLH (n=7) experiments. Filled cycles at left side represent those in DLH control, and right side represents those in DLH and KCN trials. *C*: reconstructed dPAG microinjection sites from bicuculline (n=5) experiments. The numbers to the left of images indicate location of brain section relative to bregma. Schematics of brain regions were adapted from a rat brain atlas (Paxinos et al., 1997). *****, midbrain aqueduct; *dm*, dorsomedial PAG; *dl*, dorsolateral PAG; *l*, lateral PAG; *vl*, ventrolateral PAG; *dr*, dorsal raphe.

Bic and DLH microinjections were used to activate the dPAG by different neural mechanism. DLH is a NMDA receptor angonist, and exerts direct excitatory effect on PAG neurons. Bic activates neurons by blocking $GABA_A$ inhibitory inputs and thus disinhibiting intrinsic excitatory inputs from other connected neural structures, mediated by NMDA, non-NMDA, and serotonin receptors (Albin et al., 1990; Lovick et al., 2000). Although different activation mechanisms are involved, the result was the activation of neurons in the dPAG, and consequent cardio-respiratory response. The different modes of dPAG activation led to different levels of respiratory response, and a difference in interaction with peripheral chemoreceptor stimulation.

Summary

The results of this study showed that different baseline dPAG conditions before intravenous KCN injection led to different respiratory changes with the peak respiratory response equal to KCN only response. Results from this study suggest that peripheral chemoreceptor stimulation blocks dPAG descending inputs to brainstem respiratory network, eliciting a pattern of respiratory response equal to intravenous KCN.

CHAPTER 5
INFLUENCE OF THE DORSAL PERIAQUEDUCTAL GRAY ACTIVATION ON RESPIRATORY OCCLUSION REFLEXES

Introduction

The midbrain periaqueductal gray (PAG) is an important neural structure in defense behavior, analgesia, vocalization and autonomic regulation (Hilton et al., 1982; Carrive, 1993; Bandler et al., 1994; Zhang et al., 1994; Behbehani, 1995; Bandler et al., 2000). The dorsal subdivision of the PAG (dPAG) involves in fight/flight defense behavior. Activation in this region consistently elicited excitatory effects on respiratory activity (Lovick, 1992; Huang et al., 2000; Hayward et al., 2003; Zhang et al., 2003; Hayward et al., 2004). The enhanced respiratory activities were characterized by the shortening of inspiratory time (Ti) and expiratory time (Te) with minimal effect on tidal volume (Vt). Inhibition of the NTS abolished dPAG elicited changes in breath phase timing (Huang et al., 2000). This suggests that the dPAG modulates the breath phase timing by an action on the medullar respiratory neural network (Shannon et al., 1998). The decrease in Ti or Te in the absence of a change in Vt suggests that the volume-timing relationship (Clark et al., 1972), controlling breath phase transition (off-switch), is modulated by the dPAG. If dPAG activation changes breath phase timing by acting on the respiratory neural network, it was reasoned that the dPAG may change the sensitivity of the neural network to volume related reflex regulation of breath phase transition.

Mechanosensory information from the lung transducing transpulmonary pressure in the bronchi is known to determine the timing of inspiratory and expiratory phases of the

respiratory cycle (Davenport et al., 1981; Davenport et al., 1986). Volume related mechanical information is sensed primarily by slowly adapting pulmonary stretch receptors (PSRs) that project to the central nervous system via the vagus nerves. These mechanoreceptors mediate the relationship between respiratory volume and respiratory timing during eupneic breathing, hypercapnia and loaded breathing. Decreased inspiratory volume (Vi) or expiratory volume (Ve) results in a longer Ti or Te respectively (Clark et al., 1972; Zechman et al., 1976; Davenport et al., 1981). The expiratory occlusion, by obstructing the trachea at the end of inspiration, maintains PSRs activity and inhibits subsequent inspiratory effort resulting in a longer Te (Davenport et al., 1981). Inspiratory occlusion obstructs inspiration at the end of the expiratory phase removing the Vt dependent inspiratory-inhibitory effect of lung inflation, resulting in a prolongation of Ti. While these respiratory occlusion reflexes are well known in anesthetized animals or humans during various respiratory conditions (Brown et al., 1998; Bolser et al., 2000), it is unknown if activation of the dPAG changes the sensitivity of this volume-timing reflex.

Inflation and deflation reflexes were observed during PAG evoked vocalization (Davis, et al., 1993; Zhang et al., 1994; Nakazawa et al., 1997). Activation of the dPAG changed the discharge pattern of respiratory-related NTS neurons (Sessle et al., 1981; Huang et al., 2000). Therefore, activation of the dPAG may change the volume dependent respiratory timing modulation mediated by PSRs. It was hypothesized that the activation of the dPAG would modulate volume-timing reflexes. In the current project, activation of the dPAG was elicited with the microinjection of excitatory amino acid D,L-homocysteic acid (DLH), or $GABA_A$ receptor antagonist bicuculline (Bic). Volume

related changes of respiratory timing and diaphragm EMG (dEMG) activity in response to respiratory occlusions were compared before and after dPAG activation.

Materials and Methods

The experiments were performed on adult male Sprague-Dawley rats (350 - 420g, n=14) housed in the University of Florida animal care facility. The rats were exposed to a normal 12hr light 12hr dark cycle. The experimental protocol was reviewed and approved by the Institutional Animal Care and Use Committee of the University of Florida.

General Preparation

The rat was anesthetized with urethane (1.4 g/kg, i.p.). Additional urethane (20 mg/ml) was administrated intravenously as necessary. The adequacy of anesthesia was verified by the absence of a withdrawal reflex or blood pressure and heart rate responses to a paw pinch. A tracheotomy was performed. The femoral artery and vein were catheterized. The body temperature was monitored with a rectal probe and maintained between 36 - 38°C with a thermostatically controlled heating pad (NP 50-7053-F, Harvard Apparatus). The rats respired spontaneously with room air.

Tracheal tube from each animal was connected to a pneumotachography (8431 series, Hans Rudolph) for recording airflow and tidal volume by electrical integration. The pneumotachography was connected to a non-rebreathing valve (2310 series, Hans Rudolph). The dEMG activity was recorded with bipolar Teflon-coated wire electrodes. The bared tips of the electrodes were inserted into the diaphragm through a small incision in the abdominal skin. A third wire inserted in the skin of head as an electrical ground. The recording electrodes were connected an AC preamplifier (P511, Grass Instruments) via a high-impedance probe, amplified and band-pass filtered (0.3-3.0 kHz). The analog output was fed to a computer data sampling system (CED Model 1401, Cambridge

Electronics Design) and processed by a signal analysis program (Spike 2, Cambridge Electronics Design). The arterial catheter was attached to a pressure transducer connected to a polygraph system (Model 7400, Grass Instruments). The analog outputs of the polygraph were led to the CED 1401. All signals were recorded simultaneously and stored for subsequent offline analysis.

The animal was then placed prone in a stereotaxic head-holder (Kopf Instruments). The cortex overlying the PAG was exposed by removal of small portions of the skull with a high-speed drill. Chemicals were dissolved in artificial cerebrospinal fluid (aCSF) containing (in mM): 122 NaCl, 3 KCl, 25.7 $NaHCO_3^-$, and 1 $CaCl_2$, with pH adjusted to 7.4. The chemical stimulation was performed with a single-barrel microinjection pipette, attached to a pneumatic injection system (PDES-02P, NPI, Germany). The microinjection pipette was stereotaxically lowered into the caudal dPAG with coordinates of 7.64 to 8.72 mm caudal to the bregma, 0.1 to 0.6 mm lateral to the midline and depths of 3.8 to 4.5 mm below the dorsal surface of the brain. Small amounts of fluorescent carboxylate-modified microspheres (Molecular Probes, Eugene, OR) were mixed into the microinjection solutions to facilitate later identification of the microinjection sites. The volume of injection was monitored by measuring the movement of the meniscus through a small magnifying eye-piece equipped with a calibrated reticule (50×; Titan Tools). One minute after completion of a central injection, the pipette was retracted from the brain.

At the end of the experiment, the animal was euthanized. The brain was removed and fixed in 4% paraformaldehyde solution for 72 hrs. The fixed tissue was frozen to -16°C, then cut coronally into 40-μm-thick sections with a crytostat (model HM101, Carl Zeiss). The sections were mounted and imaged with a microscope equipped with bright

field and epifluorescence. After identifying the location of fluorescence beads, the slices were then stained with neutral red, and sealed with a cover-slip. A rat brain atlas (Paxinos et al., 1997) was used to reconstruct the stimulation site.

Protocols

After the animal was surgically prepared, inspiratory and expiratory occlusions were performed in random sequence. Inspiratory occlusions were presented by occluding the inspiratory port of the non-rebreathing valve during expiration. The following inspiration was occluded. Expiratory occlusions were presented by occluding the expiratory port of the non-rebreathing valve during inspiration. The subsequent expiration was occluded. At least five occlusions of each breath phase were presented with a series of 5 unloaded breaths separating each occlusion. Two group animals were used in this study. One group (n=6) received microinjection of 45nl, 0.2M DLH into the dPAG. The occlusions were delivered after the respiratory frequency (f_R) response reached its peak. Two microinjections were delivered, one to each side of the caudal dPAG. Only one type of occlusion was performed after each unilateral microinjection. The sequence of inspiratory or expiratory occlusion was randomized. The second group (n=6) received microinjection of 45nl, 0.5mM Bic. The first set of occlusions was delivered at the respiratory frequency equal to DLH stimulation. Only one microinjection was performed. The dEMG, tracheal airflow and pressure were recorded continuously. The control animals underwent same protocols with the microinjection of aCSF.

Data Analysis

All data were analyzed off-line using Spike2 software (Cambridge Electronics Design). The EMGs were rectified and integrated (time constant = 50 ms). The Ti, Te, and f_R were calculated from the integrated dEMG signals. Ti was measured from the

onset of the dEMG burst activity to the point at which the peak dEMG activity began to decline. Te was measured from the end of Ti to the onset of following inspiration. Baseline dEMG activity was defined as the minimum value between bursts. The dEMG amplitude (ΔdEMG) was calculated as the difference between baseline and peak burst amplitude. Both dEMG baseline activity and amplitude were expressed as a percentage of control. The percentage change of Ti with occlusion was defined as the ratio between the Ti during the occlusion breath (Ti-O) divided by the Ti during the preceding control breath (Ti-C). The percentage change of Te with occlusion was defined as the ratio between the Te during the occlusion breath (Te-O) divided by the Te during the preceding control breath (Te-C). The control breath was defined as the breath immediately preceding the occlusion.

A two-way ANOVA with repeated measures (factors: treatment and occlusion) was performed to compare respiratory timing parameters (Ti and Te) and dEMG activity. A one-way ANOVA with repeated measures (factor: treatment) was performed for comparisons of f_R and percentage changes of breath phase timing. When differences were indicated, a Tukey post-hoc multiple comparison analysis was performed to identify significant effects. A *t*-test was performed to compare the difference in respiratory timing between Bic and DLH microinjections. Statistical significance was accepted at probability $p < 0.05$, and all statistic analyses were performed using SigmaStat (v2.03, SPSS software, Chicago, IL). All data are reported as means ± SE.

Results

Respiratory Response to dPAG Activation

Microinjection of DLH or Bic into the dPAG elicited an increase in respiratory activity. Baseline dEMG activity increased following dPAG activation. The resting f_R

before microinjection of DLH and Bic was 109±4 and 107±2 breaths/min, respectively. Inspiratory occlusions (Fig. 5-1) were delivered after microinjection when f_R was 126±5 breaths/min for the DLH group, and 138±7 breaths/min for the Bic group. Both f_R were significantly greater than control (p<0.05), but no significant difference between them (DLH vs Bic). At this f_R level, Ti-C was not significantly different from control (181±5 ms vs 204±5 ms for DLH, and 189±6 ms vs 185±12 ms for Bic). There was significant decrease of Te-C in both DLH (302±19 ms vs 353±21 ms, p<0.05) and Bic (252±17 ms vs 378±17 ms, p<0.05) groups (Table 5-1).

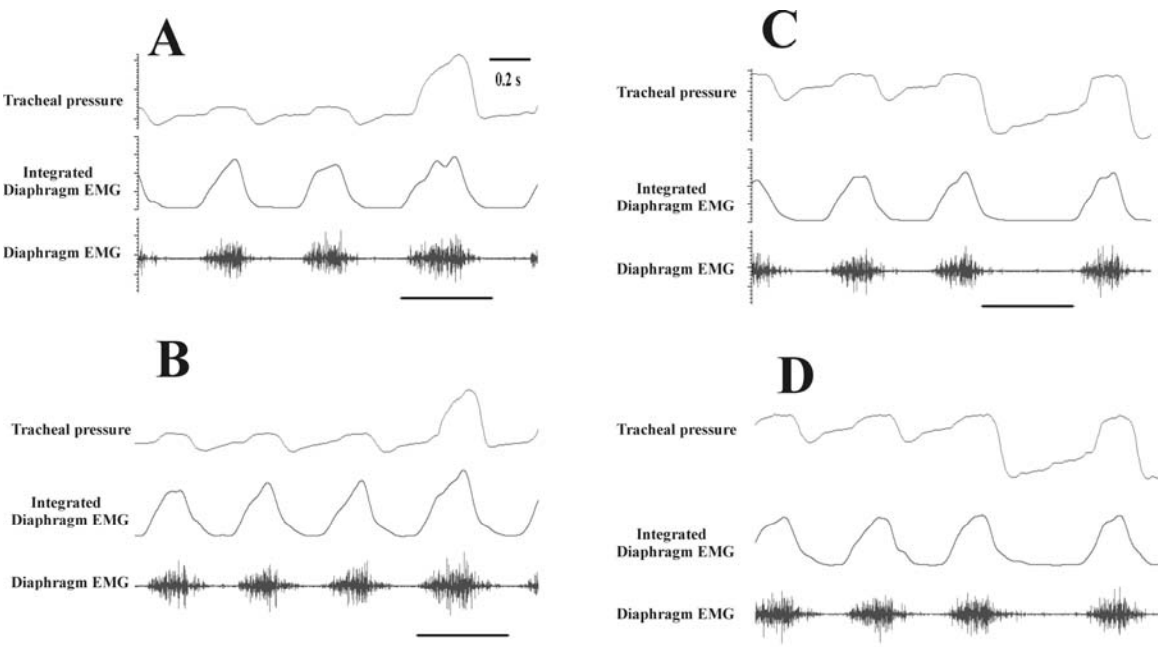

Figure 5-1. A sample of respiratory occlusions before and after microinjection of DLH in the dPAG from one single animal. *Left:* Inspiratory occlusion under control condition (A) or after DLH microinjection (B); *Right:* Expiratory occlusion under control condition (C) or after DLH microinjection (D). All panels were with same time duration. Upper direction represents inspiration.

Expiratory occlusion (Fig. 5-1) was delivered when f_R was 128±2 breaths/min, and 137±6 breaths/min for the DLH group and Bic group, respectively. Both rates were significantly greater than control group (p<0.05). At this f_R level, Ti-C was not significantly different from control (185±5 ms vs 200±2 ms for DLH, and 185±4 ms vs

183±10 ms for Bic). There was significant decrease of Te-C in Bic (258±13 ms vs 380±14 ms, $p<0.05$), and DLH groups (286±7 ms vs 351±19 ms, $p<0.05$) (Table 5-2).

Table 5-1. Effect of inspiratory occlusion on respiratory timing change following the activation of the dPAG

	control	DLH	Control	bicuculline
Ti-C (ms)	204±5	181±5	185±12	189±6
Te-C (ms)	353±21	302±19*	378±17	252±17*
Ti-O (ms)	269±9$^{\#\#}$	269±7$^{\#\#}$	265±13$^{\#\#}$	323±9$^{¤*\#\#}$
Te-O (ms)	390±26$^{\#}$	322±28$^{*\#}$	427±31$^{\#}$	283±22*
Ti-O/Ti-C	1.32±0.02	1.49±0.02**	1.46±0.06	1.73±0.10*
Te-O/Te-C	1.10±0.01	1.06±0.03	1.13±0.06	1.12±0.03
Vt-C (mL)	2.07±0.06	2.32±0.10	2.08±0.10	2.12±0.08
f_R (/min)	109±4	126±5*	107±2	138±7*
bdEMG-C (au)	1.00±0.00	1.47±0.31	1.00±0.00	6.61±4.29*
bdEMG-O (au)	0.92±0.08	1.42±0.27*	0.91±0.07	6.23±4.00$^{¤*}$
ΔdEMG-C (au)	1.00±0.00	1.19±0.08	1.00±0.00	1.12±0.20*
ΔdEMG-O (au)	1.16±0.03$^{\#\#}$	1.33±0.06$^{*\#}$	1.18±0.04$^{\#}$	1.31±0.21$^{\#\#}$

Values are means ± SE. au: arbitrary unit. ¤: significantly different from corresponding value in DLH group, $p < 0.05$. *: significantly different from corresponding value in control condition, $p < 0.05$; **: $p < 0.001$; $^{\#}$: significantly different from corresponding value in pre-occlusion breath, $p < 0.05$; $^{\#\#}$: $p < 0.001$.

The Vi-Ti Relationship with dPAG Activation

Pre-dPAG activation inspiratory occlusion significantly increased Ti-O by 134±4% (Table 5-1). Ti-O with Bic disinhibition was greater than pre-dPAG activation (323±9 ms vs 265±13 ms, $p<0.05$). The relative change in Ti (Ti-O/Ti-C) with Bic was significantly greater than pre-dPAG activation and DLH stimulation. The Ti-O with DLH stimulation

was not significantly different from Ti-O for pre-dPAG activation (Fig. 5-2 and 5-3). During DLH stimulation resulted in a significantly increased Ti-O/Ti-C compared to pre-dPAG activation. The relationships between Vi and Ti during dPAG activation were shown in Fig. 5-2 and 5-3. The relative RVi-RTi relationship (Fig. 5-3) was significantly shifted to the right for DLH and Bic compared to pre-dPAG activation. Bic was also significantly greater than DLH. Activation of the dPAG significantly increased the Te immediately following inspiratory occlusion compared with Te before occlusion (Table 5-1). No significant difference in R-Te was found with inspiratory occlusion (Table 5-1).

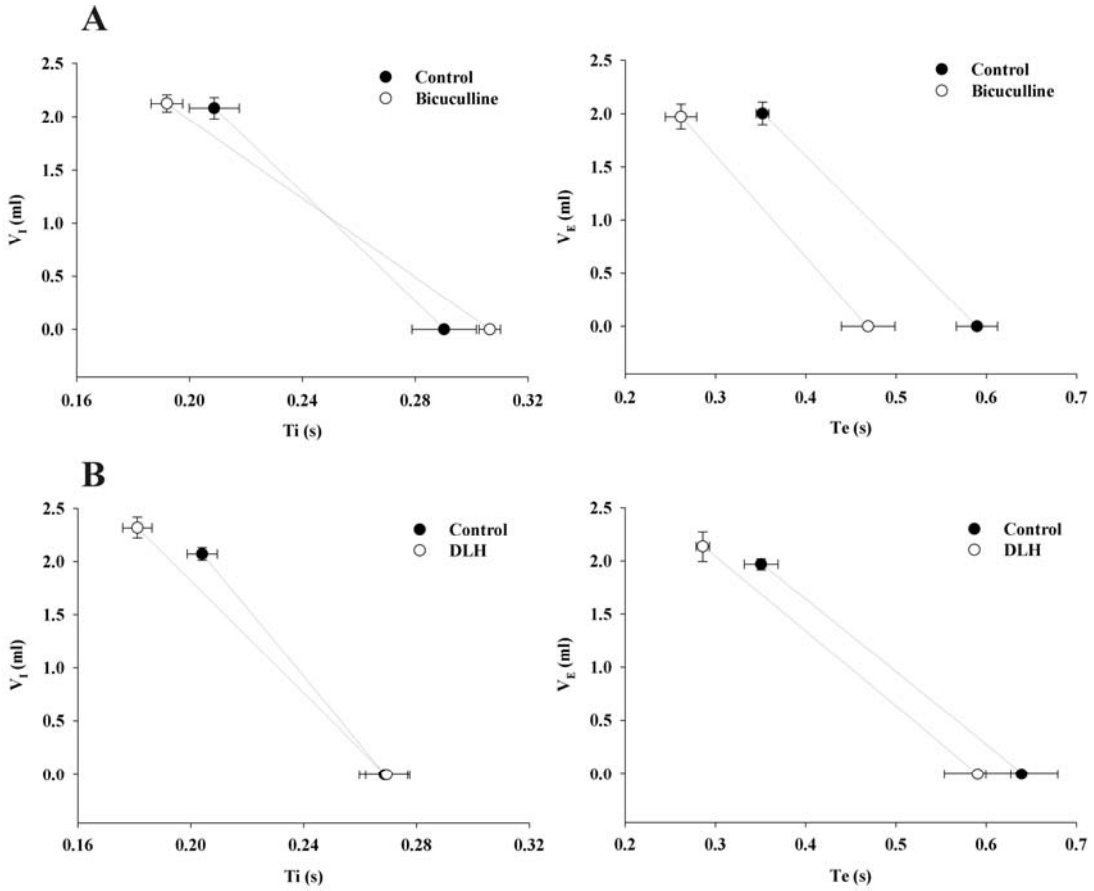

Figure 5-2. Volume-timing relationships in respiratory occlusion during dPAG activation. Relationships for volume and inspiratory (*left*) and expiratory (*right*) phase durations are shown.

The Ve-Te Relationship with dPAG Activation

Pre-dPAG stimulation, expiratory occlusion significantly increased Te-O (Table 5-2). Expiratory occlusion increased Te-O by 184±9%. Expiratory occlusion with Bic disinhibition of the dPAG significantly increased Te-O from the control breath. The Te-O with Bic was significantly less than the Te-O during pre-dPAG activation. However, the Bic control breath Te was significantly shorter than pre-dPAG activation, resulting in a significantly greater Te-O/Te-C for Bic compared to pre-dPAG activation. The Te-O with DLH was significantly less than the Te-O for pre-dPAG stimulation, but not significantly different from Bic Te-O. The Te-O/Te-C with DLH stimulation was significantly greater than during pre-dPAG activation, but not significantly different from Bic. The relationships between Ve and Te during dPAG activation were shown in Fig. 5-2 and 5-3. Activation of the dPAG significantly shifted the RVe-RTe relationship for Bic and DLH to the right of the pre-dPAG curve (Fig. 5-3). There was no significant difference in Ti-O during expiratory occlusion.

Diaphragm EMG Activity

Inspiratory occlusion elicited a significant increase in dEMG amplitude (Table 5-1). Inspiratory occlusion did not elicit a significant change in baseline dEMG activity (Table 5-1). Inspiratory occlusion with Bic and DLH stimulation of the dPAG significantly increased ΔdEMG compared to pre-dPAG activation. There was no significant difference in the ΔdEMG response to inspiratory occlusion between DLH and Bic experiments. Bic in the dPAG significantly increased ΔdEMG from control breaths (112±20% vs 100±0%, $p<0.05$). Bicuculline disinhibition did not significantly change dEMG amplitude during occlusion (131±21% vs 118±4%, $p>0.05$). Expiratory occlusion did not significantly change dEMG activity (Table 5-2).

Histology Reconstruction and Control Experiments

The dPAG microinjection sites were reconstructed from histological sections containing the highest density of fluorescent beads. Reconstructed stimulation sites from all experiments were located in the caudal dPAG (Fig. 5-4). The insertion of micropipette itself did not significantly change the cardio-respiratory parameters. Control experiments were performed with microinjection of aCSF into the dPAG (n=3). No significant difference in respiratory timing and dEMG activity was found before and after aCSF microinjection. Microinjection of aCSF in the dPAG did not elicit a significant change in respiratory timing to occlusion.

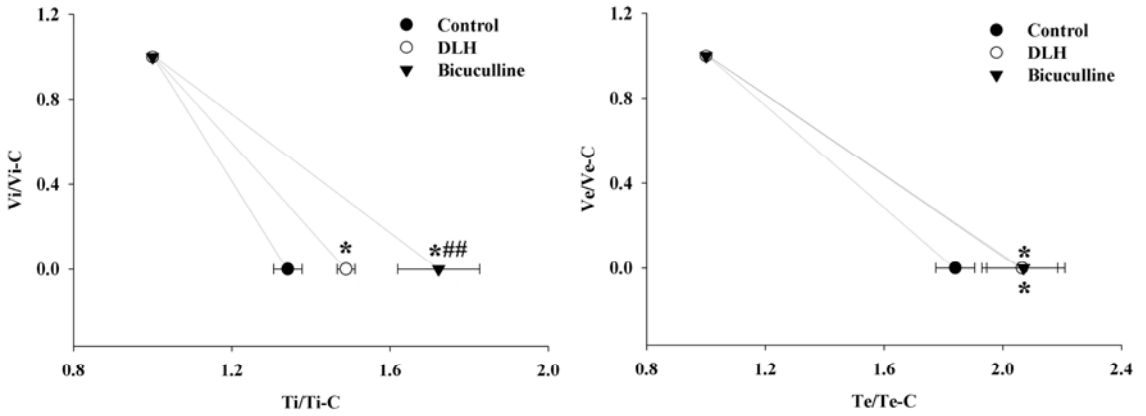

Figure 5-3. Relatiopship between respiratory volume and timing with or without dPAG activation. Both respiratory volume and timing are expressed as a percentage normalized to the control value. *: $p<0.05$, vs control; ##: $p<0.01$, vs DLH.

Discussion

This current project investigated modulation of volume-timing reflexes by dPAG activation. Both inspiratory and expiratory occlusions were delivered before and after chemical activation of the dPAG with excitatory amino acid DLH and $GABA_A$ receptor antagonist Bic. Inspiratory occlusion significantly prolonged the Ti and expiratory occlusion significantly prolonged Te under all experimental conditions. Activation of the dPAG shifted the volume-timing responses to the right suggesting that a greater change

in volume related feedback is required to elicit breath phase switching. In addition, Bic disinhibition had a greater effect than DLH on the Vi-Ti relationship. These results suggested that dPAG activation modulates respiratory mechanoreflexes.

Table 5-2. Effect of expiratory occlusion on respiratory timing change following the activation of the dPAG

	control	DLH	control	bicuculline
Te-C (ms)	351±19	286±7*	380±14	258±13*
Ti-C (ms)	200±2	185±5	183±10	185±4
Te-O (ms)	639±40$^{\#\#}$	591±37$^{\#\#}$	711±66$^{\#\#}$	537±51$^{**\#}$
Ti-O (ms)	195±3	192±6	175±13	191±6
Te-O/Te-C	1.84±0.09	2.07±0.12*	1.85±0.11	2.08±0.14*
Ti-O/Ti-C	0.98±0.02	1.04±0.02	0.96±0.03	1.04±0.01*
Vt-C (ml)	1.97±0.05	2.13±0.14	2.00±0.11	1.97±0.12
f_R (/min)	110±4	128±2*	107±2	137±6*
bdEMG-C (au)	1.00±0.00	1.25±0.16	1.00±0.00	5.76±3.43
bdEMG-O (au)	0.95±0.02	1.16±0.12	1.00±0.05	4.64±2.75
ΔdEMG-C (au)	1.00±0.00	1.11±0.06	1.00±0.00	1.19±0.24
ΔdEMG-O (au)	1.01±0.03	1.07±0.09	1.07±0.04	1.15±0.22

Values are means ± SE. au: arbitrary unit. *: significantly different from corresponding value in control condition, $p < 0.05$; **: $p < 0.001$; $^{\#}$: significantly different from corresponding value in pre-occlusion breath, $p < 0.05$; $^{\#\#}$: $p < 0.001$.

Respiratory Response Elicited from the dPAG

Both DLH and Bic microinjection in the dPAG elicited enhanced respiratory activity, as reported previously (Lovick, 1992; Huang et al., 2000; Hayward et al., 2003; Hayward et al., 2004). The f_R significantly increased after dPAG activation, which was

due to the shortening of both Ti and Te. The results suggested a descending excitatory input to the brainstem respiratory network. Activation of the dPAG has different effects on respiratory phases. Electrical stimulation with low intensity evoked a decrease in Te, but not Ti (Duffin et al., 1972; Hockman et al., 1974; Bassal et al., 1982; Hayward et al., 2003; Zhang et al., 2003). In this study, when f_R was still significantly higher than pre-activation level, Ti was similar to pre-activation level while Te was significantly shorter. Thus, the expiratory phase has a greater dPAG modulation. The result was an increased f_R and minute ventilation.

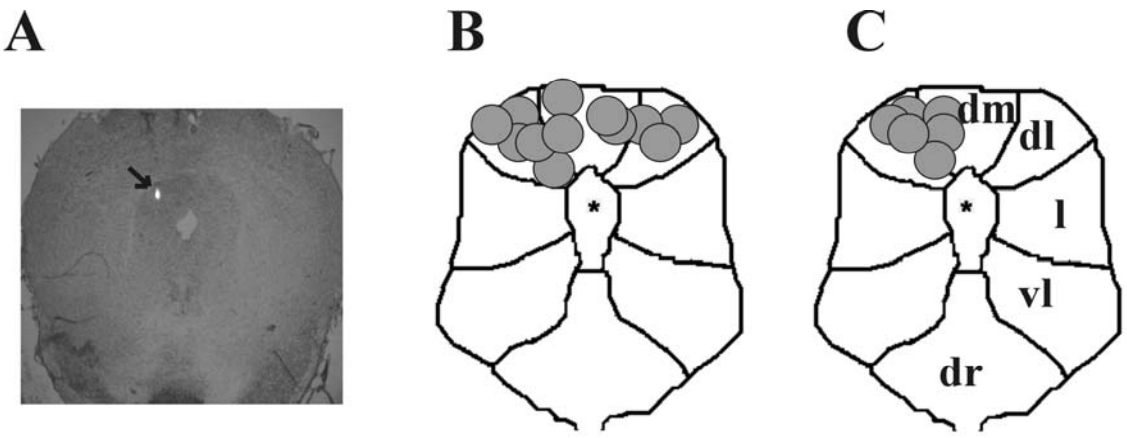

Figure 5-4. Reconstructed dPAG stimulation sites. *A*: A sample histological section taken from one animal illustrating a typical microinjection site (arrow). *B*: reconstructed dPAG microinjection sites from DLH (n=6) experiments. *C*: reconstructed dPAG microinjection sites from bicuculline (n=6) experiments. The images all represent approximate brain region at 7.8mm caudal to the bregma. Schematics of brain regions were adapted from a rat brain atlas (Paxinos et al., 1997). *****, midbrain aqueduct, *dm*, dorsomedial PAG; *dl*, dorsolateral PAG; *l*, lateral PAG; *vl*, ventrolateral PAG; *dr*, dorsal raphe.

Effect of dPAG Activation on Respiratory Occlusion Reflexes

During eupneic breathing, PSRs were recruited during the early stages of inspiration. Activation of PSRs inhibits inspiratory phase, and prolong the expiratory phase. Inspiratory occlusion was delivered at FRC. Inspiration against the occluded airway increases Ti with no increase in Vt. It has been reported that the frequency of PSR

discharges is correlated with the off-switch transition from inspiration to expiration (Davenport et al., 1981). Activation of the dPAG modulated Vi-Ti relationship and shifted the respiratory timing response to inspiratory occlusion to the right. Expiratory occlusion was delivered at the end of the inspiratory phase. It has been reported that Te is related to the summation of PSR activity (Davenport et al., 1986). Expiratory occlusion prolonged Te-O by holding the lung volume at the end inspiratory level, increasing the activity of PSRs and inhibiting the onset of the subsequent inspiration. Activation of the dPAG modulated the Ve-Te relationship and shifted the respiratory timing response to expiratory occlusion to the right. These data suggested that dPAG activation could modulate the volume-timing reflex.

The results suggest that dPAG activation can change the timing control of the brainstem respiratory network. The respiratory response elicited from the dPAG is mediated in part by the lateral parabrachial subnuclei (LPBN) (Hayward et al., 2004). The LPBN modulates neuronal activities in the ventral respiratory group (VRG) (Chamberlin et al., 1995; St. John, 1998). It is likely that pontine mechanisms play a crucial role in the dPAG modulated respiratory mechanoreflex. The parabrachial nucleus is necessary for the normal Hering-Breuer reflex (Feldman et al., 1976; Takano et al., 2003). Lesion of pontine pneumotaxic center enhanced the Ti response to non-inflation of a ventilator, a maneuver similar to inspiratory occlusion. This lesion increased the effect of high-frequency vagal stimulation on Te prolongation (Takano et al., 2003). The pontine pneumotaxic center includes the medial parabrachial nucleus (MPBN) and the Kölliker-Fuse (KF) nucleus. These two PBN subnuclei were not activated during dPAG activation (Hayward et al., 2003), and do not receive direct projections from the dPAG

(Krout et al., 1998). But the MPBN does receive projections from the ventral PAG (Krout et al., 1998), which can be activated by the dPAG (Hayward et al., 2003). This suggests that the MPBN/KF complex may be inhibited by dPAG activation. It is unknown, however, if inhibition of the MPBN/KF complex is via an intra-PAG mechanism (Sandkuhler et al., 1995; Jansen et al., 1998; Hayward et al., 2003) or intra-PBN mechanism.

It is unlikely that the dPAG mediated respiratory occlusion reflex modulation is elicited directly from the dPAG to the NTS. No significant direct connection between the dPAG and the NTS has been reported (Cameron et al., 1995; Farkas et al., 1997; Henderson et al., 1998). The dPAG may affect the neurons in the NTS through indirect pathways, including those mediated by the LPBN. Pulmonary PSR afferents mainly project to the medial subnucleus, lateral and ventrolateral subnuclei of the NTS (Jordan, 2001). In cats, neuronal discharges in the NTS were depressed following the electrical stimulation of the PAG (Sessle et al., 1981). It was reported that stimulation of the dPAG with DLH evoked a dose-dependent increase in discharge rate of respiratory-related NTS neurons, consistent with increased f_R following dPAG stimulation (Huang et al., 2000). The type of NTS respiratory neurons was, however, not characterized. It is unknown if PSR relay neurons in the NTS respond to dPAG activation. The dPAG may exert its influence on respiratory mechanoreflex sensitivity by modulating neuronal activities in the NTS via the LPBN.

The dPAG might also affect respiratory mechanoreflexes by modulating neuronal activities in the VRG, where the LPBN and the NTS have common projection targets. It has been suggested that expiratory (E-Dec) neurons in the VRG are involved in

mediating the Hering-Breuer inflation reflex (Hayashi et al., 1996). These neurons were proposed to determine the duration of the expiratory phase. Results of current project suggest that Te is modulated by dPAG activation (Duffin et al., 1972; Hockman et al., 1974; Bassal et al., 1982; Hayward et al., 2003; Zhang et al., 2003). These E-Dec neurons may play a crucial role in the dPAG evoked respiratory response. Further studies are necessary to determine the responses of respiratory neurons in the VRG to dPAG activation.

DLH vs Bicuculline

Bicuculline microinjection in the dPAG elicited similar cardio-respiratory response patterns as DLH. But at comparable f_R, Bic disinhibition prolonged Ti during inspiratory occlusion, and increased baseline dEMG activity more significantly than DLH stimulation (Fig. 5-3). This difference could be explained by the different activation mechanisms of these two drugs. DLH activates neural structures through excitatory glutamate NMDA receptors. Bic removes tonic inhibitory inputs to target structures, disinhibiting intrinsic excitatory inputs, which are mediated by NMDA receptors, non-NMDA and serotonin receptors (Barbaresi et al., 1988; Albin et al., 1990; Lovick et al., 1994; Lovick et al., 2000). Thus, these drugs may activate different neuron populations, and bicuculline disinhibition would involve a more complex neuronal mechanism. Application of Bic blocks the inhibition from medulla raphe system (Lovick et al., 2001). At the same time, the dPAG has descending projections to medulla raphe system (Cameron et al., 1995). The interruption of this neuronal circuit or other unknown circuits may modulate respiratory reflexes. The lack of information on the role of the dPAG in neural control of breathing will require further experiments to clarify the roles of specific neurotransmitter receptors in modulating respiratory reflexes.

Summary

This study found that activation of the dPAG modulated the volume-timing response to respiratory occlusion in anesthetized rats. Inspiratory or expiratory occlusion significantly prolonged corresponding Ti or Te, respectively. Activation of the dPAG enhanced the respiratory timing response to occlusion tests. This means that a greater volume, and associated PSR discharge was required to elicit breath phase switching. Bic disinhibition had a greater effect on the inspiratory occlusion Vi-Ti reflex than DLH. These findings suggested that dPAG activation modulates respiratory activity and brainstem mechanoreflexes.

CHAPTER 6
ROLE OF THE DORDAL PERIAQUEDUCTAL GRAY IN THE NEURAL CONTROL OF BREATHING

The experiments in this project studied dPAG elicited respiratory responses, and the modulatory effect of the dPAG on respiratory reflexes. The results from this project demonstrated that dPAG activation has an excitatory effect on the brainstem respiratory neural network. Furthermore, the descending excitatory inputs interact with respiratory afferent inputs to change respiratory reflex behavior.

Excitatory Effect of the dPAG on Respiratory Timing Response

In this project, activation of the dPAG with both electrical and chemical stimulation decreased inspiratory time (Ti) and expiratory time (Te) resulting an increased respiratory frequency (f_R). It was reported that activation of the dPAG with chemical microinjection evoked a dose-dependent increase in respiratory response (Huang et al., 2000; Hayward et al., 2003). In this project, respiratory response elicited by electrical stimulation in the dPAG depended on stimulus intensity and frequency. A stimulus intensity/frequency threshold eliciting cardio-respiratory responses was found in the dPAG.

The dPAG elicited respiratory timing response suggests that dPAG activation modulates neuronal activities in the brainstem respiratory network. The LPBN mediates the dPAG elicited respiratory response (Hayward et al., 2004). In our model (Fig. 6-1), the LPBN is the primary connection between the dPAG and medulla ventral respiratory group (VRG). The role of the LPBN in neural control breathing has been reported previously (Chamberlin et al., 1994; St. John, 1998). The descending excitatory inputs

from the dPAG to the LPBN could be a direct connection, or indirectly go through other subdivisions of the PAG (Cameron et al., 1995; Jansen et al., 1998; Krout et al., 1998; Hayward et al., 2003). Other subnuclei of the parabrachial nucleus (PBN) do not seem to play a significant role in the dPAG elicited respiratory response (Hayward et al., 2003). Whether the interaction among the subnuclei of the PBN is involved in the dPAG elicited respiratory response remains unknown. The LPBN may also affect other respiration-related neurons in the brainstem including the NTS (Felder et al., 1988). Activation of the dPAG modulated the discharges of respiratory-related neurons in the NTS (Sessle et al., 1981; Huang et al., 2000). The dPAG has direct descending projections to various other nuclei in the brainstem including the A5 cell group, the medullar raphe system, the rostral ventrolateral medulla (Cameron et al., 1995; Gaytan et al., 1998). Their roles in dPAG elicited respiratory response remain unknown.

This project reported that Te is the primary respiratory timing parameter modulated by dPAG activation. Electrical stimulation studies reported that only Te was decreased after dPAG activation (Duffin et al., 1972; Hockman et al., 1974; Bassal et al., 1982; Hayward et al., 2003). In this study, increasing stimulus intensity resulted in significantly decreased Ti. After the cessation of electrical stimulation, Te remained decreased from control for a longer time than Ti (Chapter 2 & 3). With chemical stimulation of the dPAG, this difference in Te and Ti recovery was shown to be due to the activation of the dPAG neurons. At 8 min after bicuculline (Bic) microinjection in the dPAG, Ti had recovered to control, while Te remained significantly decreased (Chapter 4). During the recovery stage after dPAG activation with DLH and Bic, Te was significantly decreased when Ti had returned to control (Chapter 5). These results suggest that the primary

influence of the dPAG on brainstem respiratory network is on the neurons determining expiratory phase timing (Shannon et al, 1998). The change of Ti may be the result of a recruited neural pathway and depend on stimulus intensity.

This project also reported that activation of the caudal dPAG elicited greater respiratory responses than the rostral dPAG (Chapter 3). Activation of the caudal dPAG elicited a significantly greater decrease in Ti and Te than rostral stimulation, resulting a greater increase in f_R. The LPBN mediates dPAG elicited respiratory responses (Hayward et al, 2004), which suggests that regional difference in dPAG elicited respiratory response may be due to the suprapontine neural mechanism. Anatomical studies have reported that the rostral dPAG project to the caudal dPAG before reaching brainstem respiratory network (Cameron et al., 1995; Sandkuhler et al., 1995). These results suggest that the caudal dPAG is located between the rostral dPAG and the LBPN, thus modulating the excitatory inputs to the LPBN.

Activation of the dPAG on Respiratory Muscle Activities and Ventilation

In this project, dPAG activation increased diaphragm EMG (dEMG) activity. During electrical stimulation and microinjection of Bic, significant increases occurred in baseline dEMG activity, the tonic discharge during expiratory phase, but not dEMG amplitude (Chapter 2, 3, and 4). This project also found that during DLH stimulation of the caudal dPAG, there was concurrent increase of both baseline activity and dEMG amplitude (Chapter 3). The difference may be due to different stimulation methods. Electrical stimulation activates more neural structures than DLH. Bic disinhibits normally suppressed dPAG neuronal activity. The increase in dEMG activity was not associated with a significant increase in Vt. Hence, these results suggest that increased minute ventilation after dPAG activation was contributed primarily by increased f_R.

An additional new finding of this project is the dPAG elicited recruitment of expiratory muscles (Chapter 2). Tracheal airflow was enhanced in both inspiratory and expiratory directions. During eupneic breathing, expiration is normally passive, and external abdominal oblique muscle does not show EMG activity. After dPAG activation, abdominal muscle EMG activity was recruited during the expiratory phase. Abdominal muscle EMG activity showed a dose-dependent response with stimulus intensity. In addition to the Te response to dPAG activation, these results suggest modulation of dPAG activation on the expiratory neurons in the brainstem respiratory network that control expiratory phase timing and expiratory muscle drive (Fig. 6-1). Activation of expiratory muscles is necessary to increase expiratory pressure and airflow. Increased tone of both inspiratory and expiratory muscles may represent a change in functional residual capacity (Hayward et al., 2003).

Influence of the dPAG on Respiratory Reflexes

Normal respiratory activity depends on the central generator of respiratory rhythm and respiratory afferents from mechanoreceptors and chemoreceptors located inside and outside of the respiratory system. The results from current project demonstrated an interaction between descending excitatory inputs from the dPAG and peripheral respiratory afferent inputs.

Influence of the dPAG on Peripheral Chemoreflex

Peripheral chemoreceptors are located in the carotid body, sense arterial PO_2 and $[H^+]$ and send afferent information to the CNS (Finley et al., 1992; Marshall, 1994; Gueyenet et al., 1995; Gueyenet, 2000). Most of these afferents project to the NTS. It has been demonstrated that suprapontine structures, including the hypothalamus, could modulate respiratory responses to peripheral chemoreceptor stimulation (Silva-Carvalho,

1995; Horn et al., 1998). Peripheral chemoreceptor stimulation in conscious animals may act as an alerting factor, and elicit similar autonomic and behavioral responses related to defense response (Hilton et al., 1982; Marshall, 1987).

Results from this project suggest that during dPAG activation, the respiratory responses elicited by peripheral chemoreceptor stimulation overrode the dPAG evoked response. During simultaneous dPAG activation and peripheral chemoreceptor stimulation, the respiratory response was equal to that of the peripheral chemoreflex (Chapter 4). These data suggest that peripheral chemoreceptor afferent inputs may block dPAG excitatory input to the brainstem. Activation of the dPAG elicited respiratory responses was mediated by the LPBN (Hayward et al., 2003; Hayward et al., 2004). The chemoreceptor afferents could directly block the inputs from the LPBN to the VRG (Ellenberger et al., 1990; Nunez-Abades et al., 1993). This may be mediated by the inhibitory interneurons located in ventral medulla (Gozal et al., 1994; Carrol et al., 1996). We hypothesized peripheral chemoreceptor stimulation presents the animal a stronger alerting signal than that from direct dPAG activation (Fig. 6-1). In addition, it is known that cognitive suppression of respiration during breath-holding is released when CO_2 increases to the "break-point". Thus, peripheral chemoreceptor drive in the brainstem has the capability to block higher brain control of brainstem neural respiratory drive.

Influence of the dPAG on Respiratory Occlusion Reflexes

Respiratory mechanoreceptors such as slowly adapting pulmonary stretch receptors (PSRs) are located in the tracheobronchial tree (Jordan, 2001). PSR afferents project to the brainstem via the vagus nerves. The discharge of PSRs is in phase with lung inflation. Smaller inspiratory volume (Vi) or expiratory volume (Ve) is associated with longer Ti or Te respectively, resulting in the volume-timing relationship (Zechman et al., 1976;

Davenport et al., 1981; Webb et al., 1994; Webb et al., 1996). Respiratory occlusion can elicit respiratory timing changes that follow this relationship, and prolong the corresponding respiratory phase. In the current project, dPAG activation enhanced the respiratory timing response to occlusion and shifted the volume-timing responses to the right. The shift of the Vi-Ti relationship means that it requires a greater Vi to terminate inspiration which is a desensitization of the Vi-Ti reflex. The shift of the Ve-Te relationship to the right means that the same number of PSR spikes (summation) causes a greater increase in Te. This means that the Ve-Te relationship is sensitized.

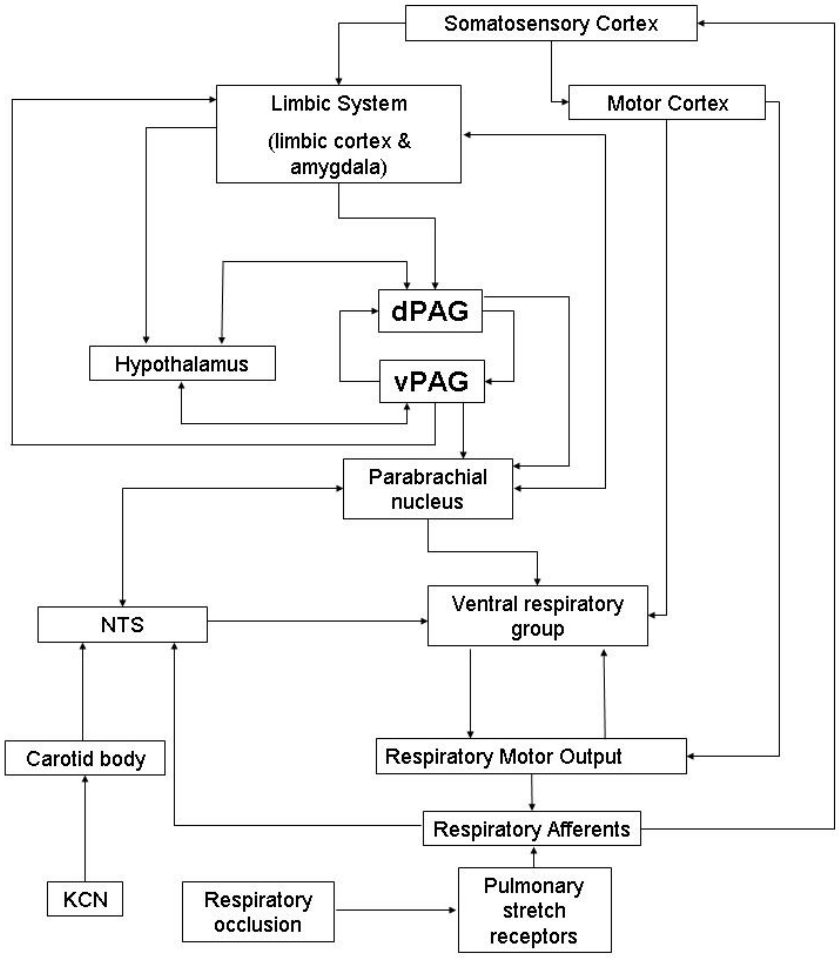

Figure 6-1. A schematic model about the role of the dPAG in the neural control of breathing.

The dPAG modulatory effect on respiratory mechanoreflex is likely due to a change in the brainstem respiratory network (Cameron et al., 1995: Cameron et al., 1995; Jansen et al., 1998). The NTS is the initial central neural termination of PSRs. Activation of the dPAG modulates the activity patterns of respiratory-related neurons in the NTS (Sessle et al., 1981; Huang et al., 2000). The modulation of the dPAG on the NTS respiratory-related neurons may change the mechanoreflex relay of PSR inputs to the VRG.

The neurons with respiratory-related discharges have been reported in the dPAG (Ni et al., 1990). The dPAG receives very few direct inputs from brainstem. These respiratory-related discharges may be indirect input from other brain nuclei. The dPAG receives afferents from medial pre-frontal cortex and pre-limbic cortex (Behbehani, 1995). These areas receive afferent information from other cortical regions. Somatosensory and limbic cortices receive vagal inputs in both rats and cats (Ito et al., 2002; Ito, 2003). These data suggest that the dPAG receives mechanical information from the respiratory system processed by higher brain regions (Fig. 6-1). Activation of the dPAG may then project to the brainstem respiratory network.

Physiological Significance of the Results

The proposed model (Fig. 6-1) implies that the dPAG is an important integration point mediating respiratory and other autonomic responses from higher brains. Thus the dPAG is a key component in autonomic regulation by the neural affective system.

The dPAG does not appear to play a significant role in neural control of eupneic breathing. The dPAG may be activated by emotional distress during respiratory challenges in humans (Brannan et al., 2001; Liotti et al., 2001; Parsons et al., 2001; Evans et al., 2002; Isaev et al., 2002). With stress, activation of the dPAG can then

modulate the activity of the brainstem respiratory network. This modulation is for survival advantage, which is consistent with the role of the dPAG in defense behavior. The hyperventilation during dPAG activation may provide extra oxygen for fight or flight motor behavior. The respiratory response to peripheral chemoreceptor stimulation is however preserved during dPAG activation. Activation of the dPAG desensitized the off-switch which allows for increased tidal volumes. Te is preferentially regulated by dPAG activation. The shortened time available for exhalation which could result in incomplete expiration and gas retention is compensated by expiratory muscle activation. The dPAG thus coordinates respiratory reflex behavior to allow for highly facilitated ventilation during periods of stress. These results increase our understanding of respiratory response to emotional and stress-related behavior which is relevant to patient responses to respiratory challenges and diseases.

CHAPTER 7
SUMMARY

This project investigated the role of the dPAG in the neural control of breathing. The dPAG was activated by both electrical and chemical stimulation. Chemical stimulation was delivered by either activation with NMDA receptor angonist DLH or disinhibition with $GABA_A$ receptor antagonist bicuculline. Experiments were performed in spontaneously breathing, vagal intact, anesthetized male Sprague-Dawley rats,

The results showed that activation of the dPAG has an excitatory effect on brainstem respiratory network, and thus increases respiratory activity. The excitatory effect is represented by respiratory timing change, characterized by increased f_R with the shortening of both Ti and Te. The increase in diaphragm EMG amplitude occurred only under DLH stimulation. Activation of the dPAG affects Te more than Ti. Respiratory pattern analysis revealed that dPAG elicited Te response persisted after the completion of electrical stimulation. This project also observed activation of abdominal expiratory muscles after dPAG stimulation. The results demonstrated that the dPAG evoked respiratory response includes both inspiratory and expiratory processes.

There was regional difference in respiratory response elicited along the rostro-caudal axis of the dPAG. Rostral and caudal dPAG are involved in different patterns of defense behavior, and sympathoexcitation. In the current project, caudal dPAG activation elicited a greater respiratory response than rostral dPAG, including a significant difference in respiratory timing and diaphragm EMG baseline activity. Cardiovascular responses of HR and MAP did not show regional differences with dPAG activation.

These data suggests that consistent with the differences in behavior patterns along the rostro-caudal axis of the dPAG, the autonomic response is also expressed in different patterns.

The influence of dPAG activation on respiratory reflexes was investigated. Peripheral chemoreceptor stimulation with KCN elicited an autonomic response pattern that was transient, consistent, reproducible and mediated by brainstem neural processes. During dPAG activation, the respiratory response to peripheral chemoreceptor stimulation was preserved. The f_R in response to peripheral chemoreceptor stimulation was the same regardless of the f_R proceeding KCN injection. The results suggest that peripheral chemoreceptor stimulation can block descending excitatory inputs from the dPAG to brainstem respiratory network. Respiratory mechanoreflexes were elicited by inspiratory or expiratory occlusion. Respiratory phase timing during the occlusion was prolonged compared with the proceeding control breath. The activation of the dPAG however further enhanced the occlusion related breath phase prolongation. This result suggests that dPAG activation modulates respiratory mechanoreflexs.

In summary, it was concluded that the dPAG has excitatory effect on the brainstem respiratory network, although the dPAG does not have an active component in the neural control of eupneic breathing. Enhanced ventilation provides essential ventilatory resources to the animal. The influence of dPAG activation on respiratory mechanoreflexs and peripheral chemoreflexs are consistent with its role in defense behavior. The results demonstrated the influence of the central neural affective system on the neural control of breathing.

LIST OF REFERENCES

Albin RL, Makowiec RL, Hollingsworth Z, Dure LS, Penney JB, Young AB, 1990, Excitatory amino acid receptors in the periaqueductal gray of the rat. Neuroscience Letter 118: 112–115.

Bandler R, 1982, Induction of 'rage' following microinjections of glutamate into midbrain but not hypothalamus of cats. Neuroscience Letter 30: 183-188.

Bandler R, Depaulis A, Vergnes M, 1985, Identification of midbrain neurones mediating defensive behaviour in the rat by microinjections of excitatory amino acids. Behavioral Brain Research 15: 107-119.

Bandler R, Keay KA, Floyd N, Price J, 2000, Central circuits mediating patterned autonomic activity during active vs. passive emotional coping. Brain Research Bulletin 53: 95-104.

Bandler R, Shipley MT, 1994, Columnar organization in the midbrain periaqueductal gray: modules for emotional expression? Trends in Neuroscience 17: 379-389.

Barbaresi P, Manfrini E, 1988, Glutamate decarboxylase-immunoreactive neurons and terminals in the periaqueductal gray of the rat. Neuroscience 27: 183-191.

Bassal M, Bianchi AL, 1982, Inspiratory onset or termination induced by electrical stimulation of the brain. Respiratory Physiology 50: 23-40.

Behbehani MM, 1995, Functional characteristics of the midbrain periaqueductal gray. Progress in Neurobiology 46: 575-605.

Behbehani MM, Liu H, Jiang M, Pun RYK, Shipley MT, 1993, Activation of serotonin 1A receptors inhibits midbrain periaqueductal gray neurons in the rat. Brain Research 612: 56-60.

Beitz AJ, 1985, The midbrain periaqueductal gray in the rat. I. Nuclear volume, cell number, density, orientation, and regional subdivisions. Journal of Comparative Neurology 237: 445-459.

Berquin P, Bodineau L, Gros F, Larnicol N, 2000, Brainstem and hypothalamic areas involved in respiratory chemoreflexes: a Fos study in adult rats. Brain Research 857: 30-40.

Blanchard RJ, Flannelly KJ, Blanchard DC, 1986, Defensive behavior of laboratory and wild *Rattus norvegicus*. Journal of Comparative Psychology 100: 101-107.

Bianchi R, Corsetti G, Rodella L, Tredici G, Gioia M, 1998, Supraspinal connections and termination patterns of the parabrachial complex determined by the biocytin anterograde tract-tracing technique in the rat. Journal of Anatomy 193: 417-430.

Bolser DC, Davenport PW, 2000, Volume-timing relationships during cough and resistive loading in the cat. Journal of Applied Physiology 89:785-790.

Bowery NG, Hudson AL, Price GW, 1987, $GABA_A$ and $GABA_B$ receptor site distribution in the rat central nervous system. Neuroscience 20: 365-383.

Brandão ML, Lopez-Garcia JA, Greaff FG, Roberts MHT, 1991, Electrophysiological evidence for excitatory 5-HT_2 and depressant 5-HT_{1A} receptors on neurones of the rat midbrain tectum. Brain Research 556: 259-266.

Brannan S, Liotti M, Egan G, Shade R, Madden L, Robillard R, Abplanalp B, Stofer K, Denton D, Fox PT, 2001, Neuroimaging of cerebral activations and deactivations associated with hypercapnia and hunger for air. Proceedings of the National Academy of Sciences of the United States of America 98: 2029-2034.

Brown K, Stocks J, Aun C, Rabbette PS, 1998, The Hering-Breuer reflex in anesthetized infants: end-inspiratory vs. end-expiratory occlusion technique. Journal of Applied Physiology 84:1437-1446.

Cameron AA, Khan IA, Westlund KN, Kliffer KD, Willis WD, 1995, The efferent projections of the periaqueductal gray in the rat: a phaseolus vulgaris-leucoagglutinin study. I. Ascending projections. Journal of Comparative Neurology 351: 568-584.

Cameron AA, Khan IA, Westlund KN, Willis WD, 1995, The efferent projections of the periaqueductal gray in the rat: a phaseolus vulgaris-leucoagglutinin study. II. Descending projections. Journal of Comparative Neurology 351: 585-601.

Carrive P, 1993, The periaqueductal gray and defensive behavior: functional representation and neuronal organization. Behavioural Brain Research 58: 27-47.

Carrive P, Bandler R, Dampney RAL, 1988, Anatomical evidence that hypertension associated with the defence reaction in the cat is mediated by a direct projection from a restricted portion of the midbrain periaqueductal grey to the subretrofacial nucleus of the medulla. Brain Research 460**:** 339–345, 1988.

Carroll JL, Gozal D, Rector DM, Aljadeff G, Harper RM, 1996, Ventral medullary neuronal responses to peripheral chemoreceptor stimulation. Neuroscience 73: 989-998.

Chamberlin NL, Saper CB, 1994, Topographic organization of respiratory responses to glutamate microstimulation of the parabrachial nucleus in the rat. Journal of Neuroscience 14: 6500-6510.

Chiou LC, Chou HH, 2000, Characterization of synaptic transmission in the ventrolateral periaqueductal gray of rat brain slices. Neuroscience 100: 829-834.

Clark FJ, von Euler C, 1972, On the regulation of depth and rate of breathing. Journal of Physiology London 222: 267-295.

Clements JR, Beitz AJ, Fletcher TF, Mullett MA, 1985, Immunocytochemical localization of serotonin in the rat periaqueductal grey: a quanititative ling and electron microscope study. Journal of Comparative Neurology 236: 60-70.

Coles SK, Dick TE, 1996, Neurones in the ventrolateral pons are required for post-hypoxic frequency decline in rats. Journal of Physiology 497: 79-94.

Davenport PW, Frazier DT, Zechman FW Jr, 1981, The effect of the resistive loading of inspiration and expiration on pulmonary stretch receptor discharge. Respiratory Physiology 43: 299-314.

Davenport PW, Wozniak JA, 1986, Effect of expiratory loading on expiratory duration and pulmonary stretch receptor discharge. Journal of Applied Physiology, 61: 1857-1863.

Davis PJ, Zhang SP, Bandler R, 1993, Pulmonary and upper airway afferent influences on the motor pattern of vocalization evoked by excitation of the midbrain periaqueductal gray of the cat. Brain Research 607: 61-80.

De Oca BM, DeCola JP, Maren S, Fanselow MS, 1998, Distinct regions of the periaqueductal gray are involved in the acquisition and expression of defensive responses. Journal of Neuroscience 18: 3426-3432.

Depaulis A, Keay KA, Bandler R, 1992, Longitudinal neuronal organization of defensive reactions in the midbrain periaqueductal gray region of the rat. Experimental Brain Research 90: 307-318.

Depaulis A, Keay KA, Bandler R, 1994, Quiescence and hyporeactivity evoked by activation of cell bodies in the ventrolateral midbrain periaqueductal gray of the rat. Experimental Brain Research 99: 75-83.

Duffin J, Hockman CH, 1972, Limbic forebrain and midbrain modulation and phase-switching of expiratory neurons. Brain Research 39: 235-239.

Eldridge FL, 1975, Relationship between respiratory nerve and muscle activity and muscle force output. Journal of Applied Physiology 39: 567–574.

Eldridge FL, 1994, Central integration of mechanisms in exercise hyperpnea. Medicine and Science in Sports and Exercise 26: 319-327.

Eldridge FL, Millhorn DE, Waldrop TG, 1981, Exercise hyperpnea and locomotion: parallel activation from the hypothalamus. Science 211: 844-846.

Ellenberger HH, Feldman JL, 1990. Brainstem connections of the rostral ventral respiratory group of the rat. Brain Research 513: 35-42.

Evans KC, Banzett RB, Adams L, Mckay L, Frackowiak RS, Corfiled DR, 2002, BOLD fMRI identifies limbic, paralimbic, and cerebellar activation during air hunger. Journal of Neurophysiology 88: 1500–1511.

Farkas E, Jansen AS, Loewy AD, 1997, Periaqueductal gray matter projection to vagal preganglionic neurons and the nucleus tractus solitarius. Brain Research 764: 257-261.

Felder RB, Mifflin SW, 1988, Modulation of carotid sinus afferent input to nucleus tractus solitarius by parabrachial nucleus stimulation. Circulation Research 63: 35-49.

Feldman JL, Gautier H, 1976, Interaction of pulmonary afferents and penumotaxic center in control of respiratory pattern in cats. Journal of Neurophysiology 31: 31-44.

Feldman JL, Mitchell GS, Nattie EE, 2003, Breathing: rhythmicity, plasticity, chemosensitivity. Annual Review of Neuroscience, 26: 239-266.

Fernandez de Molina A, Hunsperger RW, 1962, Organization of the subcortical system governing defence and flight reactions in the cat. Journal of Physiology 160:200–213.

Finley JC, Katz DM, 1992, The central organization of carotid body afferent projections to the brainstem of the rat. Brain Research 572: 108-116.

Franchini K, Krieger EM, 1992, Carotid chemoreceptos influence arterial pressure in intact and aortic denervated rats. American Journal of Physiology Regulatory, Integrative and Comparative Physiology 262: R677-R683.

Franchini KG, Krieger EM, 1993, Cardiovascular responses of conscious rats to carotid body chemoreceptor stimulation by intravenous KCN. Journal of the Autonomic Nervous System 42: 63-69.

Gaytan SP, Pasaro R, 1998, Connections of the rostral ventral respiratory neuronal cell group: an anterograde and retrograde tracing study in the rat. Brain Research Bulletin 47: 625-642.

Gozal D, Aljadeff G, Carroll JL, Rector DM, Harper RM, 1994, Afferent contributions to intermediate area of the cat ventral medullary surface during mild hypoxia. Neuroscience Letter 178: 73-76.

Graeff FG, 2004, Serotonin, the periaqueductal gray and panic. Neuroscience and Biobehavioral Reviews 28: 239-259.

Graeff FG, Silveira MCL, Nogueira RL, Audi EA, Oliveira RMW, 1993, Role of the amygdala and periaqueductal gray in anxiety and panic. Behavioural Brain Research 58: 123-131.

Griffiths JL, Lovick TA, 2002, Co-localization of 5-HT 2A -receptor- and GABA-immunoreactivity in neurones in the periaqueductal grey matter of the rat. Neuroscience Letter 326: 151-154.

Guyenet PG, 2000, Neural structures that mediate sympathoexcitation during hypoxia. Respiratory Physiology 121: 147-162.

Guyenet PG, Koshiya N, 1995, Working model of the sympathetic chemoreflex in rats. Clinical and Experimental Hypertension 17: 167-179.

Haibara AS, Tamashiro E, Olivan MV, Bonagamba LG, Machado BH, 2002, Involvement of the parabrachial nucleus in the pressor response to chemoreflex activation in awake rats. Autonomic Neuroscience: Basic & Clinical 101: 60-67.

Hayashi F, Coles SK, McCrimmon DR, 1996, Respiratory neurons mediating the Breuer-Hering reflex prolongation of expiration in rat. Journal of Neuroscience 20:6526-6536.

Hayward LF, Castellanos M, 2003, Increased c-Fos expression in select lateral parabrachial subnuclei following chemical versus electrical stimulation of the dorsal periaqueductal gray in rats. Brain Research 974: 153-166.

Hayward LF, Castellanos M, Davenport PW, 2004, Parabrachial neurons mediate dorsal periaqueductal gray evoked respiratory responses in the rat. Journal of Applied Physiology 96: 1146-1154.

Hayward LF, Felder RB, 1995, Peripheral chemoreceptor inputs to the parabrachial nucleus of the rat. American Journal of Physiology Regulatory, Integrative and Comparative Physiology 268: R707-R714.

Hayward L, Johnson AK, Felder RB, 1999, The arterial chemoreflex in conscious normotensive and hypertensive adult rats. American Journal of Physiology Heart and Circulatory Physiology 276: H1215–H1222.

Hayward LF, Von Reitzenstein M, 2002, c-Fos expression in the midbrain periaqueductal gray after chemoreceptor and baroreceptor activation. American Journal of Physiology Heart and Circulatory Physiology 283: H1975-H1984.

Hayward LF, Swartz CL, Davenport PW, 2003, Respiratory response to activation or disinhibition of the dorsal periaqueductal gray in rats. Journal of Applied Physiology 94: 913-922.

Henderson LA, Keay KA, Bandler R, 1998, The ventrolateral periaqueductal gray projects to caudal brainstem depressor regions: a functional-anatomical and physiological study. Neuroscience 82: 201-221.

Herbert H, Saper CB, 1992, Organization of medullary adrenergic and noradrenergic projections to the periaqueductal gray matter in the rat. Journal of Comparative Neurology 315: 34-52.

Hess WR, Brügger M, 1943, Das subkortikale Zentrum der affectiven Abwerreaktion. Helvetica Physiologica Acta 1:33–52.

Hilton SM, 1982, The defence-arousal system and its relevance for circulatory and respiratory control. Journal of Experimental Biology 100: 159-174.

Hilton SM, Marshall JM, 1982, The pattern of cardiovascular response to carotid chemoreceptor stimulation in the cat. Journal of Physiology 326:495-513.

Hilton SM, Redfern WS, 1986, A search for brain stem cell groups integrating the defence reaction in the rat. Journal of Physiology 378: 213-28.

Hockman CH, Duffin J, Rupert AH, Vachon BR, 1974, Phase-switching of respiration induced by central gray and hippocampal stimulation in the cat. Journal of Neural Transmission 35: 327-335.

Horn EM, Waldrop TG, 1997, Oxygen-sensing neurons in the caudal hypothalamus and their role in cardiorespiratory control. Respiratory Physiology 110: 219-228.

Huang ZG, Subramanian SH, Balnave RJ, Turman AB, Moi Chow C, 2000, Roles of periaqueductal gray and nucleus tractus solitarius in cardiorespiratory function in the rat brainstem. Respiratory Physiology 120: 185-195.

Hudson PM, Lumb BM, 1996, Neurones in the midbrain periaqueductal grey send collateral projections to nucleus raphe magnus and the rostral ventrolateral medulla in the rat. Brain Research 733: 138-141.

Hunsperger RW, 1963, Comportements affectifs provoqués par la stimulation électrique du tronc cérébral et du cerveau antérieur. Journal de Physiologie 55: 45-97.

Illing RB, Graybiel AM, 1986, Complementary and non-matching afferent compartments in the cat's superior colliculus: innervation of the acetylcholinesterase-poor domain of the intermediate gray layer. Neuroscience 18: 373-394.

Inui K, Nosaka S, 1993, Target site of inhibition mediated by midbrain periaqueductal gray matter of baroreflex vagal bradycardia. Journal of Neurophysiology 70: 2205-2214.

Ito S, 2002, Visceral region in the rat primary somatosensory cortex identified by vagal evoked potential. Journal of Comparative Neurology 444: 10–24.

Ito S, Craig AD, 2003, Vagal Input to Lateral Area 3a in Cat Cortex. Journal of Neurophysiology 90: 143–154.

Isaev G, Murphy K, Guz A, Adams L, 2002, Areas of the brain concerned with ventilatory load compensation in awake man. Journal of Physiology 539: 935-945.

Jansen AS, Farkas E, Mac Sams J, Loewy AD, 1998, Local connections between the columns of the periaqueductal gray matter: a case for intrinsic neuromodulation. Brain Research 784: 329-336.

Jordan D, 2001, Central nervous pathways and control of the airways. Respiratory Physiology 125: 67-81.

Kim JJ, Rison RA, Fanselow MS, 1993, Effects of amygdala, hippocampus, and periaqueductal gray lesions on short- and long-term contextual fear. Behavorial Neuroscience 107: 1093-1098.

Koshiya N, Guyenet PG, 1994, Role of the pons in the carotid sympathetic chemoreflex. American Journal of Physiology Regulatory, Integrative and Comparative Physiology 267: R508-R518.

Kramer JM, Nolan PC, Waldrop TG, 1999, In vitro responses of neurons in the periaqueductal gray to hypoxia and hypercapnia. Brain Research 835: 197-203.

Krout KE, Jansen ASP, Loewy AD, 1998, Periaqueductal gray matter projection to the parabrachial nucleus in rat. Journal of Comparative Neurology 401: 437-454.

Leman S, Dielenberg RA, Carrive P, 2003, Effect of dorsal periaqueductal gray lesion on cardiovascular and behavioural responses to contextual conditioned fear in rats. Behavioural Brain Research 143: 169-176.

Liotti M, Brannan S, Egan G, Shade R, Madden L, Abplanalp B, Robillard R, Lancaster J, Zamarripa FE, Fox PT, Denton D, 2001, Brain responses associated with consciousness of breathlessness (air hunger). Proceedings of the National Academy of Sciences of the United States of America 98: 2035-2040.

Lovick TA, 1985, Ventrolateral medullary lesions block the antinociceptive and cardiovascular resonses elicited by stimulating the dorsal periaqueductal grey matter in rats. Pain 21: 241-252.

Lovick TA, 1992, Inhibitory modulation of the cardiovascular defence response by the ventrolateral periaqueductal grey matter in rats. Experimental Brain Research 89: 133-139.

Lovick TA, 1993, The periaqueductal gray-rostral medulla connection in the defence reaction: efferent pathways and descending control mechanisms. Behavioural Brain Research 58: 19-25.

Lovick TA, 1994, Influence of the dorsal and median raphe nuclei on neurons in the periaqueductal gray matter: role of 5-hydroxytryptamine. Neuroscience 59: 993-1000.

Lovick TA, 2001, Involvement of GABA in medullary raphe-evoked modulation of neuronal activity in the periaqueductal grey matter in the rat. Experimental Brain Research 137: 214-218.

Lovick TA, Parry DM, Stezhka VV, Lumb BM, 2000, Serotonergic transmission in the periaqueductal gray matter in relation to aversive behaviour: morphological evidence for direct modulatory effects on identified output neurons. Neuroscience 95: 763-772.

Mansour A, Khachaturian H, Lewis ME, Akil H, Watson SJ, 1987, Autoradiographic differentiation of mu, delta, and kappa opioid receptors in the rat forebrain and midbrain. Journal of Neuroscience 7: 2445-2464.

Markgraf CG, Winters RW, Liskowsky DR, McCabe PM, Green EJ, 1991, Hypothalamic, midbrain and bulbar areas involved in the defense reaction in rabbits. Physiological Reviews 49: 493–500.

Marshall JM, 1987, Analysis of cardiovascular responses evoked following changes in peripheral chemoreceptor activity in the rat. Journal of Physiology 394: 393-414.

Marshall JM, 1994, Peripheral chemoreceptors and cardiovascular regulation. Physiological Reviews 74: 543-594.

Nakazawa K, Shiba K, Satoh I, Yoshida K, Nakajima Y, Konno A, 1997, Role of pulmonary afferent inputs in vocal on-switch in the cat. Neuroscience Research 29: 49-54.

Nashold BS, Wilson WP, Slaughter DG, 1969, Sensations evoked by stimulation in the midbrain of man. Journal of Neurosurgery 30: 14-24.

Ni H, Zhang J, Harper RM, 1990, Respiratory-related discharge of periaqueductal gray neurons during sleep-waking states. Brain Research 511: 319-325.

Nosaka S, Murata K, Inui K, Murase S, 1993, Arterial baroreflex inhibition by midbrain periaqueductal grey in anaesthetized rats. Pflügers Archiv 424: 266-275.

Nosaka SI, Murata K, Murase S, Murata K, 1996, A prejunctional mechanism in midbrain periaqueductal gray inhibition of vagal bradycardia in rats. American Journal of Physiology Regulation Integration Comparative Physiology 270: R373–R382.

Nunez-Abades PA, Morillo AM, Pasaro R, 1993, Brainstem connections of the rat ventral respiratory subgroups: afferent projections. Journal of the Autonomic Nervous System 42: 99-118.

Parsons LM, Egan G, Liotti M, Brannan S, Denton D, Shade R, Robillard R, Madden L, Abplanalp B, Fox PT, 2001, Neuroimaging evidence implicating cerebellum in the experience of hypercapnia and hunger for air. Proceedings of the National Academy of Sciences of the United States of America 98: 2041-2046.

Paxinos G, Watson G, 1997, The rat brain in stereotaxic coordinates. NY: Academic Inc..

Peano CA, Shonis CA, Dillon GH, Waldrop TG, 1992, Hypothalamic GABAergic mechanism involved in respiratory response to hypercapnia. Brain Research Bulletin 28**:** 107–113.

Pompeiano M, Palacios JM, Mengod G, 1992, Distribution and cellular localization of mRNA coding for 5-HT1A receptor in the rat brain: correlation with receptor binding. Journal of Neuroscience 12: 440-453.

Rank JB Jr, 1975, Which elements are excited in electrical stimulation of mammalian central nervous system: a review. Brain Research 98: 417-440.

Ryan JW, Waldrop TG, 1995. Hypoxia sensitive neurons in the caudal hypothalamus project to the periaqueductal gray. Respiratory Physiology 100: 185-194.

Sandkuhler J, Herdegen T, 1995, Distinct patterns of activated neurons throughout the rat midbrain periaqueductal gray induced by chemical stimulation within its subdivisions. Journal of Comparative Neurology 357: 546-553.

Sessle BJ, Ball GJ, Lucier GE, 1981, Suppressive influences from periaqueductal gray and nucleus raphe magnus on respiration and related reflex activities and on solitary tract neurons, and effect of naloxone. Brain Research 216: 145-161.

Sevoz-Couche C, Comet MA, Hamon M, Laguzzi R, 2003, Role of nucleus tractus solitarius 5-HT3 receptors in the defense reaction-induced inhibition of the aortic baroreflex in rats. Journal of Neurophysiology 90: 2521-2530.

Shannon R, Baekey DM, Morris KF, Lindsey BG, 1998, Ventrolateral medullary respiratory network and a model of cough motor pattern generation. Journal of Applied Physiology 84: 2020-2035.

Silva-Carvalho L, Dawid-Milner MS, Goldsmith GE, Spyer KM, 1995, Hypothalamic modulation of the arterial chemoreceptor reflex in the anaesthetized cat: role of the nucleus tractus solitarii. Journal of Physiology London 487: 751-760.

St. John W, 1998, Neurogenesis of patterns of automatic ventilatory activity. Progress in Neurobiology 56: 97–117.

Takano K, Kato F, 2003, Inspiration-promoting vagal reflex in anaesthetized rabbits after rostral dorsolateral pons lesions. Journal of Physiology London 550: 973-983.

van der Plas J, Maes FW, Bohus B, 1995, Electrophysiological analysis of midbrain periaqueductal gray influence on cardiovascular neurons in the ventrolateral medulla oblongata. Brain Research Bulletin 38: 447-456.

Vianna DML, Brandao NL, 2003, Anatomical connections of the periaqueductal gray: specific neural substrates for different kinds of fear. Brazilian journal of medical and biological research 36: 557-566.

Walker P, Carrive P, 2003, Role of ventrolateral periaqueductal gray neurons in the behavioral and cardiovascular responses to contextual conditioned fear and poststress recovery. Neuroscience 116: 897-912.

Wang H, Wessendorf MW, 2002, μ- and δ-opioid receptor mRNAs are expressed in periaqueductal gray neurons projecting to the rostral ventromedial medulla. Neuroscience 109: 619-634.

Weston MC, Stornetta RL, Guyenet PG, 2004, Glutamatergic neuronal projections from the marginal layer of the rostral ventral medulla to the respiratory centers in rats. Journal of Comparative Neurology 473: 73-85.

Webb B, Hutchison AA, Davenport PW, 1994, Vagally mediated volume-dependent modulation of inspiratory duration in the neonatal lamb. Journal of Applied Physiology 76: 397-402.

Webb B, Hutchison AA, Davenport PW, 1996, Contribution of vagal afferents to the volume-timing response to expiratory loads in neonatal lambs. Neuroscience Letter 207: 147-150.

Zechman FW, Frazier DT, Lally DA, 1976, Respiratory volume-time relationships during resistive loading in the cat. Journal of Applied Physiology 40: 177-183.

Zhang SP, Davis PJ, Bandler R, Carrive P, 1994, Brain stem integration of vocalization: role of the midbrain periaqueductal gray. Journal of Neurophysiology 72: 1337-1356.

Zhang W, Hayward LF, Davenport PW, 2003, The relationship between respiratory pattern and the frequency and magnitude of electrical stimulation of the dorsal periaqueductal gray matter. American Journal of Respiratory and Critical Care Medicine 167: A790.

BIOGRAPHICAL SKETCH

Weirong Zhang was born on February 25th, 1971, in the small town of Houcheng, Jiangsu Province, China. He lived with his parents, Dr. Baotian Zhang and Dr. Lianbao Xiao, and his older brother, Weihong Zhang. He graduated from the Nanjing University Medical School with a master's degree in clinical medicine (M.D. equivalent) in 1996. Then, he practiced medicine in the Department of Geriatrics, Nanjing University Medical School Affiliated Gulou Hospital, from August 1996 to October 2000. In the spring of 2001, he began his Ph.D. study in the Department of Physiological Sciences at the University of Florida, and was mentored by Dr. Paul W. Davenport. Upon receiving his Ph.D., Weirong will begin his post-doctoral training at the University of Texas Health Science Center at San Antonio to further his researches on central neural integration of cardio-respiratory activities. His new mentor will be Dr. Steven W. Mifflin.